UNIVERSITY OF CALIFORNIA SAN DIEGO

New Insights into HONO Formation from Nitrate Photochemistry in the Marine Boundary Layer

A Dissertation submitted in partial satisfaction of the requirements
for the degree Doctor of Philosophy

in

Chemistry

by

Stephanie L. Mora García

Committee in charge:

Professor Vicki H. Grassian, Chair
Professor Todd Martz
Professor Jonathan Slade
Professor Mark Young
Professor Joel Yuen Zhou

2023

The Dissertation of Stephanie L. Mora García is approved,

and it is acceptable in quality and form for publication on microfilm and electronically.

University of California San Diego

2023

DEDICATION

En dedicación a mis padres Carlos Mora Villanueva y Susana García por todo lo que han luchado y trabajado tan duro para darnos a mis hermanos y a mí oportunidades de abrir puertas. Siempre estaré agradecida.

In dedication to my parents Carlos Mora Villanueva and Susana García for everything that you've fought and worked so hard for to give my siblings and I opportunities to open doors. I will forever be grateful.

TABLE OF CONTENTS

LIST OF FIGURES

LIST OF TABLES

ACKNOWLEDGEMENTS

I would like to thank the people who have been mentors and advisors to me in my academic journey. First, a thank you to my Ph.D. advisor, Professor Vicki Grassian. Vicki, thank you for all the scientific guidance you have given me over the past five years. I have grown so much as a scientist because of your advice. But most importantly, thank you for listening to me when I shared my experiences that shaped my graduate school journey. Your support of me as a person and graduate student was key for my success. Next, I want to thank my collaborator, Professor Juan Navea. Juan, I feel lucky that I was able to work with you in all projects because your support both scientifically and personally was both needed and appreciated. Lastly, I want to thank my undergraduate research advisor and now friend, Dr. Greg Barding. Greg, thank you for the intentional help you gave me in undergrad, especially during the grad school application process. I'm not sure I'd be getting a Ph.D., at least not in the timeline that I had, if you didn't give me the help that you did. Also thank you for your unconditional support and being so vocal about it. Your belief in me has always felt like a safety net.

Next I would like to thank my family. First the biggest thank you to my husband and best friend, Eric. Eric thank you for celebrating my wins, holding space for me on bad days, always reminding me of my potential, and especially for going through this process with me. I cannot thank you enough for taking care of some of our life things to fully allow me to immerse myself in the program. I am so lucky that I had you to live my grad school experiences with. I cannot put into words how much I appreciate the role you played in my success. Next I would like to thank my parents. Mom and dad, les agradezco a ambos por todo lo que nos han dado a mí y a mis hermanos. Mi mayor motivación en este proceso fue saber lo duro que han trabajado por todo y

querer mostrarles mi agradecimiento por eso. Gracias por darme espacio para obtener este título incluso cuando no entendían completamente lo que implicaba. Gracias por expresar lo orgullosos que están de mí. A big thank you to my siblings Brian, Mia, and Ana. I hope you see I did this for you too. Brian, thank you for hyping me up and thinking so high of me. That has always kept me strong. Mia, thank you for being the most understanding when I could not be home. I always knew you would understand and that made me feel like you understood my experiences. Ana, thank you for challenging me intellectually. I always told everyone about how important my siblings were to me because I thought of you guys so much while I was away. A thank you to my second family Mimi, Jorge, Johnatan, Jorgito, and Yaella. Mimi and Jorge, thank you for treating me like your daughter and encouraging me as so. Yaella, thank you for expressing how much you look up to me. That has meant so much for me. Jorgito, thank you for trusting my advice. Johnatan for reminding me to be logical in situations. I am so rich because I have so much family backing me.

I would also like to thank my friends that I met in grad school. Starting with my best friend and sister, Deb. Deb, our friendship is the most rewarding personal aspect that I am leaving grad school with. I feel so grateful that I got to go through this experience with you. You made life in grad school so enjoyable both in the office/lab and outside. So much of our lives intertwined in the past five years starting with school. It was great to take all classes with you and be co-outreach coordinators for SWIGS. There is no better working partner than you. On a personal level we also did so much together like workout, share our love for water, experience our highest highs and lowest lows together, and even lived together. I enjoyed every single moment. Thank you for all the fun adventures that we had; I have so many memories with you that I will always hold dearly. Most importantly, thank you for being the friend that I needed these past five years; to say you supported me is an understatement. I am so excited to continue being so close and having new life

experiences together. I would also like to acknowledge Haeun. Getting closer the last two years of grad school was such a gift, especially having your support in my last six months at UCSD; I hope to do the same for you.

I also want to thank the friends in the Grassian Group that played a role in my grad school experience. Thank you to Kyle, my first friend in San Diego, for your friendship and support. Thank you to Ellen and Liora for taking me in when I joined the lab and teaching me the ropes and provided mentorship and friendship. Thank you to Mike, Victor, and Izaac for the fun times and debriefs. And thank you to Karla for a friendship where we understood each other's experiences.

Lastly, I would like to thank my friends from outside of grad school. Karla and Flor, thank you both for your omnipresent friendship. It was great to have your support in so many ways including allowing me to vent about my experiences and working on Zoom when were hundreds of miles apart to work together. Thank you for making my wins feel massive. I always know I can go to you too if I need a reminder of how far I've come. Our experience being from SB and navigating higher education and professional jobs while leaning on each other is such a unique experience that motivates me. Gil, thank you for always reminding me that I can do anything and for making our hangouts a way to forget about school problems for a little while.

Chapter 3, in full, is a reprint of the material published by ACS Earth & Space Chemistry in: Mora García, S. L.; Pandit, S.; Navea, J. G.; Grassian, V. H. Nitrous Acid (HONO) Formation from the Irradiation of Aqueous Nitrate Solutions in the Presence of Marine Chromophoric Dissolved Organic Matter: Comparison to Other Organic Photosensitizers. *ACS Earth. Space. Chem.* **2021**, *5* (11), 3056–3064. The dissertation author was the primary investigator and author of this paper.

Chapter 4 contains unpublished material that has been submitted for publication in: Mora García, S. L.; Gutierrez, I.; Navea, J. G.; Grassian, V. H. Enhanced HONO Formation from Aqueous Nitrate Photochemistry in the Presence of Marine Relevant Organics: A Study of m-DOM Concentration on HONO Kinetics and Yields and the Synergistic Enhancement of Aliphatic and Photosensitizing Compounds in m-DOM. *Submitted*. The dissertation author was the primary investigator and author of this paper.

Chapter 5 contains unpublished material that has been submitted for publication in: Mora García, S. L.; Gutierrez, I.; Navea, J. G.; Grassian, V. H. Enhanced HONO Formation from Aqueous Nitrate Photochemistry in the Presence of Marine Relevant Organics: A Study of m-DOM Concentration on HONO Kinetics and Yields and the Synergistic Enhancement of Aliphatic and Photosensitizing Compounds in m-DOM. *Submitted*. The dissertation author was the primary investigator and author of this paper. Chapter 5 also contains partial published material as found in: Karimova, N.; Alija O; Mora Garcia, S. L.; Grassian, V.; Gerber, R.B.; Navea, J.G. pH Dependence of the Optical Properties of Aqueous 4-Benzoylbenzoic Acid: A Model System for Environmentally Relevant Photosensitizers. *Phys. Chem. Chem. Phys.,* 2023, 25, 17306. The dissertation author was a contributing author of this paper.

VITA

2018 Bachelor of Science in Chemistry, California State Polytechnic University, Pomona

2020 Master of Science in Chemistry, University of California San Diego

2023 Doctor of Philosophy in Chemistry, University of California San Diego

PUBLICATIONS

Mora Garcia, S. L.; Gutierrez, I.; Navea, J.G.; Grassian, V. H. Enhanced HONO formation from aqueous nitrate photochemistry in the presence of marine relevant organics: A study of m-DOM concentration on HONO kinetics and yields and the synergistic enhancement of aliphatic and photosensitizing compounds in m-DOM. *Submitted*.

Karimova, N.; Alija O; **Mora Garcia, S. L.**; Grassian, V.; Gerber, R.B.; Navea, J.G. pH Dependence of the Optical Properties of Aqueous 4-Benzoylbenzoic Acid: A Model System for Environmentally Relevant Photosensitizers. *Phys. Chem. Chem. Phys.,* 2023, 25, 17306.

Mora Garcia, S. L.; Pandit, S.; Navea, J.G.; Grassian, V. H. Nitrous Acid (HONO) Formation from the Irradiation of Aqueous Nitrate Solutions in the Presence of Marine Chromophoric Dissolved Organic Matter: Comparison to Other Organic Photosensitizers. *ACS Earth Sp. Chem*. 2021, 5, 3056-3064.

Pandit, S.; **Mora Garcia, S. L.**; Grassian, V. H. HONO Production from Gypsum Surfaces Following Exposure to NO_2 and HNO_3: Roles of Relative Humidity and Light Source. *Environ. Sci. Technol.* 2021, 55 (14), 9761−9772.

Angle, K. J.;...; **Mora Garcia, S. L.**; ... Acidity across the Interface from the Ocean Surface to Sea Spray Aerosol. *Proc. Natl. Acad. Sci. U.S.A*. 2021, 118 (2), 1−6.

ABSTRACT OF THE DISSERTATION

New Insights into HONO Formation from Nitrate Photochemistry in the Marine Boundary Layer

By

Stephanie L. Mora García

Doctor of Philosophy in Chemistry

University of California San Diego, 2023

Professor Vicki H. Grassian, Chair

This dissertation investigates the formation mechanisms of nitrous acid (HONO) in the atmosphere, a significant source of hydroxyl and nitric oxide radicals upon photodissociation at wavelengths within the solar spectrum. It is pertinent to investigate HONO sources to better understand hydroxyl radical sources as the global budget of hydroxyl radicals, the most potent oxidizer in the atmosphere remains poorly understood. Also, nitric oxide radical sources are crucial to investigate as it is part of the nitrogen oxide atmospheric cycle, impacting photochemical smog

and acid rain. The enhancement of HONO formation in the marine boundary layer from nitrate photochemistry in the presence of marine relevant organics is explored here.

The dissertation presented in this Ph.D. dissertation explores the enhancement of HONO in the marine boundary layer from nitrate photolysis in the presence of marine-relevant organic compounds. The use of marine dissolved organic matter (m-DOM) from the Pacific Ocean, containing aliphatic and chromophoric compounds, serves as a model system to investigate HONO enhancement from both compound types, as both have been found to enhance HONO formation. Molecular proxies, such as ethylene glycol and 4-benzoylbenzoic acid, are also employed to gain mechanistic insights. To measure HONO and nitrogen dioxide (NO_2), an in lab made Incoherent Broadband Cavity Enhanced Absorption Spectrometer (IBBCEAS) was optimized for use. This instrument allows simultaneous detection of trace gases, enabling the investigation of HONO enhancement mechanisms.

The overarching objective of the dissertation is to bridge knowledge gaps regarding the role of marine-relevant organics in enhancing photolytic HONO formation in the marine boundary layer. The dissertation is structured into chapters, covering first the theoretical background, instrumental setup, data analysis, and validation of the IBBCEAS. Also presented are experimental results that reveal m-DOM as the most efficient enhancer of HONO compared to other marine relevant organics, and its concentration dependence is explored. Lastly, the synergistic enhancement of HONO by aliphatic and chromophoric compounds is investigated. The last chapter concludes the dissertation research and proposes future directions.

Chapter 1 Introduction

1.1 HONO in the atmosphere

The formation mechanisms of the atmospheric trace gas nitrous acid (HONO) are studied mainly because it is a significant source of hydroxyl and nitric oxide radicals. Nitrous acid photolyzes at wavelengths within the solar spectrum (300 to 400 nm) leading to hydroxyl and nitric oxide radicals as shown in Equation 1.1.[1–4] The hydroxyl radical (·OH) is a strong oxidizer in the atmosphere, being consider the most potent oxidizer because of its rapid reactions with traces gases and atmospheric aerosols.[5,6] Though the main source of ·OH is ozone photolysis, the known global budget of ·OH is poorly understood due to unknown sources and their significance.[7,8] Similarly, the nitric oxide radical (·NO) is an important product of HONO photolysis because it is part of the nitrogen oxide atmospheric cycle. The main sources of ·NO are natural and anthropogenic combustion processes, but all sources must be well understood as nitric oxide plays a role in creating photochemical smog and acid rain.[6] Therefore, understanding the sources of HONO which leads to such key molecules in tropospheric chemistry is pertinent.

$$HONO + h\nu\ (300 - 400nm) \rightarrow \cdot OH + \cdot NO \qquad Eq.\ 1.1$$

Sources of HONO in the outdoor atmosphere have been extensively researched. Some mechanisms are those leading to HONO in the urban, or polluted, outdoor environment. The nighttime surface mediated hydrolysis of nitrogen dioxide (NO_2) in the presence of adsorbed water was for a long time thought to be the most significant source of HONO in the atmosphere.[9,10] In the urban atmosphere, there are also proposed daytime, or photolytic, reactions leading to HONO

including the photo-enhanced hydrolysis of NO_2 to HONO and the photosensitized reduction of NO_2 on urban grime.[11–14] Forest environments were also studied and the surface mediated reactions of NO_2 hydrolysis and nitric acid (HNO_3) photolysis have been measured to lead to HONO.[15–17] Lastly, direct emissions of HONO from soil bacteria had also been observed and studied.[18] The marine boundary layer (MBL) has only recently began to be investigated as a possible environment where HONO is significantly formed.

The photolysis of HONO occurring within the solar spectrum led to the expectation that any HONO in the MBL would dissociate during the day.[19] However, field studies have observed the highest amounts of HONO during solar noon, beginning the quest to investigate photolytic sources of HONO in the MBL.[20–22] Although some evidence has been found for the photosensitized reduction of NO_2 to HONO, more recently nitrate photolysis leading to HONO has been the agreed upon mechanism. [21–25] Importantly, Ye et al. and Reed et. al. combined field measurements and computational models and found that HONO increases at solar noon at the expense of particulate nitrate, indicating that nitrate photolysis is the most likely source of daytime HONO in the atmosphere.[21,22] These same studies found photolysis rates in the MBL that were up to 300 times higher than that of HNO_3 photolysis with the increase being attributed to the enhanced cross-sections from adsorbed NO_3^-;[21,22,25] but, marine relevant organics may play a role in this increase as well.

The mechanisms of HONO formation from aqueous nitrate photolysis become more complex once factors relevant to the MBL are introduced. Aqueous nitrate photolysis happens at wavelengths (λ) greater than 280 nm leading to two major pathways as shown in Equations 1.2 and 1.3. The first product pathway leads to NO_2^- and $O(^3P)$ (ϕ=0.001), and in the presence of excess protons, NO_2^- forms HONO as shown in Equation 1.4. The other product pathway forms

NO_2 and O^- (ϕ=0.01).[26] The quantum yields for these products inform that observed NO_2 should be 10 times that of NO_2^-; but Scharko et. al. showed that acidic conditions favor the production of HONO which is formed from NO_2^- in acidic environments.[27] This is because the pKa of NO_2^-/HONO is ca. 3 with values being reported from 2.8 to 3.2.[27–29] The speciation diagram of nitrite and nitrous acid is shown in Figure 1.1. This is important to consider in HONO formation in the MBL as sea spray aerosols (SSA) have been found to exist at acidic pH values ranging from 2-4 depending on the size.[30] Another factor to consider relevant to the MBL is the presence of organics. Organic compounds have been found to enhance HONO formation via nitrate photolysis through various mechanisms.[27,31]

$$NO_3^-(aq) + h\nu \rightarrow NO_2^-(aq) + O(^3P) \qquad Eq.\,1.2$$

$$NO_3^-(aq) + h\nu \rightarrow NO_2(g) + O^- \qquad Eq.\,1.3$$

$$NO_2^-(aq) + H^+(aq) \rightarrow HONO(g) \qquad Eq.\,1.4$$

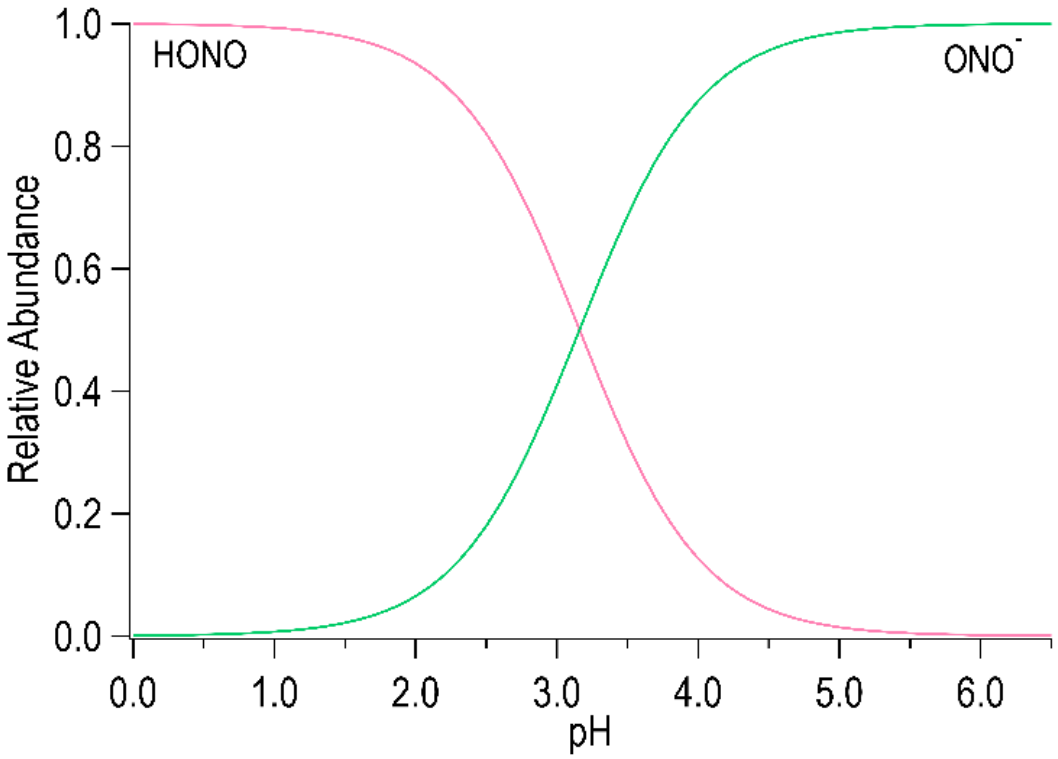

Figure 1.1 A speciation diagram of HONO (pink) and NO_2^- (green) as a function of solution pH.

1.2 Enhancement of HONO from nitrate photolysis in the presence of organics

The presence of organics in aqueous nitrate photolysis studies is of interest in the marine boundary layer because SSA are enriched with organics. The mechanisms leading to HONO in the MBL would occur in aged SSA as nitrate is present from the displacement reaction of NaCl from the ocean by gas-phase HNO_3 from the atmosphere, as shown in Equation 1.5.[32,33] Importantly, SSA have also been found to be enriched with organics, including aliphatic and chromophoric organic compounds[34–38] which are the compound types that have been found to enhance HONO formation in aqueous nitrate photolysis. Scharko et. al. measured an increase in gaseous HONO from the presence of hydroxyl radical scavenging compounds, aliphatics, in irradiated nitrate solutions.[27] More recently, Wang et. al. elucidated the reaction mechanisms that led to the enhancement was due to the formation of superoxide radicals from the reactions of hydroxyl

radicals with the aliphatic compounds. Secondary reaction of the superoxide radical with NO and NO_2, products of nitrate photolysis, lead to an enhanced amount of NO_2^- and in an acidic environment, this led to enhanced HONO observations.[31] Additionally, HONO enhancement from the photosensitized reduction of adsorbed NO_2 on thin films made of humic acid, a complex conglomerate of organic compounds derived from the decomposition of biomass, has also been observed.[39–44] The scope of the work presented in this dissertation is based on the hypothesis that both aliphatic and chromophoric marine relevant organic compounds would enhance HONO in the marine boundary layer.

$$NaCl(aq) + HNO_3(g) \rightarrow NaNO_3(aq) + HCl(aq) \qquad Eq.\,1.5$$

To study the role of marine relevant organic compounds in mechanisms leading to HONO enhancement, marine dissolved organic matter (m-DOM) collected from the Pacific Ocean was used. SSA is enriched in both aliphatic and chromophoric compounds, among other organics, due to bubble bursting mechanisms. [34–36,45] The m-DOM available was sampled during the NSF-CAICE 2019 SeaSCAPE campaign and was found to contain polycyclic, aromatic, and unsaturated compound types.[46,47] Aliphatic and chromophoric compounds can be found in the compound types in the m-DOM sample, making it a beneficial marine relevant organic system to study the possible HONO enhancement in the MBL. To gain mechanistic insight, the enhancement of HONO in the presence of humic acid and molecular proxies of aliphatic and chromophoric compounds was also explored.

Given m-DOM is composed of hundreds of different compounds, if not more, it is difficult to address specific mechanistic questions. Therefore, relatively simple molecules of each

compound type, aliphatic and chromophoric, were chosen. The chemical compounds ethylene glycol (EG) and 4-benzoylbenzoic acid (4-BBA) were used as molecular proxies of the non-light absorbing aliphatic compounds and chromophoric compounds, respectively. By probing the HONO enhancement in the presence of these compounds individually and in mixtures of the two and comparing to the enhancement due to the presence of m-DOM, insight on the mechanisms and significance of each compound should be elucidated. The different organics used in this dissertation research, their general classification, and structure (if available), are shown in Figure 1.2

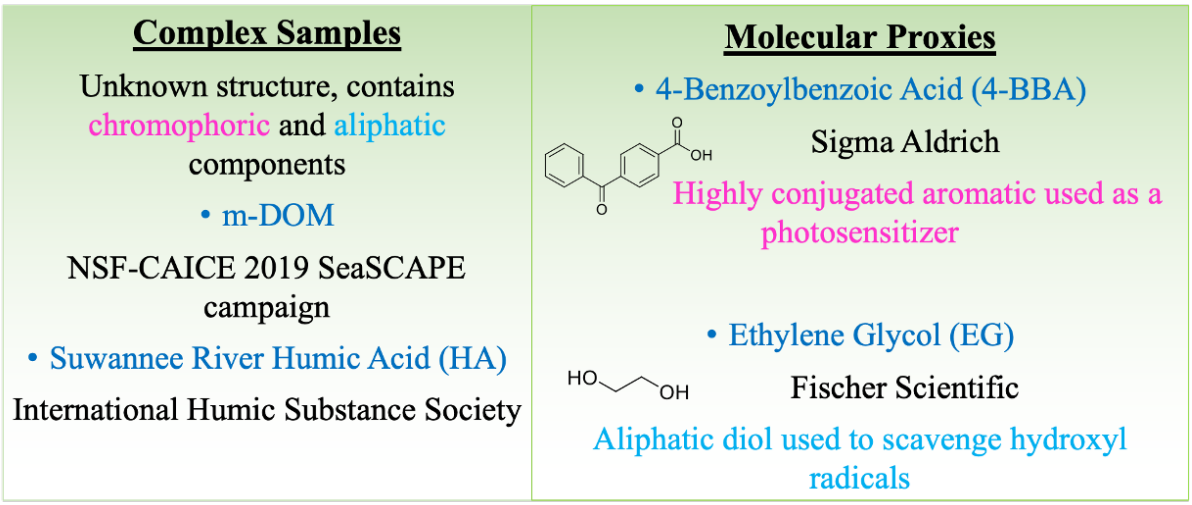

Figure 1.2 A list of the complex organic systems and molecular models used in this project to probe HONO enhancement from the presence of organics in aqueous nitrate photolysis along with a general description of why they were chosen and the structure (if available).

1.3 IBBCEAS to measure HONO and NO_2

To investigate the gaseous HONO formed from the irradiation of aqueous nitrate photolysis in the presence of marine relevant organic compounds, an inhouse made Incoherent Broadband

Cavity Enhanced Absorption Spectrometer (IBBCEAS) was built. A considerable portion of this research project comprised of reconfiguring, optimizing, and measuring HONO for the first time with this instrument. The IBBCEAS was originally designed by Dr. Jonathan Trueblood.[48] The instrument is described in detail in Chapter 2 but briefly, the instrument provides the capability of measuring trace gases in the atmosphere at atmospherically relevant pressures and concentrations.[49,50] It also allows for the simultaneous detection of trace gases without interferences as it is a direct measurement technique that utilizes the differential optical absorption spectroscopy (DOAS) theory to quantify the gases. This type of spectroscopy deconvolutes measured absorption spectra by fitting it to the narrowband (or differential) absorption features of the trace gases of interest.[51] Both HONO and NO_2, a common precursor and side product of HONO forming mechanisms, can be measured with this instrument.[49,50,52–55]

The light source for the in-lab made instrument is a light emitting diode that emits from 360 to 390 nm, a range where both HONO and NO_2 have differential absorption features. The observed HONO absorption spectrum in the range of 360 to 390 nm is due to the transition from the ground state to the first excited electronic state of $A^1A'' \leftarrow X^1A'$ having a broadband slope like shape.[56] The differential features appear as two peaks at 368 nm and 384 nm and are what the experimental data is fit to.[56] The NO_2 transition that is probed is the excitation from the electronic ground state to the first electronic excited state, $A^2B_2 \leftarrow X^2A_1$, appearing as a broadband asymmetrical bell curve with many narrowband spectral features arising from the vibrational transitions between the ground and first excited electronic states.[57,58] The capability of simultaneous HONO and NO_2 measurements of this instrument allows for the investigation of HONO enhancement mechanisms in the marine boundary layer.

1.4 Thesis Objective

The objective of this dissertation project is to fill in the gap in knowledge around how marine relevant organics enhance photolytic HONO formation in the marine boundary layer to better understand its significance as a source of HONO in the troposphere. An in-lab made spectroscopic instrument was optimized for use in the studies probing the mechanistic role that m-DOM, specifically from the non-light absorbing aliphatic compounds and the light absorbing chromophores found in m-DOM, has on HONO from nitrate photochemistry.

Chapter 2 describes the theory, instrumental setup, and data analysis for the in-lab made Incoherent Broadband Cavity Enhanced Absorption Spectrometer used to measure HONO and NO_2. It also covers the usage of UV-Vis absorption spectroscopy used as a complementary method to study the interaction of nitrate and the chosen organics (m-DOM, EG, and 4-BBA) with the solar simulator light the solutions are exposed to. Proton nuclear magnetic spectroscopy is also discussed as it was used to probe the speciation of 4-BBA in atmospheric conditions. Lastly, the chapter also discusses the chemicals used in the studies along with sample preparation.

Chapter 3 compares the HONO enhancement efficiency due to the presence of m-DOM (0.10 mg/mL) , humic acid (0.10 mg/mL), EG (0.44 mM) , and 4-BBA (0.44 mM) in the presence of irradiated aqueous nitrate solutions (100 mM) acidified to pH of 2.0 with hydrochloric acid. For the first time, m-DOM was found to be the most efficient at enhancing HONO. The findings from the solutions containing EG and 4-BBA, along with other published studies,[26,31,59] informed on the mechanistic manner that m-DOM enhances HONO formation and so a mechanistic pathway was proposed.

Chapter 4 investigates the impact of m-DOM concentration on HONO enhancement when present in irradiated nitrate solutions. It was found that HONO enhancement has a non-linear

dependence on m-DOM concentration where the enhancement increases from 0 to 0.10 mg/mL of m-DOM and decreases after that point, up to the mass concentration of 0.60 mg/mL which was the highest concentration tested. It was determined that the surface-active parts of m-DOM lead to surface coverage on the solutions introducing a physical barrier for HONO to partition out of the solution; a factor that would be significant in SSA.

Chapter 5 explores whether the HONO enhancement due to the aliphatic, non-light absorbing, compounds and the chromophoric, light absorbing, compounds in m-DOM is additive or synergistic. Mixtures of EG and 4-BBA were added to nitrate solutions and the HONO observed was compared to solutions containing only EG or 4-BBA and m-DOM. The experimental amounts of HONO from the solutions containing mixtures of EG and 4-BBA were greater than solutions only containing one of the organics at the same total organic concentration and were similar to the amounts produced when m-DOM was present. Also, the mixtures led to more HONO compared to simulated amounts of what the HONO concentration would be if the HONO resulted from each compound was linearly additive. Both findings suggest that the aliphatic and chromophoric compounds in m-DOM synergistically enhance HONO formation from nitrate photolysis. A mechanism for this synergism is proposed here for the first time.

Chapter 6 summarizes the findings from this Ph.D. dissertation research and suggests areas of future study including expanding the types of m-DOM samples investigated to determine the variability that may occur in these different samples. To further the investigation of mechanistic information, surface active compounds and nitrogen containing chromophoric compounds should also be studied as molecular proxies for m-DOM.

1.5 Bibliography

(1) Calvert, J. G.; Yarwood, G.; Dunker, A. M. An Evaluation of the Mechanism of Nitrous Acid Formation in the Urban Atmosphere. *Res. Chem. Intermed.* **1994**, 20, 463-502.

(2) Perner, D.; Platt, U. Detection of Nitrous Acid in the Atmosphere by Differential Optical Absorption. *Geophys. Res. Lett.* **1979**, *6* (12), 917–920.

(3) Platt, U. The Origin of Nitrous and Nitric Acid in the Atmosphere. In *Chemistry of Multiphase Atmospheric Systems*; Wolfgang Jaeschke, Ed.; Springer Berlin Heidelberg: Berlin, **1986**; pp 299–319.

(4) Alicke, B.; Geyer, A.; Hofzumahaus, A.; Holland, F.; Konrad, S.; Pätz, H. W.; Schäfer, J.; Stutz, J.; Volz-Thomas, A.; Platt, U. OH Formation by HONO Photolysis during the BERLIOZ Experiment. *J. Geophys. Res. D: Atmos.* **2003**, *108* (4), 3–1.

(5) Crutzen, P. J.; Zimmermann, P. H. The Changing Photochemistry of the Troposphere. *Tellus A* **1991**, *43*, 136–151.

(6) John H. Seinfeld; Spyros N. Pandis. *Atmospheric Chemistry and Physics: From Air Pollution to Climate Change*, Third.; John Wiley & Sons, Inc. : Haboken, New Jersey, **2016**.

(7) Pimlott, M. A.; Pope, R. J.; Kerridge, B. J.; Latter, B. G.; Knappett, D. S.; Heard, D. E.; Ventress, L. J.; Siddans, R.; Feng, W.; Chipperfield, M. P. Investigating the Global OH Radical Distribution Using Steady-State Approximations and Satellite Data. *Atmos. Chem. Phys.* **2022**, *22* (16), 10467–10488.

(8) Murray, L. T.; Fiore, A. M.; Shindell, D. T.; Naik, V.; Horowitz, L. W. Large Uncertainties in Global Hydroxyl Projections Tied to Fate of Reactive Nitrogen and Carbon. *Proc. Natl. Acad. Sci. USA* **2021**, *118* (43), 1–6.

(9) Pitts, J. N.; Sanhueza, E.; Atkinson, R.; Carter, W. P. L.; Winer, A. M.; Harris, G. W.; Plum, C. N. An Investigation of the Dark Formation of Nitrous Acid in Environmental Chambers. *Int. J. Chem. Kinet.* **1984**, *16* (7), 919–939.

(10) Finlayson-Pitts, B. J.; Wingen, L. M.; Sumner, A. L.; Syomin, D.; Ramazan, K. A. The Heterogeneous Hydrolysis of NO_2 in Laboratory Systems and in Outdoor and Indoor Atmospheres: An Integrated Mechanism. *Phys. Chem. Chem. Phys.* **2003**, *5* (2), 223–242.

(11) Ramazan, K. A.; Syomin, D.; Finlayson-Pitts, B. J. The Photochemical Production of HONO during the Heterogeneous Hydrolysis of NO_2. *Phys. Chem. Chem. Phys.* **2004**, *6*, 3836–3843.

(12) Baergen, A. M.; Donaldson, D. J. Formation of Reactive Nitrogen Oxides from Urban Grime Photochemistry. *Atmos. Chem. Phys.* **2016**, *16* (10), 6355–6363.

(13) Baergen, A. M.; Donaldson, D. J. Photochemical Renoxification of Nitric Acid on Real Urban Grime. *Environ. Sci. Technol.* **2013**, *47* (2), 815–820.

(14) Liu, J.; Li, S.; Mekic, M.; Jiang, H.; Zhou, W.; Loisel, G.; Song, W.; Wang, X.; Gligorovski, S. Photoenhanced Uptake of NO_2 and HONO Formation on Real Urban Grime. *Environ. Sci. Technol. Lett.* **2019**, *6* (7), 413–417.

(15) Zhang, N.; Zhou, X.; Shepson, P. B.; Gao, H.; Alaghmand, M.; Stirm, B. Aircraft Measurement of HONO Vertical Profiles over a Forested Region. *Geophys. Res. Lett.* **2009**, *36* (15), 1-5.

(16) Zhou, X.; Zhang, N.; Teravest, M.; Tang, D.; Hou, J.; Bertman, S.; Alaghmand, M.; Shepson, P. B.; Carroll, M. A.; Griffith, S.; Dusanter, S.; Stevens, P. S. Nitric Acid Photolysis on Forest Canopy Surface as a Source for Tropospheric Nitrous Acid. *Nat. Geosci.* **2011**, *4* (7), 440–443.

(17) Sörgel, M.; Trebs, I.; Serafimovich, A.; Moravek, A.; Held, A.; Zetzsch, C. Simultaneous HONO Measurements in and above a Forest Canopy: Influence of Turbulent Exchange on Mixing Ratio Differences. *Atmos. Chem. Phys.* **2011**, *11*, 841–855.

(18) Oswald, R.; Behrendt, T.; Ermel, M.; Wu, D.; Su, H.; Cheng, Y.; Breuninger, C.; Moravek, A.; Mougin, E.; Delon, C.; Loubet, B.; Pommerening-Röser, A.; Sörgel, M.; Pöschl, U.; Hoffmann, T.; Andreae, M. O.; Meixner, F. X.; Trebs, I. HONO Emissions from Soil Bacteria as a Major Source of Atmospheric Reactive Nitrogen. *Science* **2013**, *341* (6151), 1233–1235.

(19) Wojtal, P.; Halla, J. D.; McLaren, R. Pseudo Steady States of HONO Measured in the Nocturnal Marine Boundary Layer: A Conceptual Model for HONO Formation on Aqueous Surfaces. *Atmos. Chem. Phys.* **2011**, *11* (7), 3243–3261.

(20) Wen, L.; Chen, T.; Zheng, P.; Wu, L.; Wang, X.; Mellouki, A.; Xue, L.; Wang, W. Nitrous Acid in Marine Boundary Layer over Eastern Bohai Sea, China: Characteristics, Sources, and Implications. *Sci. Total Environ.* **2019**, *670*, 282–291.

(21) Ye, C.; Zhou, X.; Pu, D.; Stutz, J.; Festa, J.; Spolaor, M.; Tsai, C.; Cantrell, C.; Mauldin, R. L.; Campos, T.; Weinheimer, A.; Hornbrook, R. S.; Apel, E. C.; Guenther, A.; Kaser, L.; Yuan, B.; Karl, T.; Haggerty, J.; Hall, S.; Ullmann, K.; Smith, J. N.; Ortega, J.; Knote, C. Rapid Cycling of Reactive Nitrogen in the Marine Boundary Layer. *Nature* **2016**, *532* (7600), 489–491.

(22) Reed, C.; Evans, M. J.; Crilley, L. R.; Bloss, W. J.; Sherwen, T.; Read, K. A.; Lee, J. D.; Carpenter, L. J. Evidence for Renoxification in the Tropical Marine Boundary Layer. *Atmos. Chem. Phys.* **2017**, *17* (6), 4081–4092.

(23) Ye, C.; Zhang, N.; Gao, H.; Zhou, X. Photolysis of Particulate Nitrate as a Source of HONO and NO_x. *Environ. Sci. Technol.* **2017**, *51* (12), 6849–6856.

(24) Kasibhatla, P.; Sherwen, T.; Evans, M. J.; Carpenter, L. J.; Reed, C.; Alexander, B.; Chen, Q.; Sulprizio, M. P.; Lee, J. D.; Read, K. A.; Bloss, W.; Crilley, L. R.; Keene, W. C.; Pszenny, A. A. P.; Hodzic, A. Global Impact of Nitrate Photolysis in Sea-Salt Aerosol on NO_x, OH, and O_3 in the Marine Boundary Layer. *Atmos. Chem. Phys.* **2018**, *18* (15), 11185–11203.

(25) Andersen, S. T.; Carpenter, L. J.; Reed, C.; Lee, J. D.; Chance, R.; Sherwen, T.; Vaughan, A. R.; Stewart, J.; Edwards, P. M.; Bloss, W. J.; Sommariva, R.; Crilley, L. R.; Nott, G. J.; Neves, L.; Read, K.; Heard, D. E.; Seakins, P. W.; Whalley, L. K.; Boustead, G. A.; Fleming, L. T.; Stone, D.; Fomba, K. W. Extensive Field Evidence for the Release of HONO from the Photolysis of Nitrate Aerosols. *Sci. Adv.* **2023**, *9* (3), 1–10.

(26) Mack, J.; Bolton, J. R. Photochemistry of Nitrite and Nitrate in Aqueous Solution: A Review. *J. Photochem. Photobiol. A Chem.* **1999**, *128*, 1–13.

(27) Scharko, N. K.; Berke, A. E.; Raff, J. D. Release of Nitrous Acid and Nitrogen Dioxide from Nitrate Photolysis in Acidic Aqueous Solutions. *Environ. Sci. Technol.* **2014**, *48* (20), 11991–12001.

(28) Riordan, E.; Minogue, N.; Healy, D.; O'Driscoll, P.; Sodeau, J. R. Spectroscopic and Optimization Modeling Study of Nitrous Acid in Aqueous Solution. *J. Phys. Chem. A* **2005**, *109* (5), 779–786.

(29) Anastasio, C.; Liang, C. Photochemistry of Nitrous Acid (HONO) and Nitrous Acidium Ion (H_2ONO^+) in Aqueous Solution and Ice. *Environ. Sci. Technol.* **2009**, *43* (4), 1108–1114.

(30) Angle, K. J.; Crocker, D. R.; Simpson, R. M. C.; Mayer, K. J.; Garofalo, L. A.; Moore, A. N.; Mora Garcia, S. L.; Or, V. W.; Srinivasan, S.; Farhan, M.; Sauer, J. S.; Lee, C.; Pothier, M. A.; Farmer, D. K.; Martz, T. R.; Bertram, T. H.; Cappa, C. D.; Prather, K. A.; Grassian, V. H. Acidity across the Interface from the Ocean Surface to Sea Spray Aerosol. *Proc. Natl. Acad. Sci. USA* **2021**, *118* (2), 1–6.

(31) Wang, X.; Dalton, E. Z.; Payne, Z. C.; Perrier, S.; Riva, M.; Raff, J. D.; George, C. Superoxide and Nitrous Acid Production from Nitrate Photolysis Is Enhanced by Dissolved Aliphatic Organic Matter. *Environ. Sci. Technol. Lett.* **2021**, *8* (1), 53–58.

(32) Ault, A. P.; Guasco, T. L.; Ryder, O. S.; Baltrusaitis, J.; Cuadra-Rodriguez, L. A.; Collins, D. B.; Ruppel, M. J.; Bertram, T. H.; Prather, K. A.; Grassian, V. H. Inside versus Outside: Ion Redistribution in Nitric Acid Reacted Sea Spray Aerosol Particles as Determined by Single Particle Analysis. *J. Am. Chem. Soc.* **2013**, *135* (39), 14528–14531.

(33) Hughes, L. S.; Allen, J. O.; Bhave, P.; Kleeman, M. J.; Cass, G. R.; Liu, D. Y.; Fergenson, D. P.; Morrical, B. D.; Prather, K. A. Evolution of Atmospheric Particles along Trajectories Crossing the Los Angeles Basin. *Environ. Sci. Technol.* **2000**, *34* (15), 3058–3068.

(34) Quinn, P. K.; Collins, D. B.; Grassian, V. H.; Prather, K. A.; Bates, T. S. Chemistry and Related Properties of Freshly Emitted Sea Spray Aerosol. *Chem. Rev.*, **2015**, 115, 4383–4399.

(35) Bertram, T. H.; Cochran, R. E.; Grassian, V. H.; Stone, E. A. Sea Spray Aerosol Chemical Composition: Elemental and Molecular Mimics for Laboratory Studies of Heterogeneous and Multiphase Reactions. *Chem. Soc. Rev.* **2018**, *47* (7), 2374–2400.

(36) Cochran, R. E.; Laskina, O.; Jayarathne, T.; Laskin, A.; Laskin, J.; Lin, P.; Sultana, C.; Lee, C.; Moore, K. A.; Cappa, C. D.; Bertram, T. H.; Prather, K. A.; Grassian, V. H.; Stone, E. A. Analysis of Organic Anionic Surfactants in Fine and Coarse Fractions of Freshly Emitted Sea Spray Aerosol. *Environ. Sci. Technol.* **2016**, *50* (5), 2477–2486.

(37) Ault, A. P.; Moffet, R. C.; Baltrusaitis, J.; Collins, D. B.; Ruppel, M. J.; Cuadra-Rodriguez, L. A.; Zhao, D.; Guasco, T. L.; Ebben, C. J.; Geiger, F. M.; Bertram, T. H.; Prather, K. A.; Grassian, V. H. Size-Dependent Changes in Sea Spray Aerosol Composition and Properties with Different Seawater Conditions. *Environ. Sci. Technol.* **2013**, *47* (11), 5603–5612.

(38) Wang, X.; Sultana, C. M.; Trueblood, J.; Hill, T. C. J.; Malfatti, F.; Lee, C.; Laskina, O.; Moore, K. A.; Beall, C. M.; McCluskey, C. S.; Cornwell, G. C.; Zhou, Y.; Cox, J. L.; Pendergraft, M. A.; Santander, M. V.; Bertram, T. H.; Cappa, C. D.; Azam, F.; DeMott, P. J.; Grassian, V. H.; Prather, K. A. Microbial Control of Sea Spray Aerosol Composition: A Tale of Two Blooms. *ACS Cent. Sci.* **2015**, *1* (3), 124–131.

(39) Stemmler, K.; Ndour, M.; Kleffmann, J.; D'anna, B.; George, C. Light Induced Conversion of Nitrogen Dioxide into Nitrous Acid on Submicron Humic Acid Aerosol. *Atmos. Chem. Phys.* **2007**, *7* (16), 4248-4248.

(40) Yang, W.; Han, C.; Yang, H.; Xue, X. Significant HONO Formation by the Photolysis of Nitrates in the Presence of Humic Acids. *Environ. Pollut.* **2018**, *243*, 679–686.

(41) Stemmler, K.; Ammann, M.; Donders, C.; Kleffmann, J.; George, C. Photosensitized Reduction of Nitrogen Dioxide on Humic Acid as a Source of Nitrous Acid. *Nature* **2006**, *440* (7081), 195–198.

(42) Han, C.; Yang, W.; Wu, Q.; Yang, H.; Xue, X. Key Role of pH in the Photochemical Conversion of NO_2 to HONO on Humic Acid. *Atmos. Environ.* **2016**, *142* (2), 296–302.

(43) Han, C.; Yang, W.; Wu, Q.; Yang, H.; Xue, X. Heterogeneous Photochemical Conversion of NO_2 to HONO on the Humic Acid Surface under Simulated Sunlight. *Environ. Sci. Technol.* **2016**, *50* (10), 5017–5023.

(44) Ricker, H. M.; Leonardi, A.; Navea, J. G. Reduction and Photoreduction of NO_2 in Humic Acid Films as a Source of HONO, ClNO, N_2O, NO_X, and Organic Nitrogen. *ACS Earth Space Chem.* **2022**, *6* (12), 3066–3077.

(45) Santander, M. V.; Malfatti, F.; Pendergraft, M. A.; Morris, C.; Kimble, K.; Mitts, B. A.; Wang, X.; Mayer, K. J.; Sauer, J.; Lee, C.; Prather, K. A. Bacterial Control of Marine Humic-Like Substance Production, Composition, Size, and Transfer to Sea Spray Aerosols During Phytoplankton Blooms. *J. Geophys. Res.: Atmos.* **2023**, *128* (4), 1–14.

(46) Sauer, J. S.; Mayer, K. J.; Lee, C.; Alves, M. R.; Amiri, S.; Bahaveolos, C.; Barnes, E. B.; Crocker, D. R.; Dinasquet, J.; Garofalo, L. A.; Kaluarachchi, C. P.; Dang, D.; Kilgour, D.; Mael, L.; Mitts, B. A.; Moon, D. R.; Morris, C. K.; Moore, A. N.; Ni, C.-M.; Pendergraft, M. A.; Petras, D.; Simpson, R.; Smith, S.; Tumminello, P. R.; Walker, J. L.; DeMott, P. J.; Farmer, D. K.; Goldstein, A. H.; Grassian, V. H.; Jaffe, J. S.; Malfatti, F.; Martz, T. R.; Slade, J.; Tivanski, A. V.; Bertram, T. H.; Cappa, C. D.; Prather, K. A. The Sea Spray Chemistry and Particle Evolution Study (SeaSCAPE): Overview and Experimental Methods. *Environ. Sci.: Process. Impacts.* **2022**, *24*, 290–315.

(47) Alves, M. R.; Coward, E. K.; Gonzales, D.; Sauer, J. S.; Mayer, K. J.; Prather, K. A.; Grassian, V. H. Changes in Light Absorption and Composition of Chromophoric Marine-

Dissolved Organic Matter across a Microbial Bloom. *Environ. Sci.: Process. Impacts* **2022**, *24* (10), 1923–1933.

(48) Trueblood, J. V. Spectroscopic Investigations into Nascent and Aged Sea Spray Aerosol, University of California San Diego, 2018.

(49) Gherman, T.; Venables, D. S.; Vaughan, S.; Orphal, J.; Ruth, A. A. Incoherent Broadband Cavity-Enhanced Absorption Spectroscopy in the near-Ultraviolet: Application to HONO and NO_2. *Environ. Sci. Technol.* **2008**, *42* (3), 890–895.

(50) Ling, L.; Xie, P.; Qin, M.; Hu, R.; Zheng, N.; Si, F. Simultaneous Measurements of Atmospheric NO_2 and HONO Using IBBCEAS with a Near-Ultraviolet LED. *Proc. of SPIE* **2012**, *8563*.

(51) Platt, Ulrich.; Stutz, J. *Differential Optical Absorption Spectroscopy*; Springer, **2008**.

(52) Wu, T.; Zha, Q.; Chen, W.; Xu, Z.; Wang, T.; He, X. Development and Deployment of a Cavity Enhanced UV-LED Spectrometer for Measurements of Atmospheric HONO and NO_2 in Hong Kong. *Atmos. Environ.* **2014**, *95* (2), 544–551.

(53) Wu, T.; Chen, W.; Fertein, E.; Cazier, F.; Dewaele, D.; Gao, X. Development of an Open-Path Incoherent Broadband Cavity-Enhanced Spectroscopy Based Instrument for Simultaneous Measurement of HONO and NO_2 in Ambient Air. *Appl. Phys. B* **2012**, *106* (2), 501–509.

(54) Yi, H.; Wu, T.; Wang, G.; Zhao, W.; Fertein, E.; Coeur, C.; Gao, X.; Zhang, W.; Chen, W. Sensing Atmospheric Reactive Species Using Light Emitting Diode by Incoherent Broadband Cavity Enhanced Absorption Spectroscopy. *Opt. Express.* **2016**, *24* (10), A781.

(55) Tang, K.; Qin, M.; Duan, J.; Fang, W.; Meng, F.; Liang, S.; Xie, P.; Liu, J.; Liu, W.; Xue, C.; Mu, Y. A Dual Dynamic Chamber System Based on IBBCEAS for Measuring Fluxes of Nitrous Acid in Agricultural Fields in the North China Plain. *Atmo.s Environ.* **2019**, *196*, 10–19.

(56) Bongartz, A.; Kames, J.; Welter, F.; Schurath, U. Near-UV Absorption Cross Sections and Trans/Cis Equilibrium of Nitrous Acid. *J. Phys. Chem.* **1991**, *95* (3), 1076–1082.

(57) Volkers, E. A.; Koudijzer, M. C.; Vredenborg, A.; Bulthuis, J.; Stolte, S.; Linnartz, H.; Jost, R. The A^2B_2-X^2A_1 Electronic Transition of $^{15}NO_2$: A Rovibronic Survey Covering 14300 - 18000 cm^{-1}. *J. Mol. Spectrosc.* **2006**, *235* (1), 1–17.

(58) Kirmse, B.; Delon, A.; Jost, R. NO_2 Absorption Cross Section and Its Temperature Dependence. *J. Geophys. Res.: Atmos.* **1997**, *102* (13), 16089–16098.

(59) McKay, G.; Rosario-Ortiz, F. L. Temperature Dependence of the Photochemical Formation of Hydroxyl Radical from Dissolved Organic Matter. *Environ. Sci. Technol.* **2015**, *49* (7), 4147–4154.

Chapter 2 Experimental Methods

2.1 Solution Preparation

Aqueous solutions prepared for experiments discussed in this thesis utilized different chemicals and samples. These chemicals and samples, along with their sources, are listed in Table 2.1. Most of the chemicals are commercially available with the exception of the marine dissolved organic matter (m-DOM). The source of the m-DOM sample used in all of these studies was from the NSF – 2019 SeaSCAPE Campaign. Details of this campaign as well as how the m-DOM sample from Pacific Ocean water was collected, concentrated and characterized have been described in detail in two publications. [1,2]

Table 2.1 Chemicals used and their sources.

Chemical and Acronym	CAS No.	Supplier
sodium nitrate $NaNO_3$	7631-99-4	Sigma -Aldrich
marine dissolved organic matter m-DOM	n.a.*	Pacific Ocean from NSF-2019 SeaSCAPE Campaign[1,2]
4-benzoylbenzoic acid 4-BBA	611-95-0	Sigma-Aldrich
ethylene glycol EG	107-21-1	Fisher Chemicals
hydrochloric acid HCl	7647-01-0	Fisher Chemicals
sodium hydroxide NaOH	1310-73-2	Fisher Chemicals
Deuterium Oxide D_2O	7789-20-0	Sigma-Aldrich
trimethylsilylpropanesulfonate DSS	2039-96-5	Sigma-Aldrich

*n.a. – not applicable

The solutions prepared for IBBCEAS and UV-Vis spectroscopy experiments were similar. Stock aqueous solutions of the organic compounds were first made. For m-DOM, a 0.60 mg/mL stock solution was made by dissolving a known mass of solid m-DOM in Milli-Q (MQ) water to achieve the desired concentration. For 4-BBA, a 0.5 mM 4-BBA stock solution was made by adding solid 4-BBA to MQ water and sonicating for 48 hours to dissolve the solid. For EG solutions, a 0.5 mM EG stock solution was made by adding drops of liquid EG into a vial and then capping the vial to minimize evaporation. MQ water was then added to achieve the desired concentration. To prepare different lower concentration organic solutions containing sodium nitrate, the stock solutions were diluted and solid $NaNO_3$ was added to prepare 100 mM $NaNO_3$ solutions. These solutions were acidified with HCl (0.5 M solution) dropwise until the desired pH of 2.0 was reached. The volumes used of the sodium nitrate and organics were below the total volume so that the acid could be added and, depending on the total volume, more MQ water was added if needed to reach the final total volume.

Solutions prepared for proton nuclear magnetic resonance, ^{1}H-NMR, were made slightly differently. For NMR experiments, a 110 μM stock solution of 4-BBA was prepared in a 10% D_2O solution containing 5 μM DSS. From this stock, pH of each solution was adjusted by adding 0.5 M HCl or 0.5 M NaOH as needed. In order to reach a final concentration of 100 μM 4-BBA additional MQ water was added. The final solution pH used in these studies were 1.0, 2.0, 3.0, 3.5, 4.0, 5.0, 6.0, and 7.0 ($\pm$ 0.2).

2.2 Incoherent Broadband Cavity Enhanced Absorption Spectroscopy

The gas-phase concentrations of HONO and NO_2 were determined using Incoherent Broadband Cavity Enhanced Absorption Spectroscopy (IBBCEAS); a homebuilt spectrometer was designed specifically for these measurements. Before a full description of the instrument is given, some of the theory and background is first discussed below.

2.2.1 Theory and Background

Incoherent Broadband Cavity Enhanced Absorption Spectroscopy (IBBCEAS) is a spectroscopic method used in atmospheric chemistry that allows for the direct and simultaneous measurement of multiple trace gases at atmospherically relevant pressures and concentrations.[3–8] This method is a direct spectroscopic method because the gaseous sample does not have to be manipulated to detect the trace gas in question such as other spectrophotometric methods where the sample must be converted from the original gaseous molecule into a solute in a solution different from the starting composition. For HONO, long optical path absorption spectrophotometry and NO_x chemiluminescence analyzers are often used but both require HONO to be converted to a detectable analyte; this need for conversion introduces avenues of interferences impeding true HONO concentration measurements.[9,10] The instrument is kept at ambient pressure to ensure atmospherically relevant pressures. The employment of highly reflective mirrors at each end of the instrument, guiding the light back and forth, allows for the effective pathlength of the instrument to be in the order of kilometers. Because this is an application of the Beer-Lambert Law (Equation 2.1), the larger pathlength makes it so that absorbance of species can occur at lower concentrations of trace gases in the atmosphere which can be in the range of low ppt to low ppb

for oxides of nitrogen depending on the environment.[11] The simultaneous analyte measurement capabilities arises from the employment of Differential Optical Absorption Spectroscopy (DOAS).

The DOAS method, as described by Platt and Stutz,[12] involves using only the narrowband, or differential, absorption features of absorbing molecules to both differentiate between different absorbers of interest as well as avoid attributing light extinction from scattering due to atmospheric particles and molecules. The experimental absorption spectra are deconvoluted and fitted to only the narrow-band absorption features of the analytes of interest as these are unique and allow for fitting to reference spectra to a high degree of confidence. In the atmosphere, the extinction of a light path due to Mie and Rayleigh scattering due to aerosols and air molecules must also be considered; but, because this extinction of light only causes broadband features, it can be separated from the and narrowband features and does not cause interferences in the absorber measurements.[12] With this being accounted for, the Beer-Lambert law can be employed to relate a measured spectrum to the concentration of the species of interest. In Equation 2.1, the intensity of light after interacting through the absorbing medium, $I(\lambda,L)$, is equal to the incident light, $I_0(\lambda,L)$, multiplied by the exponential of the negative product of the absorption coefficient, $\varepsilon(\lambda)$, and the passage length, L.

$$I(\lambda, \mathrm{L}) = I_0(\lambda, \mathrm{L}) \times \exp(-(L \times \varepsilon(\lambda))) \qquad Eq.\,2.1$$

Contributing to the absorption coefficient, $\varepsilon(\lambda)$, is absorption due to the molecular species of interest $\varepsilon_s(\lambda)$ as well as loss of light not due to the atmospheric scattering mechanisms Mie $\varepsilon_{Mie}(\lambda)$ and Rayleigh scattering $\varepsilon_{Ray}(\lambda)$ therefore, Equation 2.1 can be rewritten as 2.2 with the sum of these components:

$$I(\lambda, \mathrm{L}) = I_0(\lambda, \mathrm{L}) \times \exp\left(-\left(\mathrm{L} \times \left(\varepsilon_s(\lambda) + \varepsilon_{Mie}(\lambda) + \varepsilon_{Ray}(\lambda)\right)\right)\right) \qquad Eq.\ 2.2$$

For the absorbing species, this can be rewritten in terms of concentration because the absorption coefficient for an absorbing species is the product of the wavelength dependent absorption cross-section $\sigma_s(\lambda)$ and the concentration of the absorber c_s.

$$\varepsilon_s(\lambda) = \sigma_s(\lambda) \times \mathrm{c}_s \qquad Eq.\ 2.3$$

Rewriting Equation 2.2 to include Equation 2.3 yields:

$$I(\lambda, \mathrm{L}) = I_0(\lambda, \mathrm{L}) \times \exp\left(-\left(\mathrm{L} \times \left(\left(\sigma_s(\lambda) \times \mathrm{c}_s\right) + \varepsilon_{Mie}(\lambda) + \varepsilon_{Ray}(\lambda)\right)\right)\right) \qquad Eq.\ 2.4$$

The absorption cross-section of an absorbing species *s* can be separated into the narrowband/differential $\sigma'_s(\lambda)$ and broadband $\sigma_s^b(\lambda)$ absorption cross-sections as shown in Equation 2.5.

$$\sigma_s(\lambda) = \sigma'_s(\lambda) + \sigma_s^b(\lambda) \qquad Eq.\ 2.5$$

Substituting Equation 2.5 into 2.4 yields Equation 2.6 below.

$$I(\lambda, \mathrm{L}) = I_0(\lambda, \mathrm{L}) \times \exp\left(-\left(\mathrm{L} \times \left(\left(\mathrm{c}_s \times \left(\sigma'_s(\lambda) + \sigma_s^b(\lambda)\right) + \varepsilon_{Mie}(\lambda) + \varepsilon_{Ray}(\lambda)\right)\right)\right) \qquad Eq.\ 2.6$$

To account for the changes in light intensity due to the differential molecular absorption features of the species of interest only, broadband cross-sections including the broadband absorption features of species *s*, Mie scattering, and Rayleigh scattering are removed as shown in Equation 2.7. How this is exactly done in the data analysis is discussed in section 2.2.4.

$$I(\lambda, \mathrm{L}) = I_0(\lambda, \mathrm{L}) \times \exp(-(L \times c_s \times \sigma'_s(\lambda))) \qquad Eq.\,2.7$$

To simplify, the optical density (OD), defined as the natural log of the transmitted light over the incident light, is used:

$$OD(\lambda, \mathrm{L}) = ln\frac{I(\lambda, \mathrm{L})}{I_0(\lambda, \mathrm{L})} = (L \times c_s \times \sigma'_s(\lambda)) \qquad Eq.\,2.8$$

Finally, concentration in molecules/cm^3 is calculated with Equation 2.9 where the transmitted light is the spectrum taken with the absorbing species in the cavity, the incident light is a spectrum taken when the cavity is empty, L is light's passage length, and $\sigma'_s(\lambda)$ is the cross-section of species *s* taken from literature with a high bandpass filter applied to only include narrowband features.

$$\mathrm{c}_s = \frac{OD(\lambda, \mathrm{L})}{\mathrm{L} \times \sigma'_s(\lambda)} \qquad Eq.\,2.9$$

This method was employed to measure HONO and NO_2 simultaneously as HONO is the main molecule of interest but NO_2, which absorbs in the same wavelength region, can be a precursor of HONO in the surface adsorbed hydrolysis of NO_2, the photosensitized hydrolysis of NO_2, and forms as a product during nitrate photolysis.[13–15] This method works for both molecules within the region of 360 – 390 nm because both HONO and NO_2 have differential absorption features as shown in Figure 2.1. A list of common trace gases, including HONO and NO_2, and where they absorb in the electromagnetic spectrum are shown in Figure 2.1, which is reprinted from Platt and Stutz.[12]

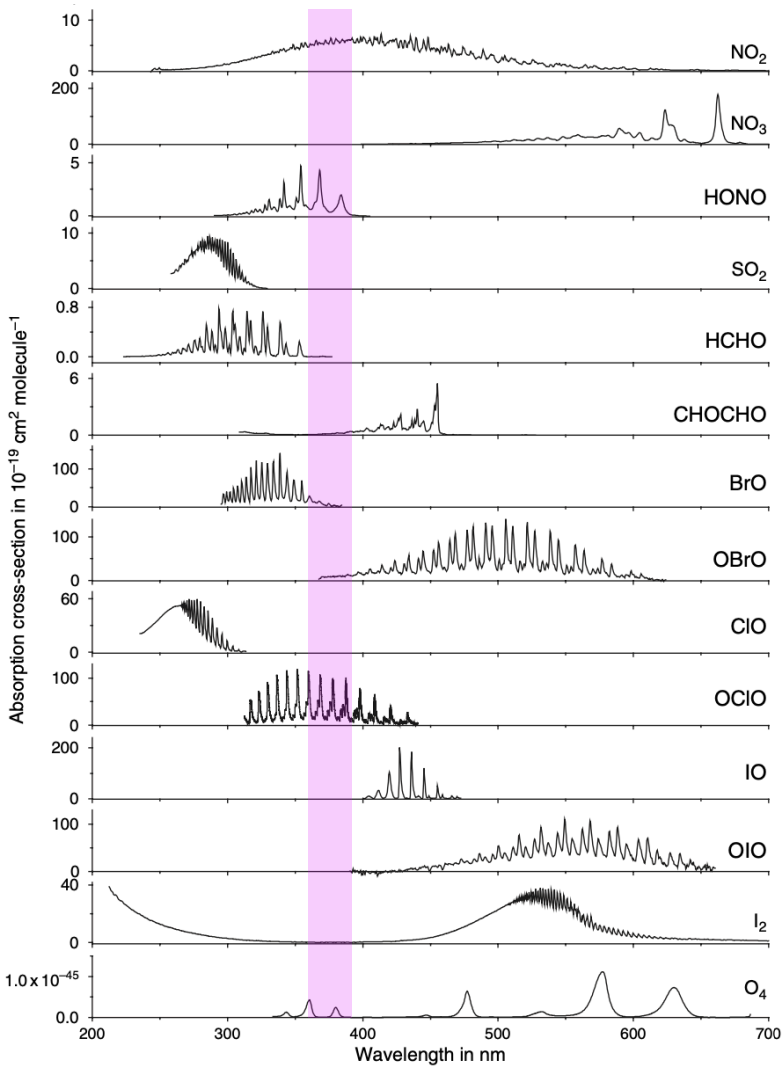

Figure 2.1 Reprint from *Differential Optical Absorption Spectroscopy* by Platt and Stutz (Springer, 2008, pp 147) that shows common atmospheric trace gases analyzed with IBBCEAS. The violet shading was added to denote the area where of irradiation for this setup's light source to denote what spectral features of HONO and NO_2 are being probed.

2.2.2 UC San Diego Homebuilt – Incoherent Broadband Cavity Enhanced Absorption Spectrometer and Reaction Cell

The measurements of HONO and NO_2 were done using a homebuilt instrument which is depicted in the schematic in Figure 2.2.[16–19] The light source is a light emitting diode (LED) that

emits in the wavelengths of 360 to 390 nm with a peak at 365 nm (Nichia Laboratories UV LED NVSU333A). The LED is mounted onto a copper printed circuit board (Cree XHP-70 MCPB) which is attached to a copper plate connecting to an aluminum block that was designed to have the capabilities to move in vertical and horizontal directions. The copper and aluminum mounting materials assist in heat dissipation created by the LED. Furthermore, to keep the temperature of the LED constant averaging 112° Fahrenheit, a Peltier cooler was mounted on the back of the copper plate and an Arctic Alpine 11 plus computer processor unit (CPU) fan was attached on the other side of the Peltier cooler. The power output of the LED and Peltier cooler are controlled using a custom LabVIEW program and circuit board interfaced with a National Instruments MyRIO device. The aluminum mount and CPU fan are shown in Figure 2.3A.

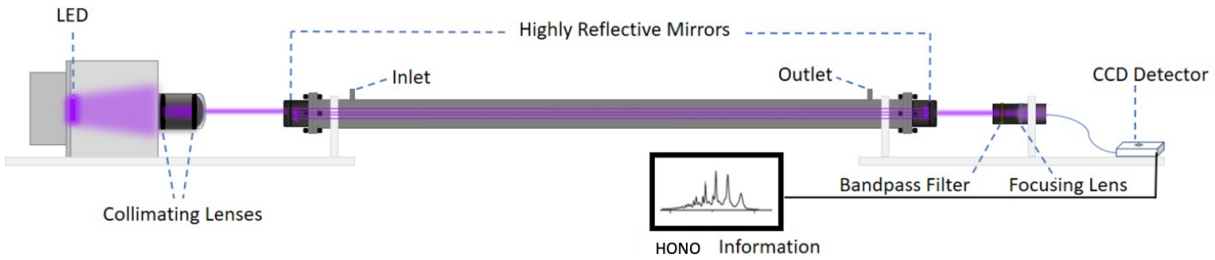

Figure 2.2 Schematic of the lab made Incoherent Broadband Cavity Enhanced Absorption Spectrometer. LED stands for light emitting diode that emits from 360 to 390 nm. The collimating lenses are aspheric condenser lenses. The mirrors are highly reflective mirrors with a peak at 370 nm. The cavity is made of PTFE. The band pass filter is a 352 to 388 nm bandpass filter and the focusing lens has a focal length of 100 mm. CCD is a charged coupled device detector.

Optics are used to direct the incoherent light emitting by the LED. As seen in Figure 2.2, the light from the LED emits in all directions (incoherent); collimating lenses are placed in an optics holder mounted in the aluminum block to collimate the light into the cavity. The optics are two aspheric condenser lenses (Thorlabs, ACL25416U-A, diameter = 1 in., NA = 0.79); this set

up is shown in Figure 2.3A. The collimated light is directed into the cavity which is a custom made 75.0 cm polytetrafluoroethylene (PTFE) tube with a diameter of 2.50 cm. At each end of the cavity are highly reflective mirrors held in place by optic holders with micrometer level adjustment capabilities and inlet holes where a nitrogen gas purge stream is introduced to avoid build up on the mirrors (mirrors, 99.99% reflectivity at 370 nm, ROC = 1 m, diameter = 2.54 cm; holders, model number 902-8010). There are inlet and outlet tubing where the gaseous sample is introduced and evacuated with PTFE tubing during the experiment. The light exiting the cavity exits through the "back" mirror where the collimated light enters and is first filtered of room light using a bandpass filter (Semrock, FF01-370/36-25, 25mm) and then focused into a fiber optic using a focusing lens (Thorlabs, LA4380-UV, diameter = 1 in., AR coated 245−400 nm, f/ 3.93, focal length = 100 mm). This setup to guide the light to the fiber optic is shown in Figure 2.3B. The fiber optic (Ocean optics, PL100-2-UV−vis, diameter = 1 mm, NA = 0.22) guides the light into a charged coupled device (CCD) detector with a 25 mm entrance slit and resolution of 0.9 nm (Ocean Optics QEPro). Spectra are taken using the accompanying software to the Ocean Optics detector, Oceanview.

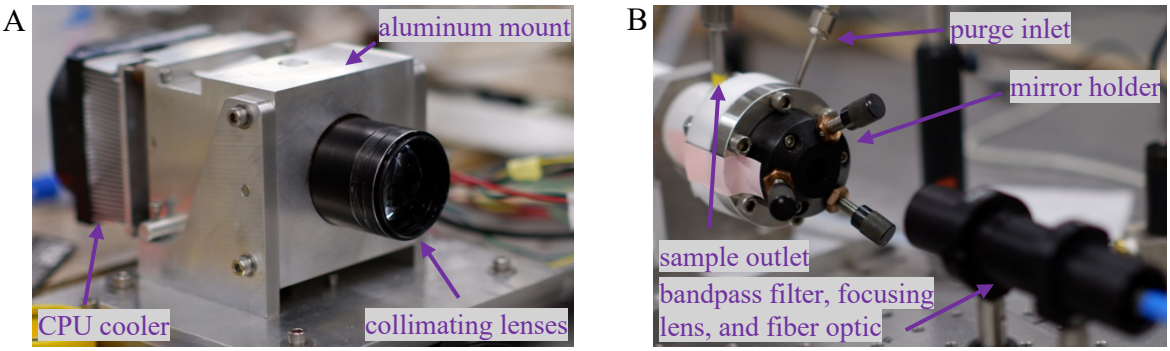

Figure 2.3 Photographs showing the set up for the (A) aluminum mount, central processing unit (CPU) cooler, and collimating lenses and (B) PTFE tube, sample outlet, mirror holders, mirror purge inlet, and the optics holder containing the bandpass filer, focusing lens, and fiber optic.

The reactions that can be studied with this instrument are many as the set up allows for the capabilities of both aqueous and thin film studies. A custom-built PTFE reaction cell is shown in Figure 2.4. The cell is a cylinder that can hold up to 7 mL of liquid sample and has 40 mL headspace volume. The inlet and outlet are placed in the same line to avoid turbulence in the reaction cell. The top of the cell is closed with a 17.35 cm^2 quartz window being held in-between an O-ring and a PTFE cap. The quartz window allows for irradiation using a Xe-Arc lamp solar simulator. All parts to the solar simulator are MKS products (lamp = 6255, housing = 67005, power supply = 69907, dichroic turning mirror = 81045). The solar simulator irradiates in the region of 200 – 2400 nm but it is an ozone free lamp making the irradiance below 260 nm minimal. Additionally, the dichroic turning mirror used only reflects wavelengths between 280 – 420 nm and a water filter removes IR irradiation. The gaseous products from reactions occurring in the reaction cell are carried out with N_2 from the outlet of the cell into the inlet of the IBBCEAS using ¼" PTFE tubing with an aerosol filter placed before the IBBCEAS inlet to avoid aerosols and buildup on the highly reflective mirrors. This set up has been used in aqueous experiments where the carrier gas was dry N_2[17] and thin film experiments where the carrier gas was wet N_2 set to specific relative humidity values.[18,19]

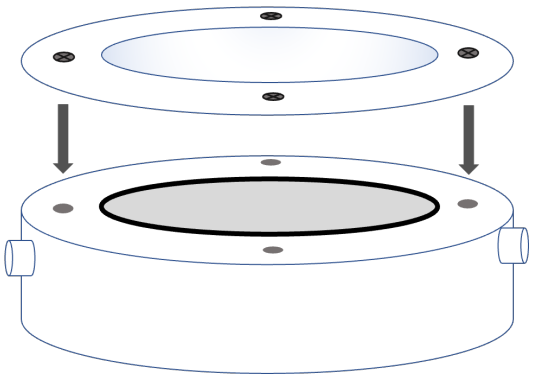

Figure 2.4 Schematic of the reaction cell used to irradiate aqueous nitrate solutions for introduction of gaseous products into the IBBCEAS or for irradiation of the solutions for UV-Vis spectroscopy experiments. The reaction cell is made of PTFE and the window is a 17.35 cm^2 quartz window that rests on a rubber O-ring with a 4.7 cm outer diameter.

2.2.3 Mirror Reflectivity and Pathlength Determination

The concentrations of HONO and NO_2 are calculated using Equation 2.9, where the effective pathlength is required so it can be rewritten as Equation 2.10 below. Effective pathlength is the effective length of the cavity that is achieved due to the light source being reflected off the highly reflective mirrors; and therefore, it is dependent on the mirror reflectivity. To obtain the wavelength dependent mirror reflectivity, spectra of the intensity of the LED were taken when nitrogen and helium were flowed through the cavity at a flow rate of 100 standard cubic centimeters per minute (sccm). The reflectivity is then calculated using Equation 2.11 where d is the physical length of the cavity (75.0 cm), I_{N_2} and I_{He} are the intensity of the light detected when the respective gases are flowing through the cavity. The Rayleigh extinction coefficients for nitrogen and helium are denoted as $\alpha_{Ray}^{N_2}(\lambda)$ and $\alpha_{Ray}^{He}(\lambda)$, respectively[16,20,21]. The effective pathlength, Equation 2.12, is then calculated by dividing the physical length of the cavity by one minus the wavelength dependent reflectivity.[12,16]

$$c_s = \frac{OD(\lambda, L)}{L_{eff} \times \sigma'_s(\lambda)} \qquad Eq.\ 2.10$$

$$R(\lambda) = 1 - d\frac{\left(\frac{I_{N_2}(\lambda)}{I_{He}(\lambda)}\alpha_{Ray}^{N_2}(\lambda)\right) - \left(\alpha_{Ray}^{He}(\lambda)\right)}{1 - \left(\frac{I_{N_2}(\lambda)}{I_{He}(\lambda)}\right)} \qquad Eq.\ 2.11$$

$$L_{eff}(\lambda) = \frac{d}{1-R(\lambda)} \qquad Eq.\ 2.12$$

Figure 2.5 displays the mirror reflectivity (A) and effective pathlength (B) for the setup of the IBBCEAS. The reflectivity of the mirrors is wavelength dependent and increases with increasing wavelength number. This is reflected in the effective pathlength as it is a function of the reflectivity. The effective pathlength average across the light source wavelength range (360 - 390 nm) is 1.05 km and the maximum, which occurs at the lower energy end of the range is 1.57 km.

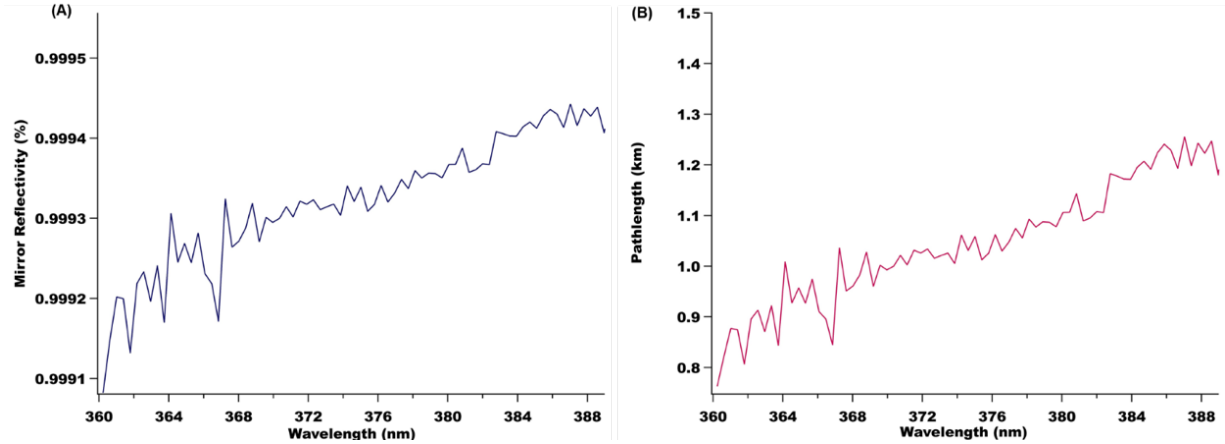

Figure 2.5 (A) The wavelength-dependent reflectivity of the mirrors used in the IBBCEAS setup for the wavelength range of the LED light source used in the experiments. The y-axis is in percentage. (B) The calculated wavelength-dependent effective pathlength, in kilometers, used for the determination of HONO and NO_2 concentration.

2.2.4 Data Acquisition and Analysis

The detector measures the intensity of the LED with and without absorbers present. At the start of every experiment, after the CCD detector has cooled down (ca. 30 minutes), a dark spectrum is taken which is done by physically blocking the path of the LED output into the detector. Then a spectrum with only the carrier gas set at the flowrate that the experiments will have, 200 sccm for most experiments, is acquired this is $I_0(\lambda, \mathrm{L})$. The spectra under experimental conditions are then acquired, $I(\lambda, \mathrm{L})$. It was determined that the conditions that allowed for best signal to noise ratio for all spectra was to average 10 scans where the acquisition time (slit opening time) was 20s. This gave information every 200 s which was an average for that period.

The next step is to calculate the optical density for each spectra using Equation 2.8. The dark spectrum that was collected is subtracted from $I(\lambda, \mathrm{L})$ and $I_0(\lambda, \mathrm{L})$ to account for electrical noise of the instrument.[12] Next, the OD of each spectrum is calculated by taking the natural log of the intensity of the LED with the absorbing medium present, $I(\lambda, \mathrm{L})$, divided by the intensity of the incident LED light, $I_0(\lambda, \mathrm{L})$. This can be done individually for each spectrum or by using the MATLAB file in the Appendix section 2.6.1 which automates this process for all $I(\lambda, \mathrm{L})$. Once the OD's are determined for all spectra, the OD's can be fit reference HONO and NO_2 absorption cross-sections.

Differential Optical Absorption Spectroscopy Intelligent System (DOASIS) can be used to deconvolute the OD into HONO and NO_2 absorption cross-sections. DOASIS is a software that can be used to interpret spectral data and in this set up, it is used to deconvolute the acquired spectra into the two components contributing to the overall spectra.[22] A step-by-step guide on how to do this can be found in the DOASIS Tutorial available in the Help Tab of the DOASIS software. First, the literature reference absorption cross-section spectra taken for HONO[23] and NO_2[24] were

convoluted to match the resolution of the detector, which was determined by taking spectra of a Mercury pen lamp, on DOASIS. A high pass binomial filter is then applied to remove broadband absorption features, this is also done in DOASIS under the Math Tab. This is $\sigma'_{HONO}(\lambda)$ and $\sigma'_{NO_2}(\lambda)$ in Equation 2.10. The entire denominator of Equation 2.10 can be uploaded onto DOASIS to fit the optical density to if $L_{eff}(\lambda)$ is multiplied by $\sigma'_s(\lambda)$ where it would be done to both $\sigma'_{HONO}(\lambda)$ and $\sigma'_{NO_2}(\lambda)$. To be able to do this multiplication, $L_{eff}(\lambda)$ needs to be interpolated to match the same wavelength intervals of $\sigma'_{HONO}(\lambda)$ and $\sigma'_{NO_2}(\lambda)$. Once the reference spectra are in the forms of $L_{eff}(\lambda) \times \sigma'_{HONO}(\lambda)$ and $L_{eff}(\lambda) \times \sigma'_{NO_2}(\lambda)$, they can be uploaded into DOASIS program for spectral fitting. To manually fit individual experimental OD data in DOASIS, the fitting range for the experimental OD data and both HONO and NO_2 reference spectra were selected using the Marker tool. To fit the data to the reference spectra, the OD spectrum is selected and in the Fitting dock the two reference spectra for HONO and NO_2 are selected along with the polynomial degree (polynomials 5 and 6 are suggested). The OD is fit to Equation 2.13 where the broadband features of molecular absorption, Mie, and Rayleigh scattering are fit to a polynomial.

$$OD = \ln\left(\frac{I_0(\lambda)}{I(\lambda)}\right) = L_{eff}(\lambda) \times \left[\sum_i \sigma'_s \times c_s + polynomial\right] \qquad Eq.\,2.13$$

The resulting output are coefficients to Equation 2.13 where a table will show the main coefficients for HONO and NO_2 and the secondary coefficients correspond to the error in the fitting. These values are in concentration units of molecules cm^{-3} and then be converted to ppb by multiplying by 2.46×10^{10}.[25] From this process, the spectra of the fitting of the experimental OD to HONO, NO_2, and the polynomial can also be extracted. Figure 2.6 shows this fitting for the spectra

of a 100 mM $NaNO_3$ solution acidified to pH 2 with HCl at the three-hour mark. The residual trace corresponds to any light extinction process that was not able to be fit to the HONO or NO_2 differential features or the broadband features grouped in the polynomial. This process has been automated using a JavaScript code which DOASIS is compatible with where these fitted parameters have been specified. The code is provided in the Appendix section 2.6.2.

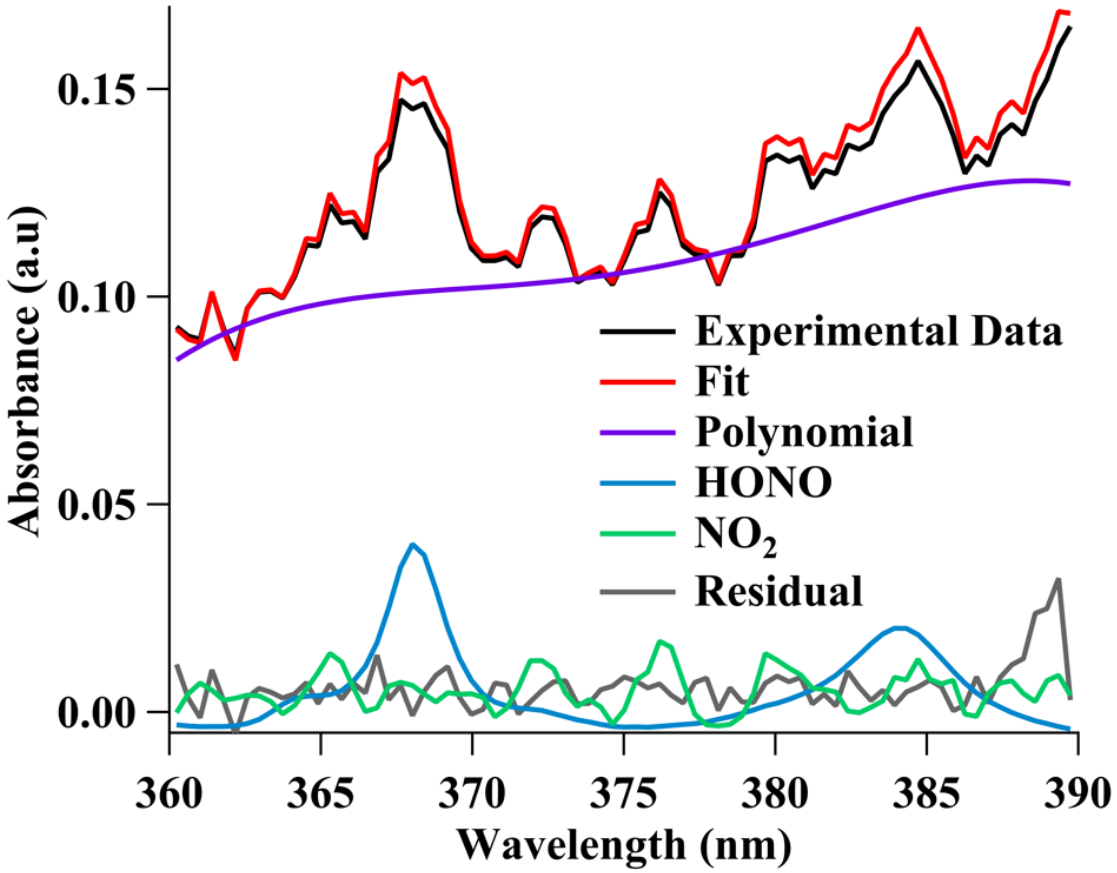

Figure 2.6 The experimental spectrum (black trace) is fit by DOASIS (red trace) and then separated into the absorbance due to HONO (blue trace) and NO_2 (green trace) by fitting them to literature HONO and NO_2 spectra. Also displayed are the absorbance due to Mie and Rayleigh scattering and any other non-HONO and NO_2 absorptions fitted to a polynomial (purple trace) and any wavelength dependent residual absorption data not able to be fitted (gray trace). This is the deconvolution of one spectrum for an experiment involving broadband irradiation of 100 mM $NaNO_3$ at pH 2.00.

2.2.5 Optimization and Validation of UC San Diego Homebuilt IBBCEAS Spectrometer

This thesis describes the current IBBCEAS experimental setup since its initial development.[16] In particular, the cavity tube material was originally 100 cm long and made of stainless steel. This was changed to a 75 cm cavity made of PTFE. The change in cavity material was done to address HONO values for the same experiment not being reproducible. It was hypothesized that HONO was sticking to the stainless-steel walls and creating unquantifiable loss via deposition or reactions with hydroxyl radicals making H_2O and NO_2.[26] In addition, the aluminum block was realigned in the horizontal and vertical planes to be to better collated with the end of the fiber optic. This allowed for maximum capacity of light reflections in the cavity. Furthermore, different mirror cleaning techniques were tested, and the best technique was found to be to clean the non-reflective side of the mirrors first by putting a lens wipe over the mirror, adding a drop of methanol and pulling the lens wipe over the mirror. This was repeated two more times with methanol and then three more times with acetone. Following cleaning with the lens wipes, the mirror was cleaned with lint-free cotton swabs with a drop of methanol and then with acetone again. It is to be ensured that a side of the cotton swab is not reused as to not drag debris over the mirror. This is all to be repeated on the reflective side of the mirrors. Mirror alignment was optimized. The method that gave the best results, i.e., the highest cavity reflectivity and thus highest pathlength, involved using an optical iris to collimate the LED light and then aligning the "back" mirror, the mirror closest to the fiber optic, to reflect back into the iris, by overlapping the reflection circle to the incident light circle. A sturdy white piece of paper (e.g., the back of an index card) was used for this process. The "front" mirror is then mounted into the cavity and aligned by adjusting the micrometers while monitoring at the detector output in real time and maximizing the

LED intensity. The implementation of cleaning and aligning the mirrors in this manner increased the maximum effective pathlength from 1.0 to 1.57 km, lowering the limit of quantification for HONO and NO_2, to 10 and 15 ppb respectively.

The NO_2 transition that is probed within the region of the LED emission of 360 to 390 nm is excitation from the electronic ground state to the first electronic excited state, $A^2B_2 \leftarrow X^2A_1$ transition, appearing as a broadband asymmetrical bell curve with narrowband spectral features arising from the vibrational transitions between the ground and first excited electronic states.[27,28] The reference spectrum used here was taken from Burrows et al. and treated to match the CCD detector resolution and remove broadband features as discussed in section 2.2.4.[24] The HONO absorption in the range of 360 to 390 nm is the ground state to first excited state electronic transition of $A^1A'' \leftarrow X^1A'$ having a broadband slope like shape.[29] Like NO_2, HONO has differential spectral features arising from vibronic transitions, which is what is utilized for the DOAS analysis. The reference absorption cross-section spectrum of HONO was taken from Bongartz et al. and treated like the NO_2 reference spectrum.[29] A calibration curve of true concentration to measured concentration of NO_2 was done with known concentrations of NO_2 gas. The slope, shown in Figure 2.7, for this was 0.96, validating the instrument and analysis process.[18] A modified version of Febo et al.'s HONO generation system was set up where diluted and humidified HCl was passed through a bed of $NaNO_2$ leading to gaseous HONO being generated.[30] However, a similar calibration curve could not be done as the HONO generation system had wide variability in the efficiency of HONO generation and so the values were not reproducible.

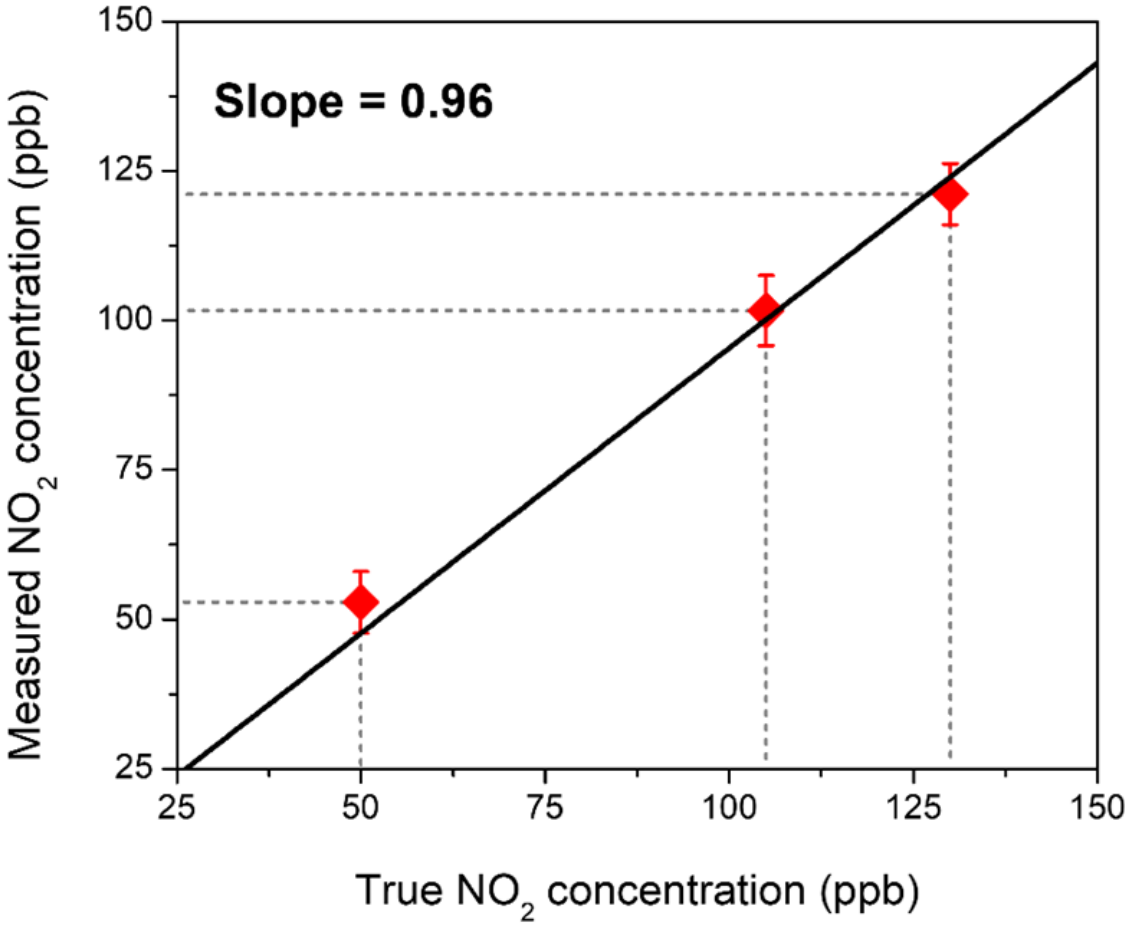

Figure 2.7 Validation of the IBBCEAS system by graphing true amounts of NO_2 in the ppb range with the measured amounts from the DOAS data analysis procedure. The black solid line is a linear fit to the experimentally measured data points and the true concentration amounts. The slope of the line (0.96), close to 1, validates the accuracy of the measurement.

2.3 Ultraviolet – Visible Absorption Spectroscopy

UV-Vis spectroscopy was used as complementary technique to measure the electronic excitation spectra of the solutions used in these experiments and to measure changes in the spectrum following irradiation with the Xe-Arc lamp solar simulator. Using Beer-Lambert Law, as shown in Equation 2.14, where the absorbance, A, of a solution is equal to the molar absorptivity constant of the molecule(s) in the solution, ε ($M^{-1}cm^{-1}$), times the concentration of the absorber(s),

c (M), and the pathlength that the light is interacting with the absorber, b (cm), [31] the changes in absorbance following irradiation were measured.

$$A = \varepsilon cb \qquad Eq. 2.14$$

Since this dissertation research focuses on solution phase photochemistry of aqueous nitrate solutions in the presence of light absorbing marine relevant organics, it is important to measure the absorption spectra of these different light absorbing components in the aqueous phase and how the absorption changes upon broadband irradiation. For all UV-Vis absorption experiments, the wavelength range probed was 280 – 500 nm. For aqueous nitrate, the transition probed was the $n \rightarrow \pi^*$ transition that peaks at 305 nm.[15] Marine dissolved organic matter has continuous absorption from 500 nm to well below 200, or 280 as probed in this project.[2,32] Similarly, 4-BBA has a continuous absorption profile from 500 to 200 nm[33] whereas EG does not absorb in the region being probed in for these studies, only having absorption below 240 nm.[34]

An Agilent Cary 5000 UV-Vis-NIR Spectrophotometer was used to measure the absorbance of all solutions. The instrument was set to acquire in double beam mode where the reference cuvette contained Milli-Q (MQ) water. Both cuvettes were 10 mm quartz cuvettes. The acquisition parameters were kept to default except that the light source, grating, and detector changeovers were set to outside of the acquisition wavelength range. The resolution was set to 0.5 nm over the spectral region from 280 to 500 nm.

2.4 Proton Nuclear Magnetic Resonance

Proton nuclear magnetic resonance (^{1}H-NMR) experiments were done to determine the speciation of 4-BBA at MBL conditions as it allowed for the measurement of the hydrogens in the samples with varying pH values. The chemical shifts in the NMR spectrum are representative of how a hydrogen nucleus interacted with the magnetic field applied and can be used to characterize the protonated and deprotonated form of 4-BBA.[35] The NMR was a 500 MHz Jeol Spectrometer.

The solutions were prepared as detailed in section 2.1 and put in NMR tubes. The acquisition parameters were as follows. One spectrum that was an average of 8 spectra was taken before the start of each sample to locate the water peak. To take the spectra, autogain, auto lock, and force tune were enabled. To suppress the water peak, presaturation mode was chosen and the water peak from the first spectrum taken was entered as offset. One ^{1}H-NMR spectrum was an average of 1024 scans in efforts to increase the signal to noise ratio (S/N) as the intensity of 100 μM 4-BBA was very weak. Analysis of the ^{1}H-NMR chemical shift spectra was done using the software MestreNova (Mnova) following a basic analysis procedure including blocking the water peak and auto baseline correction. Manual peak fitting was done because the S/N was not high enough for all peaks to be auto detected. In addition, simulated ^{1}H-NMR spectra of the different forms of 4-BBA were compared to the experimental ^{1}H-NMR chemical shift profile.

2.5 Acknowledgements

The author would like to thank past members of the Grassian group including Dr. Jonathan Trueblood for the initial building of the IBBCEAS along with Dr. Michael N. Sullivan for his assistance in the optimization of the instrument and Dr. Kristin Wall for the HONO generation

setup. I also want to thank to Dr. Shubhrangshu Pandit for also assisting in the optimization and for automizing the analysis procedure. Thank you to Anthony Mrse at the UCSD Chemistry and Biochemistry NMR Facility for his helpful discussions.

2.6 Appendix

Several different codes were developed for the analysis of the data from the UC San Diego homebuilt spectrometer. These were written by Dr. Shubhrangshu Pandit in the effort to minimize data analysis time requirements.

2.6.1 Automated Optical Density Calculation

If there are multiple spectra to calculate optical densities (OD) for, the recommended method is to run the following MATLAB code below. The name of the file for the experimental spectra is written in line number 12. The number of spectra to calculate OD for is written in line number 8. The name of the new OD files created will have the name listed in line number 23. Note that for this code to work, an empty and dark spectrum must be present in the same folder. This code can be copied into MATLAB and ran, the resulting files will be saved in the same folder the MATLAB is told to run the code in. The numbering was added to describe the code, it must be removed to be used.

```
1. clear;
2. begin=158;
3. finish=234;
4. D=readtable('dark.txt');
5. w=table2array(D(:,1));
6. E=readtable('empty.txt');
7. cE=table2array(E(:,2))-table2array(D(:,2));
```

```
8.  num=92; %number of scan to average
9.  step=1;
10. start=1;
11. S=zeros(size(w));
12. fname='ON_QEP011461_';

13. for nn=start:step:num
14. f=strcat(fname,num2str(nn),'.txt');
15. S1=readtable(f);
16. cS1=table2array(S1(:,2))-table2array(D(:,2));
17. cS=log(cE./cS1);

18. plot(w(begin:finish),cS(begin:finish));
19. hold on
20. xlabel('Wavelength (nm)');
21. ylabel('OD (a.u.)');

22. scan=table(w(begin:finish),cS(begin:finish));
23. fs='ON_';
24. t=0+(nn*200);
25. fscan=strcat(fs,num2str(t),'s.txt');
26. writetable(scan, fscan);
27. end
```

2.6.2 JavaScript File to Run DOASIS for Multiple Spectra Collected as a Function of Time

After having the OD files from section 2.6.1, they can be fit to the reference HONO and NO_2 spectra on DOASIS which is compatible with JavaScript. The following code can be used to automate the fittings for multiple OD spectra. Lines 13 and 14 are where the code is saved. Lines 17-19 are where the reference spectra are saved and under which file name. Line 41 is where the results file will be saved. Lines 49-50 is the name and location of OD spectra to be analyzed. Lines 52 and 53 are the channels correlated to the wavelengths in DOASIS (channel 10 = 360 nm and channel 64 =389 nm). Line 54f is the polynomial equation order to fit the data to. This code can

be copied into Notepad++ and selected in DOASIS under the Script docking window. The numbering was added to describe the code, it must be removed to be used.

```
1.  //|---------DOAS Fit for Time scan----------|
2.  //|----------------------------------------|

3.  import System;
4.  import System.Threading;
5.  import DoasCore;
6.  import DoasCore.Spectra;
7.  import DoasCore.IO;
8.  import DoasCore.Device;
9.  import DoasCore.Script;
10. import DoasCore.HMI;
11. import DoasCore.Math;

12. //**************      Fit file and Result file
            ****************************************

13. var Path = "W:\\Mora Garcia Stephanie\\Java Script Copy\\";
14. var FitFile = "fit_scenario.fs";

15. var ResultSpec : ISpectrum = Specbar.GetSpectrum("FitResult");

16. //**************      Load Reference Spectra
            *********************************************

17. var refHONO = "diff_HONO_20220701.txt";
18. var refNO2 = "diff_NO2_20220701.txt";
19. var refPath = "W:\\_Alumni Folders\\Pandit\\Ref Spec\\";

20. var HONOfile : ISpectrum = Specbar.GetSpectrum(refHONO);
21. var NO2file : ISpectrum = Specbar.GetSpectrum(refNO2);

22. HONOfile.Open(refPath + refHONO);
23. NO2file.Open(refPath + refNO2);

24. //***************  Create an Excel File
            ***********************************************

25. // Start Excel and get Application object.
26. var oXL = new ActiveXObject("Excel.Application");
27. // Make the Excel program visible.
28. oXL.Visible = true;
```

```
// Get a new workbook and add a worksheet
var oWB = oXL.Workbooks.Add();
// Make the opened worksheet ready for modifying
var oSheet = oWB.ActiveSheet;
// Add table headers going cell by cell.
oSheet.Cells(1, 1).Value = "Time (s)";
oSheet.Cells(1, 2).Value = "HONO";
oSheet.Cells(1, 3).Value = "error";
oSheet.Cells(1, 4).Value = "NO2";
oSheet.Cells(1, 5).Value = "error";

//*****************    Create the AutoFileName object to store the files
**************

var afnFile = new AutoFileName();
afnFile.BasePath = "W:\\Mora Garcia Stephanie\\IBBCEAS Exps\\Preliminary
Exps\\20221005 100 mM NaNO3  + 0p2mgml mDOM pH2\\DOASIS Fit Comparison\\";
afnFile.Prefix = "a";
afnFile.Suffix = ".std";
afnFile.FilesPerFolder = 100,
afnFile.NumberOfDigits = 5;
// look for the first existing file
afnFile.FindFirstIndex();

//****************  Load Time-scan Spectra and Modify Fit Scenario
          ***************************

var fname ="ON_OldRef_";
var specPath = "W:\\Mora Garcia Stephanie\\IBBCEAS Exps\\Preliminary
Exps\\20221005 100 mM NaNO3  + 0p2mgml mDOM pH2\\DOASIS Fit Comparison\\";

var n=1
var FitLow = 10;
var FitHigh = 64;

var fit = new DoasCore.Math.DoasFit( );
    a. fit = DoasCore.Math.DoasFit.Open(Path + FitFile);

    b. Console.WriteLine("Old file name: " + fit.PolynomialOrder);

    c. fit.FitRanges[0].LimitLow = FitLow;
    d. fit.FitRanges[0].LimitHigh = FitHigh;
    e. fit.FitModel = "DOAS";
    f. fit.PolynomialOrder = 6;
    g. fit.OffsetPolynomialOrder = -1;
```

h. fit.ReferencesInfo[0].ReferenceSpectrum = HONOfile;
i. fit.ReferencesInfo[1].ReferenceSpectrum = NO2file;

55. if (DoasFit.Save(fit, Path + FitFile))
    a. {
        i. Console.WriteLine("Fit scenario saved!");
    b. }
56. else {
        i. Console.WriteLine("Error while saving!");
    b. }

    c. Console.WriteLine("Old file name: " + fit.PolynomialOrder);

57. //********** Run the loop
    ****

58. var i;
59. for(i = 1; i <= n; i++)
60. {
    a. var fspec = fname+i*200+"s.txt";
    b. var specfile : ISpectrum = Specbar.GetSpectrum(fspec);
    c. specfile.Open(specPath + fspec);

    d. Specbar.CurrentSpectrum = specfile;
    e. System.Threading.Thread.Sleep(1000);
    f. fit.TargetSpectrum = specfile;

    g. if (fit.DoFit (specfile))
        i. {
            1. Console.WriteLine("Fit successful for spectrum");
            2. fit.PrepareFitResultSpectrum(ResultSpec);
            3. Specbar.CurrentSpectrum = ResultSpec;
            4. fit.AppendResultToFile(specPath + "result.txt");
            5. oSheet.Cells(1 + i, 1).Value = i*200;
            6. oSheet.Cells(1 + i, 2).Value = fit.ReferencesInfo[0].FitCoefficient;
            7. oSheet.Cells(1 + i, 3).Value = fit.ReferencesInfo[0].FitCoefficientError;
            8. oSheet.Cells(1 + i, 4).Value = fit.ReferencesInfo[1].FitCoefficient;
            9. oSheet.Cells(1 + i, 5).Value = fit.ReferencesInfo[1].FitCoefficientError;
        ii. }
    h. else

i. { System.Console.WriteLine("Fit failed for spectrum");
    1. oSheet.Cells(1 + i, 1).Value = i*200;
    2. oSheet.Cells(1 + i, 2).Value = fit.ReferencesInfo[0].FitCoefficient;
    3. oSheet.Cells(1 + i, 3).Value = fit.ReferencesInfo[0].FitCoefficientError;
    4. oSheet.Cells(1 + i, 4).Value = fit.ReferencesInfo[1].FitCoefficient;
    5. oSheet.Cells(1 + i, 5).Value = fit.ReferencesInfo[1].FitCoefficientError;
ii. }

61. }

62. import System.Windows.Forms;
63. MessageBox.Show("Done!");

2.7 Bibliography

(1) Sauer, J. S.; Mayer, K. J.; Lee, C.; Alves, M. R.; Amiri, S.; Bahaveolos, C.; Barnes, E. B.; Crocker, D. R.; Dinasquet, J.; Garofalo, L. A.; Kaluarachchi, C. P.; Dang, D.; Kilgour, D.; Mael, L.; Mitts, B. A.; Moon, D. R.; Morris, C. K.; Moore, A. N.; Ni, C.-M.; Pendergraft, M. A.; Petras, D.; Simpson, R.; Smith, S.; Tumminello, P. R.; Walker, J. L.; DeMott, P. J.; Farmer, D. K.; Goldstein, A. H.; Grassian, V. H.; Jaffe, J. S.; Malfatti, F.; Martz, T. R.; Slade, J.; Tivanski, A. V.; Bertram, T. H.; Cappa, C. D.; Prather, K. A. The Sea Spray Chemistry and Particle Evolution Study (SeaSCAPE): Overview and Experimental Methods. *Environ. Sci.: Process. Impacts.* **2022**, *24*, 290–315.

(2) Alves, M. R.; Coward, E. K.; Gonzales, D.; Sauer, J. S.; Mayer, K. J.; Prather, K. A.; Grassian, V. H. Changes in Light Absorption and Composition of Chromophoric Marine-Dissolved Organic Matter across a Microbial Bloom. *Environ. Sci. Process. Impacts.* **2022**, *24* (10), 1923–1933.

(3) Ling, L.; Xie, P.; Qin, M.; Hu, R.; Zheng, N.; Si, F. Simultaneous Measurements of Atmospheric NO_2 and HONO Using IBBCEAS with a Near-Ultraviolet LED . *Proc. of SPIE* **2012**, *8563*.

(4) Gherman, T.; Venables, D. S.; Vaughan, S.; Orphal, J.; Ruth, A. A. Incoherent Broadband Cavity-Enhanced Absorption Spectroscopy in the near-Ultraviolet: Application to HONO and NO_2. *Environ. Sci. Technol.* **2008**, *42* (3), 890–895.

(5) Scharko, N. K.; Berke, A. E.; Raff, J. D. Release of Nitrous Acid and Nitrogen Dioxide from Nitrate Photolysis in Acidic Aqueous Solutions. *Environ. Sci. Technol.* **2014**, *48* (20), 11991–12001.

(6) Zheng, K.; Zheng, C.; Zhang, Y.; Wang, Y.; Tittel, F. K. Review of Incoherent Broadband Cavity-Enhanced Absorption Spectroscopy (Ibbceas) for Gas Sensing. *Sensors*. 2018, 18, 3646.

(7) Yi, H.; Wu, T.; Wang, G.; Zhao, W.; Fertein, E.; Coeur, C.; Gao, X.; Zhang, W.; Chen, W. Sensing Atmospheric Reactive Species Using Light Emitting Diode by Incoherent Broadband Cavity Enhanced Absorption Spectroscopy. *Opt. Express.* **2016**, *24* (10), A781.

(8) Wu, T.; Chen, W.; Fertein, E.; Cazier, F.; Dewaele, D.; Gao, X. Development of an Open-Path Incoherent Broadband Cavity-Enhanced Spectroscopy Based Instrument for Simultaneous Measurement of HONO and NO_2 in Ambient Air. *Appl. Phys. B* **2012**, *106* (2), 501–509.

(9) Payne, Z. C.; Dalton, E. Z.; Gandolfo, A.; Raff, J. D. HONO Measurement by Catalytic Conversion to NO on Nafion Surfaces. *Environ. Sci. Technol.* **2023**, *57* (1), 85–95.

(10) Crilley, L. R.; Kramer, L. J.; Ouyang, B.; Duan, J.; Zhang, W.; Tong, S.; Ge, M.; Tang, K.; Qin, M.; Xie, P.; Shaw, M. D.; Lewis, A. C.; Mehra, A.; Bannan, T. J.; Worrall, S. D.; Priestley, M.; Bacak, A.; Coe, H.; Allan, J.; Percival, C. J.; Popoola, O. A. M.; Jones, R. L.; Bloss, W. J. Intercomparison of Nitrous Acid (HONO) Measurement Techniques in a Megacity (Beijing). *Atmos. Meas. Tech.* **2019**, *12* (12), 6449–6463.

(11) John H. Seinfeld; Spyros N. Pandis. *Atmospheric Chemistry and Physics: From Air Pollution to Climate Change*, Third.; John Wiley & Sons, Inc., 2016.

(12) Platt, Ulrich.; Stutz, J. *Differential Optical Absorption Spectroscopy*; Springer, 2008.

(13) Finlayson-Pitts, B. J.; Wingen, L. M.; Sumner, A. L.; Syomin, D.; Ramazan, K. A. The Heterogeneous Hydrolysis of NO_2 in Laboratory Systems and in Outdoor and Indoor Atmospheres: An Integrated Mechanism. *Phys. Chem. Chem. Phys.* **2003**, *5* (2), 223–242.

(14) Ramazan, K. A.; Syomin, D.; Finlayson-Pitts, B. J. The Photochemical Production of HONO during the Heterogeneous Hydrolysis of NO_2. *Phys. Chem. Chem. Phys.* **2004**, *6*, 3836–3843.

(15) Mack, J.; Bolton, J. R. Photochemistry of Nitrite and Nitrate in Aqueous Solution: A Review. *J. Photochem. Photobiol. A Chem.* **1999**, *128*, 1–13.

(16) Trueblood, J. V. Spectroscopic Investigations into Nascent and Aged Sea Spray Aerosol, University of California San Diego, 2018.

(17) Mora García, S. L.; Pandit, S.; Navea, J. G.; Grassian, V. H. Nitrous Acid (HONO) Formation from the Irradiation of Aqueous Nitrate Solutions in the Presence of Marine Chromophoric Dissolved Organic Matter: Comparison to Other Organic Photosensitizers. *ACS Earth. Space. Chem.* **2021**, *5* (11), 3056–3064.

(18) Pandit, S.; Mora García, S. L.; Grassian, V. H. HONO Production from Gypsum Surfaces Following Exposure to NO_2 and HNO_3: Roles of Relative Humidity and Light Source . *Environ. Sci. Technol.* **2021**, *55* (14), 9761–9772.

(19) Pandit, S.; Grassian, V. H. Gas-Phase Nitrous Acid (HONO) Is Controlled by Surface Interactions of Adsorbed Nitrite (NO_2^-) on Common Indoor Material Surfaces. *Environ. Sci. Technol.* **2022**, *56* (17), 12045–12054.

(20) Thalman, R.; Zarzana, K. J.; Tolbert, M. A.; Volkamer, R. Rayleigh Scattering Cross-Section Measurements of Nitrogen, Argon, Oxygen and Air. *J. Quant. Spectrosc. Radiat. Transf.* **2014**, *147*, 171–177.

(21) Sneep, M.; Ubachs, W. Direct Measurement of the Rayleigh Scattering Cross Section in Various Gases. *J. Quant. Spectrosc. Radiat. Transf.* **2005**, *92*, 293–310.

(22) Kraus, S. DOASIS: A Framework Design for DOAS, University of Mannheim, Mannheim, 2006.

(23) Stutz, J.; Kim, E. S.; Platt, U.; Bruno, P.; Perrino, C.; Febo, A. UV-Visible Absorption Cross Sections of Nitrous Acid. *J. Geophys. Res. Atmos.***2000**, *105* (D11), 14585–14592.

(24) Burrows, J. P.; Dehn, A.; Deters, B.; Himmelmann, S.; Richter, A.; Voigt, S.; Orphal, J. Atmospheric Remote-Sensing Reference Data from GOME: Part 1. Temperature-Dependent Absorption Cross-Sections of NO_2 in the 231-794 nm Range. *J. Quant. Spectrosc. Radiat. Transf.* **1998**, *60* (6), 1025–1031.

(25) Finlayson-Pitts, B. J.; Pitts, J. N.; Pitts, J. N. Jr. *Chemistry of the Upper and Lower Atmosphere Theory, Experiments, and Applications*; Elsevier Science, 1999.

(26) Sörgel, M.; Regelin, E.; Bozem, H.; Diesch, J. M.; Drewnick, F.; Fischer, H.; Harder, H.; Held, A.; Hosaynali-Beygi, Z.; Martinez, M.; Zetzsch, C. Quantification of the Unknown

HONO Daytime Source and Its Relation to NO_2. *Atmos. Chem. Phys*. 2011, 10433–10447.

(27) Volkers, E. A.; Koudijzer, M. C.; Vredenborg, A.; Bulthuis, J.; Stolte, S.; Linnartz, H.; Jost, R. The A^2B_2-X^2A_1 Electronic Transition of $^{15}NO_2$: A Rovibronic Survey Covering 14300-18000 cm^{-1}. *J. Mol. Spectrosc.* **2006**, *235* (1), 1–17.

(28) Kirmse, B.; Delon, A.; Jost, R. NO_2 Absorption Cross Section and Its Temperature Dependence. *J. Geophys. Res. Atmos.* **1997**, *102* (13), 16089–16098.

(29) Bongartz, A.; Kames, J.; Welter, F.; Schurath, U. Near-UV Absorption Cross Sections and Trans/Cis Equilibrium of Nitrous Acid. *J. Phys. Chem.* **1991**, *95* (3), 1076–1082.

(30) Febo, A.; Perrino, C.; Gherardi, M.; Sparapani, R. Evaluation of a High-Purity and High-Stability Continuous Generation System for Nitrous Acid. *Environ. Sci. Technol.* **1995**, *29* (9), 2390–2395.

(31) Skoog, D. A.; Holler, F. J.; Crouch, S. R. *Principles of Instrumental Analysis*, 7th ed.; Sunder College Publisher, 2017.

(32) Karimova, N. V.; Alves, M. R.; Luo, M.; Grassian, V. H.; Gerber, R. B. Toward a Microscopic Model of Light Absorbing Dissolved Organic Compounds in Aqueous Environments: Theoretical and Experimental Study. *Phys. Chem. Chem. Phys.* **2021**, *23* (17), 10487–10497.

(33) Karimova, N.; Alija, O.; Mora García, S. L.; Grassian, V. H.; Gerber, R. B.; Navea, J. G. PH Dependence of the Speciation and Optical Properties of 4-Benzoylbenzoic Acid. *Phys. Chem. Chem. Phys.* **2023**, *25*, 17306–17319.

(34) Zhang, J.; Zhang, P.; Ma, K.; Han, F.; Chen, G.; Wei, X. Hydrogen Bonding Interactions between Ethylene Glycol and Water: Density, Excess Molar Volume, and Spectral Study. *Sci. China. B Chem.* **2008**, *51* (5), 420–426.

(35) Günther, H. *NMR Spectroscopy: Basic Principles, Concepts, and Applications in Chemistry*, 3rd ed.; Wiley-VCH, 2013.

Chapter 3 Nitrous Acid (HONO) Formation from Irradiation of Aqueous Nitrate Solutions in the Presence of Marine Chromophoric Dissolved Organic Matter: Comparison to Other Organic Photosensitizers

3.1 Abstract

Nitrous acid (HONO), a highly reactive trace atmospheric gas, is often underestimated in global atmospheric models due to the poor understanding of its sources and sinks, especially in the marine boundary layer (MBL). Herein we have investigated HONO formation from the irradiation of nitrate solutions in the presence of increasingly complex photosensitizers including marine dissolved organic matter (m-DOM), that contains chromophoric organic matter, collected from a large-scale mesocosm experiment. In particular, aqueous nitrate solutions in the presence of m-DOM, humic acid, and 4-benzoylbenzoic acid (4-BBA) as well as ethylene glycol were irradiated with a solar simulator. Gas-phase HONO and NO_2 produced during irradiation of these samples were detected using incoherent broad band cavity enhanced absorption spectroscopy (IBBCEAS). The relative amounts of HONO and NO_2 formation varied for these different samples. The addition of all of these different organic containing samples (m-DOM, HA, 4-BBA, and EG) to nitrate solutions caused an enhancement in HONO formation, with m-DOM showing the greatest total amount over a six-hour time period. Mechanisms for this enhancement are discussed as well as the strong pH dependence, with the greatest amount of HONO at low pH. Overall, HONO formation from nitrate photolysis in the presence of m-DOM provides insights into the HONO formation pathway in the MBL and ultimately contributes to improving atmospheric models.

3.2 Introduction

Trace chemical oxidizers like nitrous acid (HONO), are highly reactive and as such, play a large role in the chemistry of the atmosphere. Reactions that lead to nitrous acid formation have been studied extensively for over the past 30 years due to the rapid photolysis of HONO into OH and NO at wavelengths between 300-400 nm which falls within the solar spectrum as well as some indoor light sources, relevant to photochemistry in indoor environments[1–6]. It has been reported that in some conditions, HONO photolysis can be the major source of OH formed outdoors[7]. Understanding sources of OH is important as it is the most significant oxidant in the atmosphere[8] and contributions to the oxidation of volatile organic carbons (VOCs) to form secondary organic aerosols.[7,9]

There are many reaction pathways that lead to the formation of HONO in the atmosphere which can be separated into two categories: nighttime and daytime sources. Nighttime sources include direct emissions from soil bacteria, as well as reactions that occur in the absence of a light source, such as the hydrolysis of NO_2 in the presence of adsorbed water[10,11]. Daytime sources include aqueous and particulate nitrate photolysis and the photosensitized reduction of NO_2 in the presence of organic chromophores[12–15].

In recent years, HONO has been measured in clean marine boundary layer (MBL) environments where there is no significant influence from pollution, and maximum values have been found at noon, highly suggesting photochemical sources are of great significance[4,16]. Measurements of HONO in the MBL along with complementary modeling analysis indicated that the most likely source of HONO is due to the photosensitized reduction of NO_2 or particulate nitrate photolysis, with the latter being more common[16–18]. Furthermore, although previous models of the NO_x cycle have treated HNO_3 as a sink, recent models, including work from Ye et. al., have

incorporated particulate nitrate as a daytime source of HONO[17]. It is well known that the displacement reaction of chloride in sodium chloride, a component of sea spray aerosol (SSA), with nitrate, from nitric acid and other nitrogen oxides, in polluted atmospheres leads to sodium nitrate[19,20]. Furthermore, SSA have also been shown to contain organics compounds including aliphatic molecules such as fatty acids and amino acids and condensed aromatics that can act as photosensitizers and as notes above, the presence of these can enhance HONO formation. [21]. All of this suggests that aged SSA in the MBL could be a source of HONO.

Laboratory studies can provide insights into the mechanisms and kinetics of HONO formation; therefore, we have investigated the photochemistry of nitrate solutions to represent aged sea spray aerosols, in the presence of different photosensitizers and organic compounds to elucidate information into the relevant environmental conditions leading to HONO formation. Specifically, we have focused on measurements of gas-phase NO_2 and HONO produced from the simulated solar irradiation of nitrate in the presence of marine dissolved organic matter (m-DOM) collected from a large scale mesocosm campaign, SeaSCAPE.[22] We compared these results to nitrate solutions in the presence and absence of humic acid (HA), 4-benzoylbenzoic acid (4-BBA), and ethylene glycol (EG). HA has been used as a terrestrial proxy for m-DOM in many heterogeneous and photochemical studies, though recently deemed not a good proxy in a comparison study.[23] 4-BBA has also been used as a much simpler chemical proxy when studying photochemical sources of HONO and is a derivative of benzophenone, also a commonly used photosensitizer and also a proxy for m-DOM.[7,23] Ethylene glycol has been used in studies as a hydroxyl radical scavenger and found to also lead to an enhancement of HONO formation in the nitrate photolysis pathway[12]. These complementary measurements were used to help elucidate the enhancement mechanisms of HONO when m-DOM is present.

Additionally, the impact of pH was explored on the relative yields of NO_2 and HONO. Previously, Scharko et al. found that aqueous nitrate photolysis is a viable source of gaseous HONO, and NO_2 at pH values lower than 3.2, the pKa value for HONO[12]. Relevant to this current study is the measurements of Angle et al. that showed SSA produced from ocean waters can easily become acidified to values between pH 2 and 4 depending on size.[24] Therefore, experiments conducted in this work on the irradiation of nitrate solutions at low pH give insights into HONO and NO_2 formation in aqueous SSA aerosols due to nitrate photolysis and the effects of organics when present.

3.3 Experimental Section

3.3.1 Incoherent Broadband Cavity Enhanced Absorption Spectroscopy (IBBCEAS).

The simultaneous and quantitative measurements of gaseous HONO and NO_2 formed in these studies are accomplished using an in-house designed and constructed incoherent broadband cavity enhanced absorption spectrometer (IBBCEAS).[5,25] A simple schematic of the instrument is shown in Figure 3.1. The spectrometer consists of a 75 cm long cavity made of polytetrafluoroethylene (PTFE) with inner diameter of 2.5 cm. High reflectivity mirrors are mounted on optics holders both from CRD optics with micrometer adjustments (mirrors: 99.99% reflectivity at 370 nm, radius of curvature = 1 meter, diameter = 2.54 cm, holders: model number 902-8010). Closing caps attached to each of the mounts have inlet tubes to introduce N_2 as purge gas to keep the mirrors clean. There are an inlet and outlet ports at both ends of the cavity. The nitrogen flow containing the trace gases flows through these ports and is set using mass flow controllers. Atmospheric pressures are maintained inside the cavity.

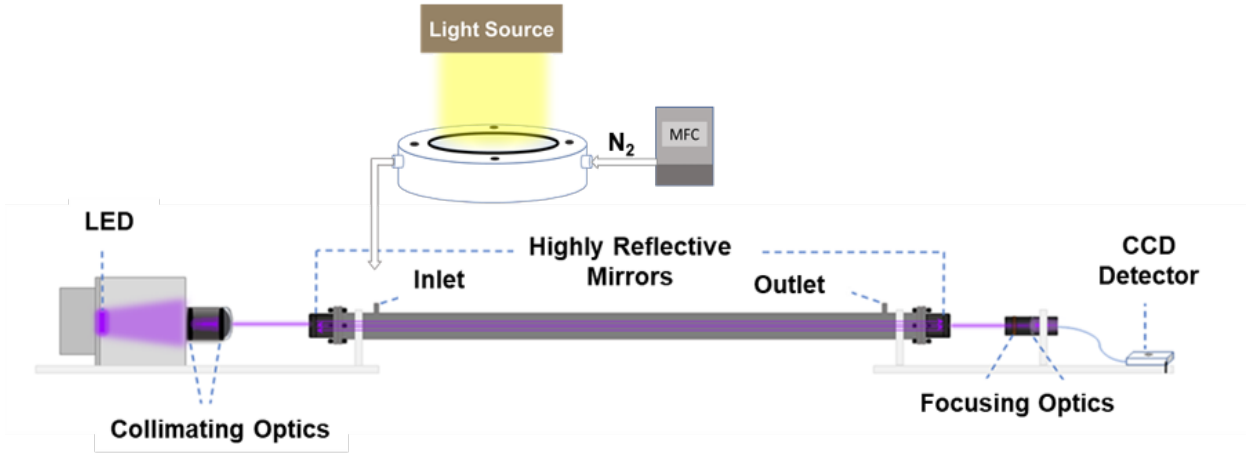

Figure 3.1 Schematic of the IBBCEAS used for NO_2 and HONO detection. The aqueous sample cell is irradiated with a solar simulator. A continuous flow of nitrogen guiding the gases produced from the irradiation of the nitrate containing solutions above the sample is sent into the cavity. LED = light emitting diode, MFC = mass flow controller, CCD = charged coupled device.

The IBBCEAS light source used is a Nichia Labs UV LED (NVSU333A, 3.640 W) that emits from 360-390 nm with a peak at 365 nm. It is mounted on a copper printed circuit board (Cree XHP-70 MCPB) which is attached to a copper plate to dissipate heat. This copper plate is further cooled by a Peltier cooler attached to an Arctic Alpine 11 plus CPU fan. To further decrease thermal heating, the copper plate is placed inside a custom aluminum housing that allows for movement in the yz and xy planes. The power output for the LED and Peltier cooler are controlled using a custom Labview program and custom circuit board interfaced with a National Instruments MyRIO device.

To align and collimate the light from the LED, the housing also contains an optics holder where two aspheric condenser lenses (Thorlabs, ACL25416U-A, diameter = 1 inch, NA = 0.79) are placed to direct the collimated light into the first mirror and then the cavity. On the other end of the cavity, a bandpass filter (Semrock, FF01-370/36-25, 25 mm) is first used to eliminate light outside the range 300-400 nm. This filtered light is directed onto a focusing lens (Thorlabs,

LA4380-UV, diameter = 1 inch, AR coated 245-400 nm, f/3.93, focal length = 100 mm) with a focal point of 10 cm onto a fiber optic (Ocean optics, PL100-2-UV-VIS, diameter = 1 mm, NA = 0.22) into a CCD detector (Ocean Optics QEPro) with a 25nm entrance slit. The resolution of the spectrometer was determined to be 0.9 nm. Spectra are taken using the accompanying software to the OceanOptics detector.

The experimental setup gives an average effective pathlength in the cavity of 1.05 km across the spectral region from 360 to 390 nm with a maximum of 1.57km at the higher wavelength region. The reflectivity and effective pathlength are determined by comparing the loss of light due to Rayleigh scattering by He and N_2, this calculation can be found in the Supporting Information. To validate the instrument, the r^2 value of actual NO_2 concentration versus instrument derived NO_2 concentration in the range from 50-125 ppb was determined to be 0.96[5].

3.3.2 Reaction cell, solar irradiation experimental setup and solution preparation.

A reaction cell was custom made of PTFE to minimize wall loss; a schematic of the experimental setup is shown in Figure 3.1. The reaction cell is custom-built and can hold 7 mL of liquid solution and has a headspace volume of 40 ml. The inlet and outlet fittings are in line with each other so as to ensure there is no unnecessarily increase of residence time of the gaseous products in the cell. The top of the sample holder is fit with a 17.35 cm^2 quartz window. The mount is kept in place through a set of screws holding the top and bottom parts of the reaction cell together. The carrier gas, Praxair UHP nitrogen, is guided into the cell at 100 sccm with PTFE ¼" tubing and is directed into the inlet of the cavity. After the reaction cell, all tubing is wrapped with black electrical tape to avoid light exposure. Directly after the reaction cell is a PTFE Pellparts

(PN 4251) aerosol filter to avoid water droplets in the lines and in the cavity. The reaction cell rests on top of aluminum blocks which is in direct contact with the metal laser table to dissipate any heat from the solar simulator.

A Newport (67005) solar simulator with a Xenon Arc lamp with the spectral output shown in Figure 3.2 is used to irradiate the samples. The reaction cell is placed 5 cm from the output to reach an irradiation intensity of 1 sun (1000 Wm^{-2}). A water filter is placed in between the reaction cell and the solar simulator and cooled with a flowing water cooler to filter out IR radiation. The spectral output in photon flux is displayed in Figure 3.2. In the same figure, the absorbance of a 100 mM $NaNO_3$ aqueous solution is also shown to show the overlap in the $n \rightarrow \pi^*$ transition of nitrate to the output of the solar simulator used in the experiments.[12]

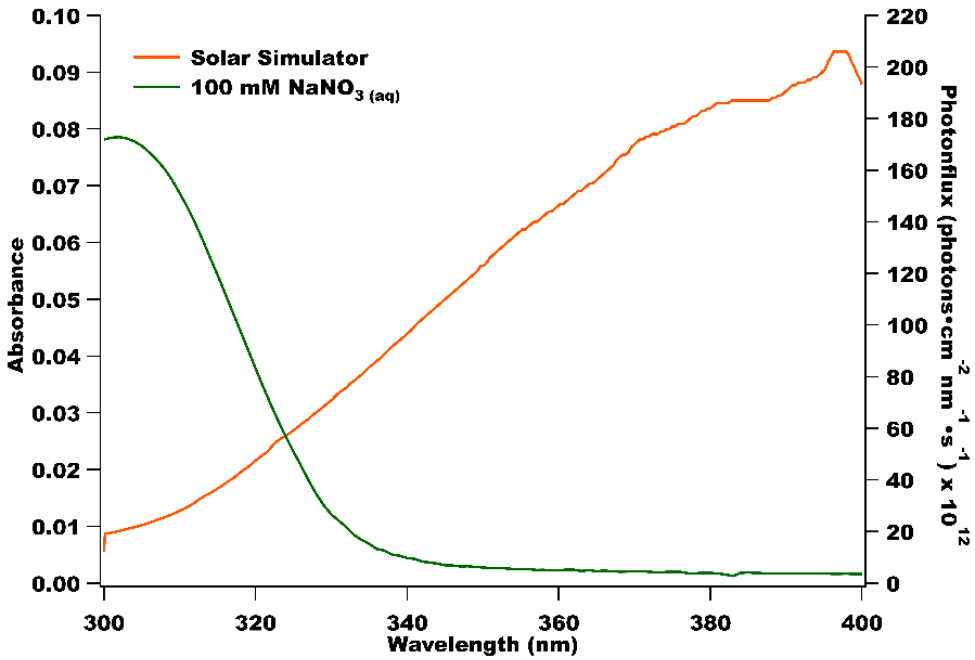

Figure 3.2 The absorption of a 100 mM $NaNO_3$ aqueous solution taken using a UV-VIS spectrophotometer is graphed in green with the y-axis of absorbance on the left and an x-axis of wavelength in nm. The spectral output of the solar simulator used for the experiments is graphed in orange. The x-axis is the same and the y-axis is on the right in units of photon flux.

All experiments were carried out in aqueous solutions of sodium nitrate with added organics and acidified to the desired pH as described in more detail below. The m-DOM used was collected from the NSF-SeaSCAPE 2019 campaign.[23] The desired concentration of m-DOM is created by weighing the dried sample and then placing in Milli-Q water and dissolved by sonication for 3 hours. The humic acid used was Suwannee River humic acid from the International Humic Substance Society, 4-BBA was from Sigma Aldrich and the ethylene glycol used was from Fischer Chemicals. Both m-DOM and HA were used at the concentration of 0.1 mg/mL. The concentration used for 4-BBA and ethylene glycol was 0.44 mM which is equivalent to 0.1mg/mL of 4-BBA. After dissolving the m-DOM in MQ water, the desired amount of Sigma Aldrich $NaNO_3$ was added and sonicated for an additional 5 minutes. Once this was completed, the pH was adjusted to the desired pH with dilute HCl. The pH for the comparison studies of the effects of the organics was adjusted to 2.0, to stay below the pKa of HONO. For the pH studies with m-DOM present, the pH was adjusted to 2.0, 3.0, 3.5, 4.0, and 7.0.

3.3.3 Determination of gas-phase HONO and NO_2 concentrations.

Prior to the beginning of the experiments, the cavity, reaction cell, and all lines are evacuated of any HONO or NO_2 by flowing N_2 for at least an hour. Following this, an off period prior to irradiation is acquired for an hour followed by the acquisition of spectra for 5 hours of irradiation and 5 hours after irradiation. The spectra are averaged 10 times and are integrated for 20 seconds, giving information every 200 seconds. The data are deconvoluted and analyzed using the Differential Optical Absorption Spectroscopy Intelligent System (DOASIS) software.[26] The software fits the experimental data and separates the contribution from different components of

the gas mixtures from the transmittance into the absorption due to HONO and NO_2 by comparing to their respective cross section reference spectra and the rest is fit to a polynomial.[27,28] More information on this can be found in a previously published paper.[5]

3.4 Results and Discussion

3.4.1 Gas-phase HONO and NO_2 from irradiated nitrate solutions

To get a baseline concentration of HONO formation from nitrate photolysis without the organic compounds present, an acidic aqueous nitrate solution at pH 2 was irradiated and the gaseous HONO and NO_2 was measured. Figure 3.3A shows the formation of HONO while the solutions were irradiated. After 2 hours, the HONO formation plateaus around 80 ppb. Figure 3.3B shows the immediate formation NO_2, which occurs within the first 200 seconds following irradiation by the solar simulator. In contrast to the HONO time course measurements, NO_2 concentrations increase sharply upon the irradiation with the solar simulator and decrease sharply with irradiation ceases. This behavior for NO_2 formation is also seen when organics are present in the solutions.

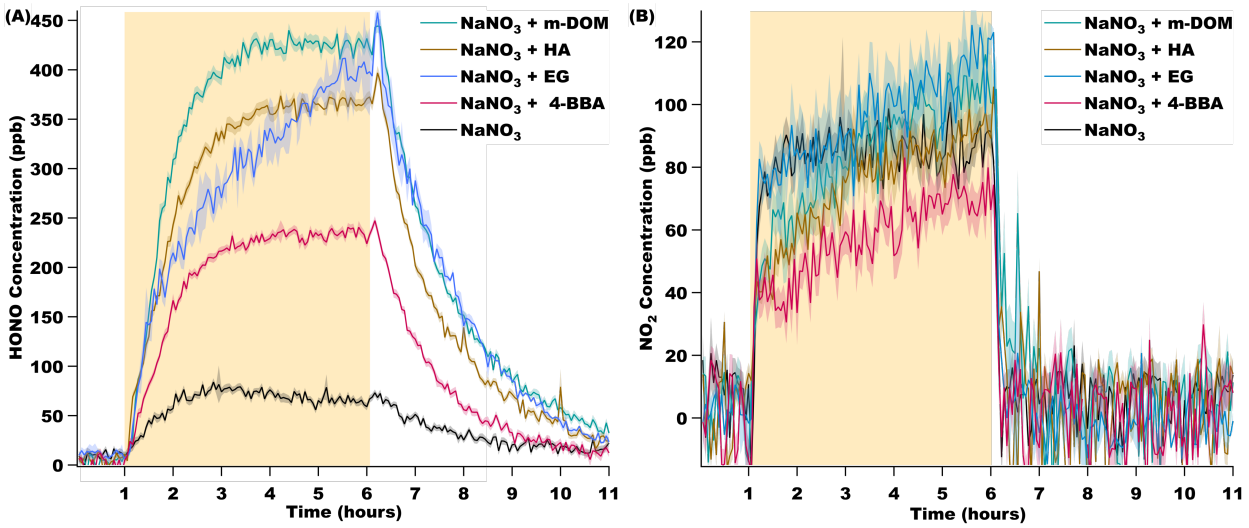

Figure 3.3 Time course profiles of HONO (A) and NO_2 (B) concentrations (in ppb) detected for solutions with 100 mM $NaNO_3$ in the presence of different organic compounds. The yellow box indicates when solutions were irradiated with the solar simulator. The error displayed on the figure as shading is one standard deviation calculated from triplicate experiments. For HONO values above the limit of detection, the error is an average of 4% of the HONO values for each point and for NO_2 it is an average of 10%. (Note: m-DOM = marine dissolved organic matter, teal; HA = humic acid, brown; EG = ethylene glycol, blue; and 4-BBA = 4-benzoylbenzoic acid, pink.)

The presence of organic compounds significantly enhances HONO concentrations by a factor of 2 to 5. In contrast, NO_2 concentrations decrease in the presence of organic compounds by 0.6 to 0.9 times that of the pure nitrate solution. In the presence of m-DOM, HONO formed up to an average 425 ppb once it reached a steady state which occurs 2 hours after the start of irradiation. Figure 3 shows that at the period in which the maximum amount of HONO was formed, NO_2 was detected at about 100 ppb. When comparing the values of HONO and NO_2 with and without m-DOM present, m-DOM enhances HONO by a factor of ca. 5 and the amount of NO_2 decreased by 10 percent. Figure 3 shows 4-BBA had a HONO enhancement factor of ca. 3. In comparison to the different compounds added to the nitrate solutions, 4-BBA had lowest enhancement, but it is still significantly more HONO than that measured from pure sodium nitrate solutions without the presence of organic compounds. Additionally, Figure 3.3B shows 4-BBA had the lowest amount

of NO_2 with the concentration being 0.6 times the amount measured in the nitrate solution alone. Interestingly for EG containing solutions, the time profile for the HONO during irradiation differed in shape compared to other solutions (Figure 3.3A). EG also showed an enhancement factor of 3.6 at 2 hours of irradiation (Figure 3.4). The solutions with EG were the only ones that did not reach a steady state emission of HONO at 2 hours of irradiation, instead HONO concentrations increased steadily for the entire time the sample was irradiated with the solar simulator. Lastly, humic acid had a similar HONO formation profile to m-DOM and 4-BBA and had an enhancement factor of ca. 4 whereas the amount of NO_2 measured at the 2-hour irradiation point decreased and was 0.8 times that of the pure sodium nitrate solution.

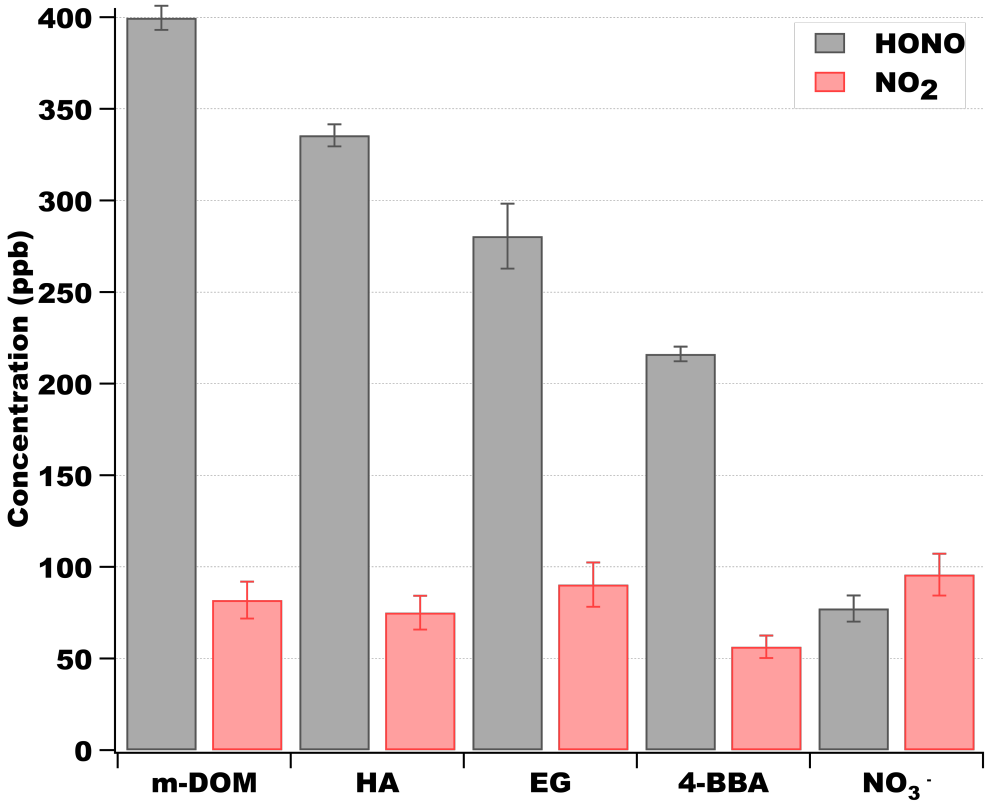

Figure 3.4 HONO (gray bars) and NO_2 (red bars) concentrations (in ppb) at 2 hours of irradiation for the different nitrate solutions. The bin labeled NO_3^- is just the sodium nitrate solution without any organic compounds added to the solution. The error bars represent the experimental error which was found to be the largest source of error. For HONO in this region, the error was about 4% of total HONO values and 10% for NO_2.

3.4.2 Surface tension measurements

To better understand the surface activity of these various organic compounds, the surface tensions were measured. Table 3.1 displays the surface tension measurements of the organic solutions at 1mg/ml without nitrate present. Samples containing EG, HA and 4-BBA show very similar surface tensions as Milli-Q water, however, samples containing m-DOM showed a marked decrease in the surface tension with a value of 65.9 ± 0.5 mN/m. Thus, components within m-DOM are highly surface active. HA has been found to lower surface tension of aqueous solutions due to the amphiphilic functional groups.[29] Compared to HA, the m-DOM solution has a lower surface tension, suggesting that m-DOM is composed of more surface-active molecules than HA. This surface activity can impact the degassing of HONO and NO_2. Table 3.1 and Figure 3.4 show that solutions containing m-DOM, the organic photosensitizer with the highest surface activity, yields the largest amount of HONO. Ongoing studies are investigating concentration dependence of HONO formation with m-DOM to determine the impact on the rate and yield of HONO with decreasing surface tension.

Table 3.1 The surface tension values of the solutions used in the experiments. The first row is the surface tension of MQ water.

Organic Present	Surface Tension without the presence of $NaNO_3$ (mN/m)
None / Milli-Q Water	72.8±0.1
Ethylene glycol	73.1±0.1
4-benzoylbenzoic acid	72.3±0.2
Suwanee River Humic Acid	72.3±0.1
m-DOM	65.9±0.5

Interestingly, solutions with EG were the only ones that slightly increased in surface tension compared to pure water. In general, there is no effect in the degassing of products as there is no microlayer of organics at the surface of the solutions containing EG. This suggests that the slow decrease of HONO concentration after the irradiation period (Figure 3.3A) is mostly due to a slower HONO formation rather than a slow degassing of products. The higher surface activity that m-DOM and HA introduce affects the rate of degassing for HONO and NO_2 differently. HONO slowly increases and decrease for all the solutions, including the ones without the presence of an organic whereas NO_2 promptly, within seconds, responds to irradiation. In a previous study, Reeser et.al reported seeing a significant change in both the degassing profiles and steady state concentrations of NO_2 detected after the irradiation of aqueous nitrate solutions in the presence of organic monolayers on the surface of the solutions and it was concluded that the difference was likely due to the orientation of the molecules at the interface, inhibiting surface adsorption and/or degassing of NO_2.[30] In the current study, there is no detectable change in the degassing of NO_2 with regards to the different organics present but there is for HONO, specifically the different profile of HONO evolution. Additionally, the different kinetic profiles found for the different organics present signifies that interactions with the walls of the experimental setup is not the main contributing factor for slow HONO kinetics.

3.4.3 Mechanisms for HONO Enhancement in the presence of organic compounds and complex organic samples (m-DOM, HA, 4-BBA and EG).

Without the presence of organics, irradiation of the acidified aqueous nitrate solutions leads to the formation of HONO and NO_2. Interestingly, NO_2 was not measured at an order of magnitude

higher than that of HONO, in contrast to the nitrate photolysis mechanism shown in Scheme 3.1A Reaction 3.1 and 3.2 would to the associated quantum yields.[31] Scharko et al. similarly reported a $HONO/NO_2$ ratio of about 1:1 for acidic sodium nitrate solutions as seen in Figure 3.4.[12] Likely, as nitrite is turned into HONO after protonation in the acidic solutions, it drives the nitrite forming reaction forward (Reaction 3.2) leading to more HONO formation. As noted previously, HONO increases and decreases slowly after a change in light, and this is presumably due to the that additionally protonation step of NO_2^- to form HONO.

Introducing organics increased the measured amount of HONO, with m-DOM being the most efficient. The chromophoric and aliphatic components of m-DOM have the ability to enhance HONO formation via two different pathways, one photochemical and another via secondary reactions[23,32–34]. Measuring HONO and NO_2 formation of irradiated sodium nitrate samples with m-DOM gives information on the significance of enhancement abilities as it would pertain to a real MBL, but it gives little information regarding the enhancement mechanisms.

Scheme 3.1 Mechanisms for HONO production. A) Nitrate photolysis in acidic aqueous solutions. B) Secondary reactions involving the superoxide radical. C) Aqueous electron reduction. D) The formation of ROS (hydroxyl radicals) from the irradiation of m-CDOM.

A. Nitrate photolysis

3.1) $NO_3^-{}_{(aq)} \xrightarrow{h\nu} NO_2^-{}_{(aq)} + O(^3P)$ Φ=0.001

3.2) $NO_3^-{}_{(aq)} \xrightarrow{h\nu\ H^+} NO_2 + OH$ Φ=0.01

3.3) $NO_2^-{}_{(aq)} + H^+ \rightarrow HONO_{(g)}$

B. Secondary reactions with superoxide radical

3.4) 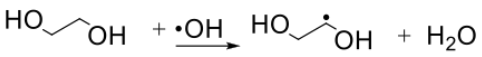

3.5) 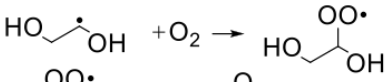

3.6) 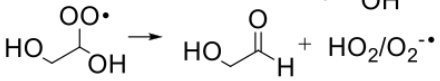

3.7) $O_2^{-\bullet} \xrightarrow{NO_2} OONO_2^- \rightarrow O_2 + NO_2^-$

3.8) $O_2^{-\bullet} \xrightarrow{NO} OONO^- \underset{}{\overset{pKa\ 6.5}{\rightleftharpoons}} OONOH$

3.9) $OONO^- + OONOH \rightarrow O_2 + 2NO_2^- + H^+$

C. Aqueous electron reduction

3.10) ^{1}m-CDOM $\xrightarrow{h\nu}$ ^{1}m−CDOM$^{+\bullet/-\bullet}$

3.11) ^{1}m−CDOM$^{+\bullet/-\bullet} \rightarrow {}^1$m−CDOM$^{+\bullet} + e^-_{(aq)}$

3.12) $e^-_{(aq)} + NO_3^-{}_{(aq)} \rightarrow NO_2^-{}_{(aq)} + O^-$

3.13) $e^-_{(aq)} + O_{2(aq)} \rightarrow O_2^{-\bullet}$

D. Release of hydroxyl radical from irradiated m-CDOM

3.14) ^{1}m-CDOM $\xrightarrow{h\nu}$ ^{3}m−CDOM*

3.15) ^{3}m−CDOM* + $H_2O \rightarrow$ m-CDOM-H + ·OH

Marine dissolved organic matter contains a significant amount of aliphatic compounds that have been proposed to enhance HONO formation in a non-photochemical pathway[23,32]. Aliphatic compounds will form superoxide radicals by reacting with OH in solution, a reaction that is dependent on the presence of dissolved oxygen[35–37]. These radicals then have secondary reactions with any NO_2 or NO solvated in the solutions that lead to an enhanced amount of HONO[38–40].

Ethylene glycol was chosen to probe this mechanism; any enhancement that is observed is assumed to be from secondary reactions with superoxide. In Scheme 3.1B, proposed mechanisms from Wang et al. were adapted to incorporate ethylene glycol as the molecule that leads to the superoxide radical (Scheme 3.1C Reactions 3.4 to 3.6)[38]. Reactions 3.7 to 3.9 in Scheme 3.1B show that NO_2 and NO present in the solution react with the superoxide radical to form more nitrite. This leads to an increase in nitrite in the solution leads to more HONO (Scheme 3.1A Reaction 3.3). Interestingly, Figure 3.3B shows more NO_2 detected in this solution compared to that with just sodium nitrate present for irradiation times over two hours. It is possible that the secondary reactions consuming the NO_2 and NO drive Reaction 3.2 forward. In turn, this may be what causes the different profile for HONO and NO_2 as well as the highest NO_2 concentrations measured after 2 hours of light exposure. Additionally, the slower formation of HONO may be attributed to the requirement of more reaction steps to occur to lead to the enhancement or the effect of the surface interactions leading to a slower degassing.

To probe the contribution due to the chromophoric components of m-DOM, the enhancement due to 4-BBA, a highly conjugated molecule, was also investigated. The literature has proposed that the highly conjugated m-DOM systems can absorb light, undergo a radical charge separation, leading to an aqueous electron (Scheme 3.1C Reactions 3.10 and 3.11)[34]. With nitrate present in the solution, we are proposing that the aqueous electron reduces nitrate into nitrite as shown in Scheme 3.1C Reaction 3.12. An enhanced amount of nitrite in an acidic solution would protonate and lead to more gaseous HONO, as shown in Reaction 3.3. The molecular compound 4-BBA was chosen as a proxy that would undergo a similar mechanism; a molecule specific mechanism is depicted in Scheme 3.2. It is highly conjugated and has the carbonyl group that can charge separate after being in the triplet state, like that shown for m-CDOM in Scheme

3.1C.[23,41]The solutions with 4-BBA present were the only ones that showed a significant difference in the amount of NO_2 measured and that can be understood by Scheme 3.1C. As nitrate is decreased in the solution, less would be available to form NO_2 via the nitrate photolysis reaction in Scheme 3.1A Reaction 3.2. However, when solvated electrons are in an aqueous solution, the more likely reaction to occur is Reaction 3.13 where the electron will form the superoxide radical when it reacts with dissolved oxygen.[37] In this scenario, the photochemical formation of the solvated electron further enhances HONO formation by feeding into reaction Scheme 3.1B Reactions 3.7-9 due to the increase in superoxide radical.

Scheme 3.2: Upon absorption of light, the molecular proxy, 4-benzoylbenzoic acid, undergoes a radical charge separation which results in the formation of a solvated electron in the solution.

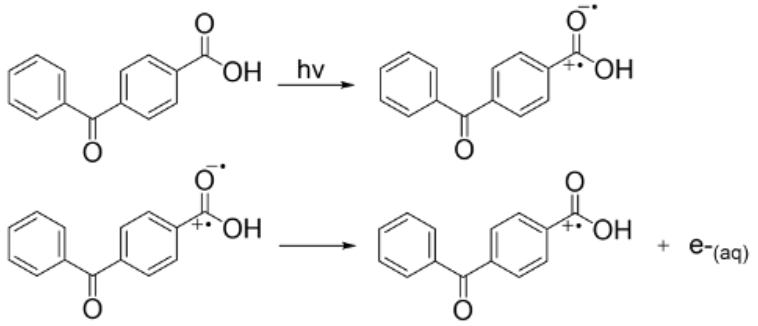

Humic acid thin films have been studied as a possible source of HONO via the photosensitized reduction of NO_2. Though it has been shown that HA is not an appropriate chemical proxy for m-DOM, mainly due the compositional differences, it was also used in this study as it is a complex system that has both chromophores and other components that are not light absorbing.[23] Previous studies of HONO formation from HA have flowed NO_2 over thin films of HA[7,13,42,43]. In the presented study, this mechanism less likely because the HA is not present in a thin film, and as seen in Figure 3.3A and B, there is an increase of HONO detected but no

corresponding decrease NO_2 detected. If HONO was being formed via this pathway, a decrease of NO_2 would be observed. Furthermore, given the amount of nitrate in solution is much greater the nitrate photochemistry pathway (Scheme 3.1A) would be more favorable. HA has been found to have high amounts of ketone, carboxylic, aromatic, and aliphatic functional groups like m-DOM[40]. However, a comparative study of HA and m-DOM found that there are compositional differences[23]. HA has a lower nitrogen content but was found to have more aromatic, condensed aromatic, and aliphatic function groups. Additionally, HA displayed lower photosensitization efficiency compared to m-DOM. A lower photosensitization efficiency may mean there is a lower triplet state efficiency. Future studies are designed to probe these mechanisms in greater detail.

Marine dissolved organic matter and humic acid are complex organic systems that contain many compounds including aliphatic compounds and light absorbing, chromophoric compounds, so it is likely that the enhancement of HONO that is measured is due to multiple enhancement pathways. In addition to an increase of superoxide radicals, it has been shown that the irradiation of m-DOM and isolates like humic acid will form hydroxyl radicals via different reaction pathways.[34] Scheme 3.1D shows the proposed pathway of H abstraction of water by triplet state m-DOM (^{3}m-DOM*) following excitation to the singlet state (^{1}m-DOM*) and subsequent intersystem crossing(Reactions 3.14 and 3.15).[45] Other photochemical mechanisms of hydroxyl radical formation include the photolysis of hydrogen peroxide which has also been measured in irradiated m-DOM samples,[46,47] low energy hydroxylation and photo-Fenton reactions all of which are discussed in detail by McKay and Rosario-Ortiz.[45] The enhancement in hydroxyl radicals with aliphatics present in m-DOM would further enhance Reaction Scheme 3.1B starting at Reaction 3.4. The OH secondary mechanism (1B) and the photochemical production of $O_2^{\cdot-}$ and ·OH (Scheme 3.1 C and D) which feed into Scheme 3.1B all are significant pathways for the

enhancement of HONO when m-DOM and HA are present in aqueous nitrate solutions. A comparison of HONO formation with EG and 4-BBA present suggests that non-photochemical superoxide formation might be greater than the photochemical formation of superoxide and hydroxyl radicals. However, it is important to note that EG and 4-BBA may not be the most efficient molecular models to show the enhancements of each enhancement mechanism. Nevertheless, seeing that m-DOM has a larger enhancement of HONO formation is important and suggests that marine organic compounds play an important role in HONO formation in the MBL.

3.4.4 HONO Formation Probed as a f(pH).

In addition to organic content of SSA, the pH of the aerosol is another factor that must be considered with regards to how it affects the HONO formation efficiency from nitrate photolysis due to the need of excess protons to protonate the nitrite ion in solution into gaseous HONO. The role of pH was previously studied for aqueous nitrate solutions by Scharko et al[12]. In the current study, the dependence of pH on HONO and NO_2 formation was also investigated in the presence of m-DOM. Figure 3.5 shows that at pH 2 and 3, a high amount of HONO is detected but at pH 3.5 it begins to decrease significantly. Even less is detected at pH 4 and at pH 7. This is due to the pH being above the pKa of HONO, causing nitrite to remain deprotonated and remaining in the solution. Interestingly, at pH 7 NO_2 decreases which was not the case for any of the other pH ranges. Reaction 3.2 of Scheme 3.1A shows that free protons are required for the reaction that forms NO_2 to progress because it is needed to form the secondary product, OH. This suggests that pH is more important for HONO formation than it is for NO_2 but most importantly, it informs that the HONO:NO_2 ratio can change as a function of pH. Recent measurements by Angle et al. have

shown that SSA is quite acidic upon formation. Total suspended aerosol pH measurements, which is a measure of the mostly supermicron sized particle, found a pH of 4 whereas for submicron SSA a value of 2 was measured.[24] These measurements of HONO and NO_2 as a function of SSA pH show that in the conditions chosen for this study, HONO formation is favorable over NO_2.

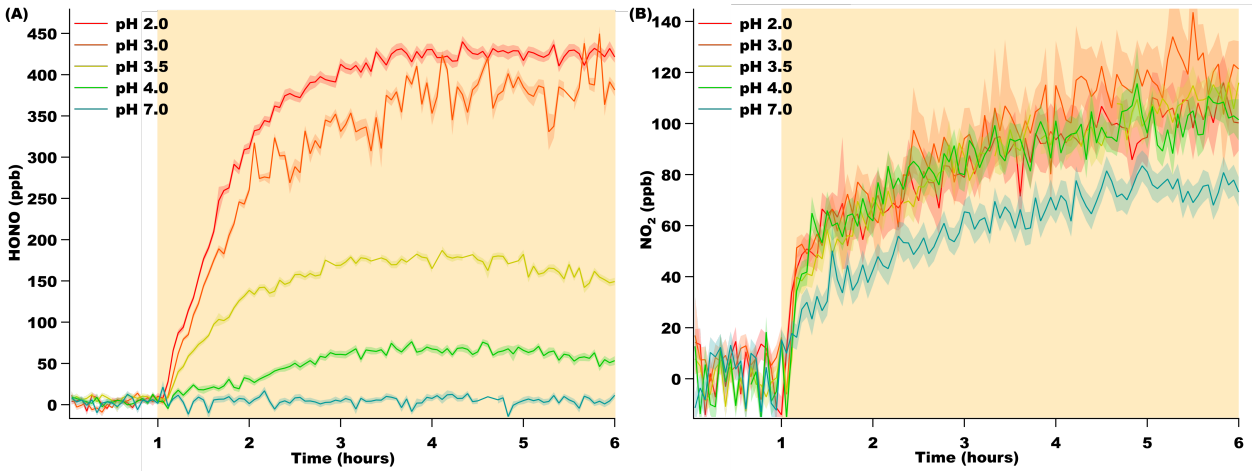

Figure 3.5 Left (A) HONO and Right (B) NO_2 values for 100 mM $NaNO_3$ + 0.1 mg/mL m-DOM solutions at varied pH values. The concentration of HONO and NO_2 are on the y-axis in ppb and the time in hours is on the x-axis. The irradiation period is denoted by the highlighted yellow region.

3.4.5 Validation of Experimental Results

The largest source of error was found to be experimental error between triplicate runs. This can be seen in Figure 3.6 where the error of each time point, denoted by shading, is larger for the average value of HONO measured compared to the single measurements. The error in the average value comes from random error is found to be less than 6% for most data points. The error displayed for the individual trials is the error calculated by the fitting program, DOASIS.[26] Furthermore, HONO and NO_2 formation was determined to be only due to nitrate photolysis and not the irradiation of the organic solutions, specifically irradiated m-DOM, 0.1mg/mL solutions of

m-DOM acidified to pH 2 were irradiated in the same manner as the solutions that contained nitrate. In Figure 3.7, it is shown that HONO and NO_2 were below the detection limit of our instrument, about 10 ppb for HONO and 15 ppb for NO_2, for the solutions that did not contain sodium nitrate. Therefore, it is confidently deduced that in this study, the HONO formation is due to nitrate photolysis with enhancements when m-DOM is present.

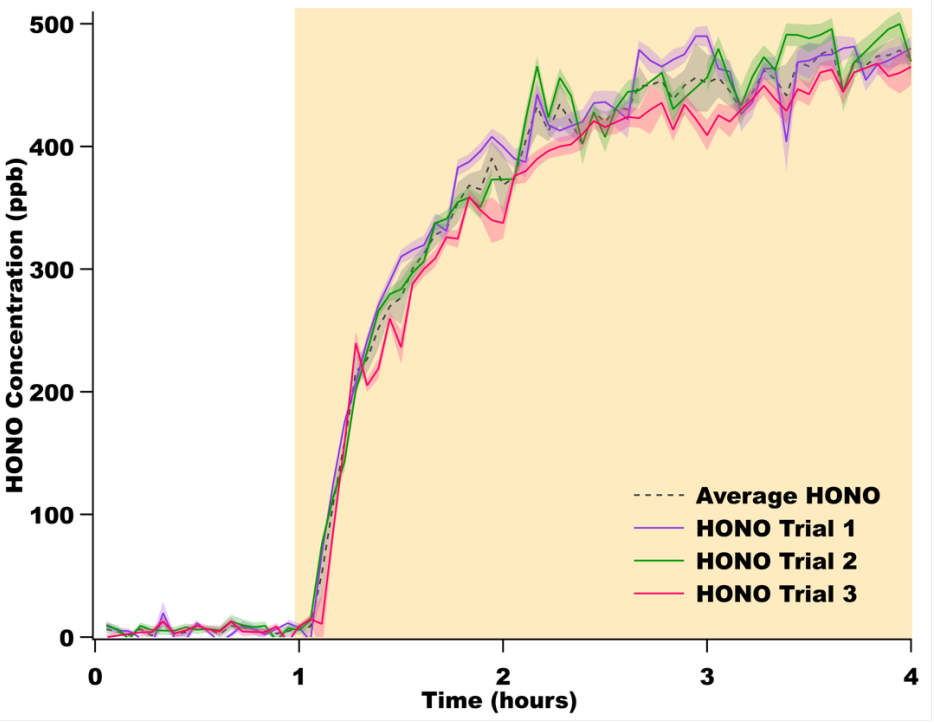

Figure 3.6 The concentration of HONO in parts per billion for three different trials of independently prepared solutions of 100 mM $NaNO_3$ + 0.1 mg/mL m-DOM adjusted to pH 2.00. The concentration is on the y-axis and the time in hours is on the x-axis. The light was turned on after a 1 hour off period and is denoted by the yellow shading. The different trials were done on separate days and their associated error, the shading, is calculated using the analysis software, DOASIS. The average was calculated and plotted in black dashed line with the error (gray shade) of 1σ.

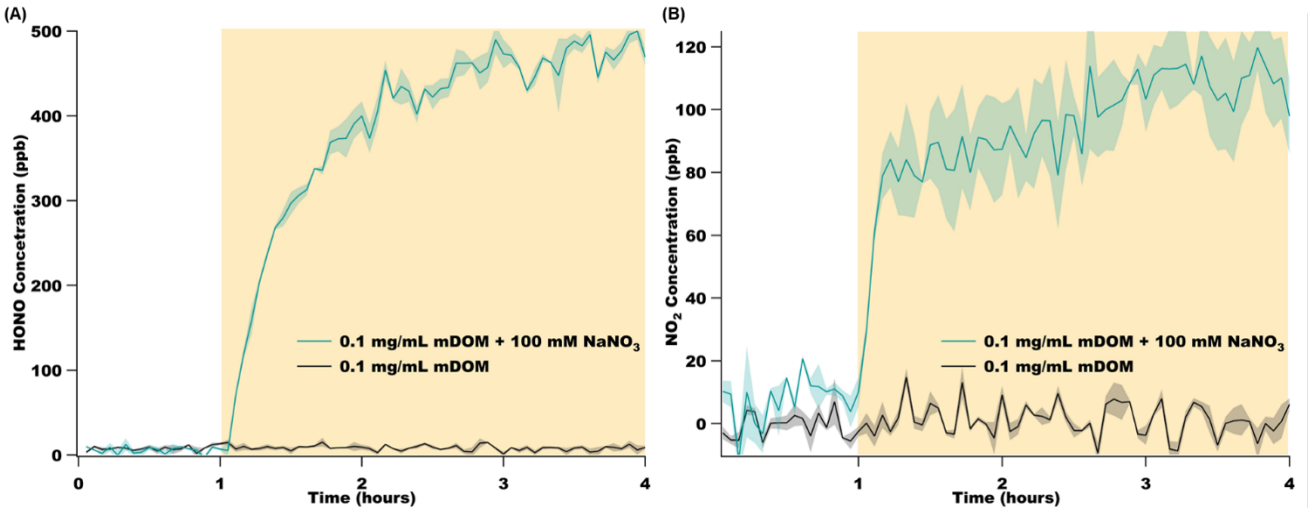

Figure 3.7 HONO (A) and NO_2 (B) concentrations in ppb for 0.1mg/mL solutions of m-DOM at pH 2.00 with and without nitrate present. Irradiation began 1 hour after the beginning of the experiment, and it is highlighted by the yellow box.

3.5 Conclusion and Atmospheric Implications

The main goal of this study was to gain insight into the sources of HONO in the marine boundary layer during the day. The findings suggest that aged sea spray aerosols that contain nitrate and m-DOM are likely a significant contributor to the elevated amounts of measured HONO in the MBL during the daytime. m-DOM from the NSF-SeaSCAPE 2019 mesocosm campaign was found to enhance HONO formation the most compared to commonly used model systems humic acid and 4-benzoylbenzoic acid as well as the non-chromophoric ethylene glycol. It is proposed that m-DOM enhances HONO formation via one pathway which is the secondary reactions of the superoxide radical with NO_2 and NO. This pathway can be enhanced photochemically by the formation of superoxide radicals when solvated electrons are formed by the charge splitting of excited m-DOM and are in the presence of water and by the formation of

hydroxyl radicals from the irradiation of m-DOM. These enhancement pathways lead to higher levels of nitrite in the solution, leading to elevated HONO formation.

These results support observations of HONO in the MBL where HONO concentrations are seen to display a diurnal cycle with a peak at noon. Nitrate photochemistry within SSA has been proposed to be the source and this current study gives insight into how marine organics present within SSA can enhance HONO formation from nitrate photolysis. This is the first study to use a complex m-DOM sample and compared to commonly used model systems as well as other complex samples such as HA. Furthermore, this study aids in the overall picture of HONO production in the atmosphere. These findings can inform atmospheric chemistry models to better understand and predict HONO formation in the MBL.

3.6 Acknowledgements

Chapter 3, in full, is a reprint of the material published by ACS Earth & Space Chemistry in: Mora García, S. L.; Pandit, S.; Navea, J. G.; Grassian, V. H. Nitrous Acid (HONO) Formation from the Irradiation of Aqueous Nitrate Solutions in the Presence of Marine Chromophoric Dissolved Organic Matter: Comparison to Other Organic Photosensitizers. *ACS Earth. Space. Chem.* **2021**, *5* (11), 3056–3064. The dissertation author was the primary investigator and author of this paper.

This work is supported by the National Science Foundation through the NSF Center for Aerosol Impacts on the Chemistry of the Environment, a Center for Chemical Innovation (CHE-1801971). The authors would like to thank Michael R. Alves for leading the effort in the large-scale collection of m-DOM from the NSF-SeaSCAPE campaign as well as his contributions to the

project in the form of discussions. Thank you to Dr. Michael N. Sullivan for his guidance and help to optimize the instrument to be used in this study as well as Dr. Jonathan Trueblood and Dr. Kristin Wall for their work in developing the instrument and experimental setup. Thank you to Prof. Mark Young and Heather Ricker for their helpful discussions.

3.7 Bibliography

(1) Alicke, B.; Geyer, A.; Hofzumahaus, A.; Holland, F.; Konrad, S.; Pätz, H. W.; Schäfer, J.; Stutz, J.; Volz-Thomas, A.; Platt, U. OH Formation by HONO Photolysis during the BERLIOZ Experiment. *J. Geophys. Res.: Atmos.* **2003**, *108* (D4), 8247.

(2) Ramazan, K. A.; Syomin, D.; Finlayson-Pitts, B. J. The Photochemical Production of HONO during the Heterogeneous Hydrolysis of NO_2. *Phys. Chem. Chem. Phys.* **2004**, *6*, 3836–3843.

(3) Kleffmann, J. Daytime Sources of Nitrous Acid (HONO) in the Atmospheric Boundary Layer. *Chem. Phys. Chem.* **2007**, *8* (8), 1137–1144.

(4) Ye, C.; Zhou, X.; Pu, D.; Stutz, J.; Festa, J.; Spolaor, M.; Tsai, C.; Cantrell, C.; Mauldin, R. L.; Campos, T.; et al. Rapid Cycling of Reactive Nitrogen in the Marine Boundary Layer. *Nature* **2016**, *532* (7600), 489–491.

(5) Pandit, S.; Mora García, S. L.; Grassian, V. H. HONO Production from Gypsum Surfaces Following Exposure to NO_2 and HNO_3 : Roles of Relative Humidity and Light Source . *Environ. Sci. Technol.* **2021**, *55* (14), 9761–9772.

(6) Perner, D.; Platt, U. Detection of Nitrous Acid in the Atmosphere by Differential Optical Absorption. *Geophys. Res. Lett.* **1979**, *6* (12), 917–920.

(7) Han, C.; Yang, W.; Wu, Q.; Yang, H.; Xue, X. Heterogeneous Photochemical Conversion

of NO_2 to HONO on the Humic Acid Surface under Simulated Sunlight. *Environ. Sci. Technol.* **2016**, *50* (10), 5017–5023.

(8) Stutz, J.; Alicke, B.; Neftel, A. Nitrous Acid Formation in the Urban Atmosphere: Gradient Measurements of NO_2 and HONO over Grass in Milan, Italy. *J. Geophys. Res. Atmos.* **2002**, *107* (22), 8192.

(9) Hofzumahaus, A.; Rohrer, F.; Lu, K.; Bohn, B.; Brauers, T.; Chang, C.; Fuchs, H.; Holland, F.; Kita, K.; Kondo, Y.; et al. Amplified Trace Gas Remocal in the Troposphere. *Science* **2009**, *324*, 1702–1705.

(10) Oswald, R.; Behrendt, T.; Ermel, M.; Wu, D.; Su, H.; Cheng, Y.; Breuninger, C.; Moravek, A.; Mougin, E.; Delon, C.; et al. HONO Emissions from Soil Bacteria as a Major Source of Atmospheric Reactive Nitrogen. *Science* **2013**, *341* (6151), 1233–1235.

(11) Finlayson-Pitts, B. J.; Wingen, L. M.; Sumner, A. L.; Syomin, D.; Ramazan, K. A. The Heterogeneous Hydrolysis of NO_2 in Laboratory Systems and in Outdoor and Indoor Atmospheres: An Integrated Mechanism. *Phys. Chem. Chem. Phys.* **2003**, *5* (2), 223–242.

(12) Scharko, N. K.; Berke, A. E.; Raff, J. D. Release of Nitrous Acid and Nitrogen Dioxide from Nitrate Photolysis in Acidic Aqueous Solutions. *Environ. Sci. Technol.* **2014**, *48*

(13) Stemmler, K.; Ammann, M.; Donders, C.; Kleffmann, J.; George, C. Photosensitized Reduction of Nitrogen Dioxide on Humic Acid as a Source of Nitrous Acid. *Nature* **2006**, *440* (7081), 195–198.

(14) Han, C.; Yang, W.; Yang, H.; Xue, X. Enhanced Photochemical Conversion of NO_2 to HONO on Humic Acids in the Presence of Benzophenone. *Environ. Pollut.* **2017**, *231* (2), 979–986.

(15) Yang, W.; Han, C.; Yang, H.; Xue, X. Significant HONO Formation by the Photolysis of

Nitrates in the Presence of Humic Acids. *Environ. Pollut.* **2018**, *243*, 679–686.

(16) Reed, C.; Evans, M. J.; Crilley, L. R.; Bloss, W. J.; Sherwen, T.; Read, K. A.; Lee, J. D.; Carpenter, L. J. Evidence for Renoxification in the Tropical Marine Boundary Layer. *Atmos. Chem. Phys.* **2017**, *17* (6), 4081–4092.

(17) Ye, C.; Zhou, X.; Pu, D.; Stutz, J.; Festa, J.; Spolaor, M.; Tsai, C.; Cantrell, C.; Mauldin Iii, R. L.; Campos, T.; et al. Rapid Cycling of Reactive Nitrogen in the Marine Boundary Layer. *Nature* **2016**, *532*, 489–491.

(18) Wen, L.; Chen, T.; Zheng, P.; Wu, L.; Wang, X.; Mellouki, A.; Xue, L.; Wang, W. Nitrous Acid in Marine Boundary Layer over Eastern Bohai Sea, China: Characteristics, Sources, and Implications. *Sci. Total Environ.* **2019**, *670*, 282–291.

(19) Ault, A. P.; Guasco, T. L.; Ryder, O. S.; Baltrusaitis, J.; Cuadra-Rodriguez, L. A.; Collins, D. B.; Ruppel, M. J.; Bertram, T. H.; Prather, K. A.; Grassian, V. H. Inside versus Outside: Ion Redistribution in Nitric Acid Reacted Sea Spray Aerosol Particles as Determined by Single Particle Analysis. *J. Am. Chem. Soc.* **2013**, *135* (39), 14528–14531.

(20) Hughes, L. S.; Allen, J. O.; Bhave, P.; Kleeman, M. J.; Cass, G. R.; Liu, D. Y.; Fergenson, D. P.; Morrical, B. D.; Prather, K. A. Evolution of Atmospheric Particles along Trajectories Crossing the Los Angeles Basin. *Environ. Sci. Technol.* **2000**, *34* (15), 3058–3068.

(21) Bertram, T. H.; Cochran, R. E.; Grassian, V. H.; Stone, E. A. Sea Spray Aerosol Chemical Composition: Elemental and Molecular Mimics for Laboratory Studies of Heterogeneous and Multiphase Reactions. *Chem. Soc. Rev.* **2018**, *47* (7), 2374–2400.

(22) Sauer, J. S.; Mayer, K. J.; Lee, C.; Alves, M. R.; Amiri, S.; Bahaveolos, C.; Barnes, E. B.; Crocker, D. R.; Dinasquet, J.; Garofalo, L. A.; et al. The Sea Spray Chemistry and Particle

Evolution Study (SeaSCAPE): Overview and Experimental Methods. *Environ. Sci.: Process. Impacts.* **2022**, *24*, 290–315.

(23) Trueblood, J. V; Alves, M. R.; Power, D.; Santander, M. V; Cochran, R. E.; Prather, K. A.; Grassian, V. H. Shedding Light on Photosensitized Reactions within Marine-Relevant Organic Thin Films. *ACS Earth Space Chem.* **2019**, *3*, 1614–1623.

(24) Angle, K. J.; Crocker, D. R.; Simpson, R. M. C.; Mayer, K. J.; Garofalo, L. A.; Moore, A. N.; Mora García, S. L.; Or, V. W.; Srinivasan, S.; Farhan, M.; et al. Acidity across the Interface from the Ocean Surface to Sea Spray Aerosol. *Proc. Natl. Acad. Sci. USA* **2021**, *118* (2), 1-6.

(25) Gherman, T.; Venables, D. S.; Vaughan, S.; Orphal, J.; Ruth, A. A. Incoherent Broadband Cavity-Enhanced Absorption Spectroscopy in the near-Ultraviolet: Application to HONO and NO_2. *Environ. Sci. Technol.* **2008**, *42* (3), 890–895.

(26) Kraus, S. DOASIS: A Framework Design for DOAS, University of Mannheim Germany, 2006.

(27) Stutz, J.; Kim, E. S.; Platt, U.; Bruno, P.; Perrino, C.; Febo, A. UV-Visible Absorption Cross Sections of Nitrous Acid. *J. Geophys. Res.: Atmos.* **2000**, *105* (D11), 14585–14592.

(28) Burrows, J. P.; Dehn, A.; Deters, B.; Himmelmann, S.; Richter, A.; Voigt, S.; Orphal, J. Atmospheric Remote-Sensing Reference Data from GOME: Part 1. Temperature-Dependent Absorption Cross-Sections of NO_2 in the 231-794 nm Range. *J. Quant. Spectrosc. Radiat. Transf.* **1998**, *60* (6), 1025–1031.

(29) Gyula, K.; Tombacz, E.; Hansson, H. Surface Tension Effects of Humic-Like Substances in the Aqueous Extract of Surface Tension Effects of Humic-Like Substances in the Aqueous Extract of Tropospheric Fine Aerosol. *J. Atmos. Chem.* **2005**, *50*, 279–294.

(30) Reeser, D. I.; Kwamena, N. O. A.; Donaldson, D. J. Effect of Organic Coatings on Gas-Phase Nitrogen Dioxide Production from Aqueous Nitrate Photolysis. *J. Phys. Chem. C* **2013**, *117* (43), 22260–22267.

(31) Zellner, R.; Exner, M.; Herrman, H. Absolute OH Quantum Yields in the Laser Photolysis of Nitrate , Nitrite and Dissolved H_2O_2 at 308 and 351 nm in the Temperature Range 278-353 K. *J. Atmos. Chem.* **1990**, *10*, 411–425.

(32) Repeta, D. J.; Quan, T. M.; Aluwihare, L. I.; Accardi, A. M. Chemical Characterization of High Molecular Weight Dissolved Organic Matter in Fresh and Marine Waters. *Geochim. Cosmochim. Acta* **2002**, *66* (6), 955–962.

(33) Carpenter, L. J.; Nightingale, P. D. Chemistry and Release of Gases from the Surface Ocean. *Chem. Rev.* **2015***, 115,* 4015-4034.

(34) Sharpless, C. M.; Blough, N. V. The Importance of Charge-Transfer Interactions in Determining Chromophoric Dissolved Organic Matter (CDOM) Optical and Photochemical Properties. *Environ. Sci.: Process. Impacts.* **2014**, *16*, 654–671.

(35) von Sonntag, C.; Schuchmann, H. -P. The Elucidation of Peroxyl Radical Reactions in Aqueous Solution with the Help of Radiation-Chemical Methods. *Angew. Chemie Int. Ed. English* **1991**, *30* (10), 1229–1253.

(36) Karpel Vel Leitner, N.; Dore, M. Hydroxyl Radical Induced Decomposition of Aliphatic Acids in Oxygenated and Deoxygenated Aqueous Solutions. *J. Photochem. Photobiol. A Chem.* **1996**, *99* (2–3), 137–143.

(37) Draper, W. M.; Crosby, D. G. Photochemical Generation of Superoxide Radical Anion in Water. *J. Agric. Food Chem.* **1983**, *31* (4), 734–737.

(38) Wang, X.; Dalton, E. Z.; Payne, Z. C.; Perrier, S.; Riva, M.; Raff, J. D.; George, C.

Superoxide and Nitrous Acid Production from Nitrate Photolysis Is Enhanced by Dissolved Aliphatic Organic Matter. *Environ. Sci. Technol. Lett.* **2021**, *8* (1), 53–58.

(39) Goldstein, S.; Czapski, G.; Lind, J.; Merenyi, G. Mechanism of Decomposition of Peroxynitric Ion (O_2NOO^-): Evidence for the Formation of $O_2^{\cdot-}$ and $^{\cdot}NO_2$ Radicals. *Inorg. Chem.* **1998**, *37* (16), 3943–3947.

(40) Gupta, D.; Harish, B.; Kissner, R.; Koppenol, W. H. Peroxynitrate Is Formed Rapidly during Decomposition of Peroxynitrite at Neutral pH. *Dalt. Trans.* **2009**, No. 29, 5730–5736.

(41) Ma, J.; Liu, Y.; Han, C.; Ma, Q.; Liu, C.; He, H. Review of Heterogeneous Photochemical Reactions of NO_y on Aerosol - A Possible Daytime Source of Nitrous Acid (HONO) in the Atmosphere. *J. Environ. Sci. (China)* **2013**, *25* (2), 326–334.

(42) George, C.; Strekowski, R. S.; Kleffmann, J.; Stemmler, K.; Ammann, M. Photoenhanced Uptake of Gaseous NO_2 on Solid Organic Compounds: A Photochemical Source of HONO *Faraday Discuss.* **2005**, *130* (2), 195–210.

(43) Scharko, N. K.; Martin, E. T.; Losovyj, Y.; Peters, D. G.; Raff, J. D. Evidence for Quinone Redox Chemistry Mediating Daytime and Nighttime NO_2-to-HONO Conversion on Soil Surfaces. *Environ. Sci. Technol.* **2017**, *51* (17), 9633–9643.

(44) Thorn, K.; Folan, D.; MacCarthy, P. Characterization of the International Humic Substances Society Standard and Reference Fulvic and Humic Acids by Solution State Carbon-13 (^{13}C) and Hydrogen (^{1}H) Nuclear Magnetic Resonance Spectrometry. *Water-Resources Investig. Rep.* **1989**, *13*, 4189-4196.

(45) McKay, G.; Rosario-Ortiz, F. L. Temperature Dependence of the Photochemical Formation of Hydroxyl Radical from Dissolved Organic Matter. *Environ. Sci. Technol.*

2015, *49* (7), 4147–4154.

(46) Cooper, W. J.; Zika, R. G.; Petasne, R. G.; Plane, J. M. C. Photochemical Formation of H_2O_2 in Natural Waters Exposed to Sunlight. *Environ. Sci. Technol.* **1988**, *22* (10), 1156–1160.

(47) Bielski, B. H. J.; Allen, A. O. Mechanism of the Disproportionation of Superoxide Radicals. *J. Phys. Chem.* **1977**, *81* (11), 1048–1050.

Chapter 4 Enhanced HONO Formation from Aqueous Nitrate Photochemistry in the Presence of Marine Relevant Organics: A Study of m-DOM Concentration on HONO Kinetics and Yields

4.1 Abstract

Nitrous acid (HONO) is a trace atmospheric gas that can photodissociate to form hydroxyl (·OH) and nitric oxide (·NO) radicals and therefore considered an important source of ·OH and a key molecule in the reactive nitrogen cycle in the atmosphere. However, sources and sinks for HONO, along with their respective significance in the chemistry of the atmosphere, are not fully understood. Recent field measurements of daytime HONO in the marine boundary layer (MBL) suggests that there is a previously unrecognized photolytic pathway, with particulate nitrate photochemistry being the most likely source. Furthermore, environmental organic compounds are hypothesized to play a role in the enhancement of photochemical formation of HONO from nitrate. Thus, marine relevant organic compounds are important to understand in the context of HONO formation in the MBL. In this study, the amount of HONO produced from aqueous nitrate photochemistry with varying concentrations of marine dissolved organic matter was quantified using an Incoherent Broadband Cavity Enhanced Absorption Spectrometer (IBBCEAS). It was found that HONO enhancement has a non-linear dependence on m-DOM concentration, with the enhancement increasing with increasing m-DOM mass concentrations (0.01 – 0.60 mg/mL) up to 0.10 mg/mL of m-DOM and decreasing after that. Here, we show that surface activity of m-DOM plays a role in both the steady state HONO yields as well as partitioning rates of HONO into the gas phase. Overall, rates of HONO formation decrease with m-DOM present in the irradiated nitrate solutions getting as low as $2.2 \pm 0.1 \times 10^{-4}$ s^{-1} for experiments where there is 0.60 mg/mL

m-DOM present compared to $6.8 \pm 0.4 \times 10^{-4}$ s^{-1} for just nitrate solutions. This study emphasizes the balance between HONO enhancement from chemical mechanisms and physical barrier caused by the surface-active compounds within m-DOM, both factors can play a role within sea spray aerosols.

4.2 Introduction

The hydroxyl (·OH) radical is the most significant atmospheric oxidizer, as it reacts with trace tropospheric gases and it is critical in the formation of both secondary organic aerosols as well as secondary marine aerosols.[1–6] Despite its significance, ·OH has been largely underrepresented in atmospheric models, mainly due to uncertainties in its sources.[7,8] A major source of ·OH in the troposphere is the photodissociation of nitrous acid, or HONO, which occurs at wavelengths between 300 to 400 nm.[9,10] Over the last decade, several formation pathways of atmospheric HONO have been reported. These include direct emissions from soils,[11] NO_2 hydrolysis,[12,13] NO_2 reduction in the presence of photosensitizers,[14,15] surface mediated reactions of nitrated surfaces,[16–19] and aqueous and particulate nitrate photolysis.[20–25] For nitrate photolysis, there are two reaction pathways, one leading to gas-phase NO_2 and the other HONO at low pH (and NO_2^- at pH greater than ca. 4).[20] These reactions occur in the wavelength region below within the tail of the solar spectrum of (i.e. 300 nm).

Most studies over the last decade have focused on photochemical pathways for HONO formation from urban areas, ice sheets, and plant leafs.[26–32] However, recently it has been suggested that the marine boundary layer (MBL) is likely a more significant source of daytime HONO, with the photoinduced reduction of nitrate as a likely source.[21–23] Additionally, despite HONO photo-dissociating within the solar actinic spectral region, its daytime concentration,

especially in the MBL, has been found to reach quasi-steady-state levels, suggesting daytime photolytic sources.[21,22,25,33] Recent field studies have found that nitrate photolysis reactions are likely the main contributor of photochemical HONO formation in the marine boundary layer (MBL).[21–23,25] The source of nitrate in the MBL comes from the displacement of chloride with nitrate in aged sea spray aerosols due to heterogeneous chemistry with gas-phase nitrogen oxides (NO_2, HNO_3, N_2O_5).[34,35]

Marine-dissolved organic matter (m-DOM) present in sea spray aerosols (SSA) has been shown to enhance the formation of HONO in the MBL due to the presence of light absorbing, photosensitizing molecular species.[36] The photosensitized reduction of NO_2 to HONO has been extensively investigated using humic acid as a chemically complex environmental photosensitizer.[14,15,20,37] Importantly, studies combining computational models and experimental work have found that the UV-Vis absorption of m-DOM falls within the range of nitrate absorption which opens up the photosensitization pathways of nitrate photolysis due to m-DOM.[38–41] We have recently shown that irradiation ($\lambda > 280$ nm) of aqueous nitrate solutions containing m-DOM, as well as solutions containing the known photosensitizer 4-benzoyl benzoic acid (4-BBA), enhance HONO formation by a factor of 5 and 3, respectively.[36] This is due to the H-abstraction of water by the photosensitizer in the triplet state generating ·OH radicals which then reacts with aliphatic compounds leading to superoxide radicals that react with the NO_2 or NO (products of nitrate photolysis) leading to enhanced amount of nitrite to yield HONO in acidic environments.[36]

In addition to evidence of photosensitized formation of HONO by m-DOM, recent studies have shown that the presence of aliphatic organic compounds, also referred to as ·OH radical scavenging organic compounds, can impact and enhance HONO formation from nitrate photolysis.[15,20,36,42] More recently, it was determined that the enhancement is due to the formation of superoxide

radicals which react with NO_2 and NO to lead to more HONO.[42] Thus the presence of aliphatic compounds, such as ethylene glycol (EG), in m-DOM also play a role in enhanced HONO yields from nitrate photochemistry. Both mechanisms are relevant in SSA because marine organic species are known to be concentrated in SSA as a result of bubble bursting mechanisms, where both aliphatic and chromophoric components have been found in SSA at higher concentrations than bulk seawater.[43–46]

Although these initial studies point to the role of m-DOM in enhancing HONO formation from nitrate photochemistry, questions remain on the effect of m-DOM concentration on the rate and amount of conversion of nitrate into HONO. In this study we investigate the impact that m-DOM concentration has on the maximum yields and partitioning rates of gas-phase HONO from nitrate photochemistry in aqueous solutions using an Incoherent Broadband Enhanced Cavity Absorption Spectrometer (IBBCEAS).

4.3 Experimental Section

4.3.1 Sample preparation, reaction cell and solar simulator light source

The experimental setup and protocol have been previously described.[36] Briefly, aqueous solutions containing 100 mM $NaNO_3$ and varying amounts of m-DOM were acidified to pH 2.00 using HCl. All irradiated m-DOM solutions were prepared from a stock 0.6 mg/mL solution. The stock solution was made by dissolving a known mass of dry m-DOM collected from the NSF-CAICE 2019 SeaSCAPE campaign[47] in Milli-Q (MQ) water, rotating the mixture at room temperature overnight. The desired amount of $NaNO_3$ (Sigma Aldrich) was added to make 100 mM $NaNO_3$ solutions and were acidified to pH 2.00 using 0.5 M HCl (Fisher Chemical). The

aqueous solutions were then placed in a custom-made PTFE (polytetrafluoroethylene) reaction cell equipped with a quartz window to allow for sample irradiation. A broadband ($\lambda > 300$ nm) ozone free 150-Watt xenon arc lamp (Newport Oriel) with an average output of 1000 Wm^{-2}, equivalent to 1 sun irradiation intensity, was positioned above the reaction cell, as shown in Figure 4.1. A water optical filter removes infrared radiation to ensure isothermal 298 K reaction conditions. The irradiation time was three hours and a steady-state HONO concentration was reached at 2.5 hours after the start of irradiation (*vide infra*).

4.3.2 Measurements of gas-phase HONO and NO_2

Gas-phase products, HONO and NO_2, formed during the photochemical reaction were measured using an in-house designed Incoherent Broadband Cavity Enhanced Absorption Spectrometer (IBBCEAS).[16,36] The experimental setup gives an average effective pathlength (L_{eff}) of 1.05 km across the spectral region from 360 to 390 nm with a maximum at the lower energy end of 1.57 km. The limit of detection for HONO and NO_2 is 10 and 15 ppb, respectively. Before conducting the experiments, the experimental system including the cavity, reaction cell, and all connecting tubing are purged with N_2 for at least one hour. After the purge, data acquisition started for an hour under dark conditions, followed by the 3 hours of irradiation. The rate of the inlet flow was set to 100 sccm into the IBBCEAS and the spectra are averaged 10 times and are integrated for 20 seconds, giving information every 200 seconds. A tensiometer (AquaPi by Kibron) was used to measure the surface tension of the solutions.

An Agilent Cary 5000 UV-Vis-NIR Spectrophotometer was used to measure the absorbance of all solutions. For the samples containing m-DOM, spectra were taken before and after three hours of

irradiation to determine m-DOM optical changes due to irradiation. The absorbance spectra of the irradiated samples were compared to that for non-irradiated solutions. Spectra were recorded for non-irradiated and irradiated solutions of 100 mM $NaNO_3$, 0.10 mg/mL m-DOM, and 100 mM $NaNO_3$ plus 0.10 mg/mL m-DOM all acidified to pH 2.

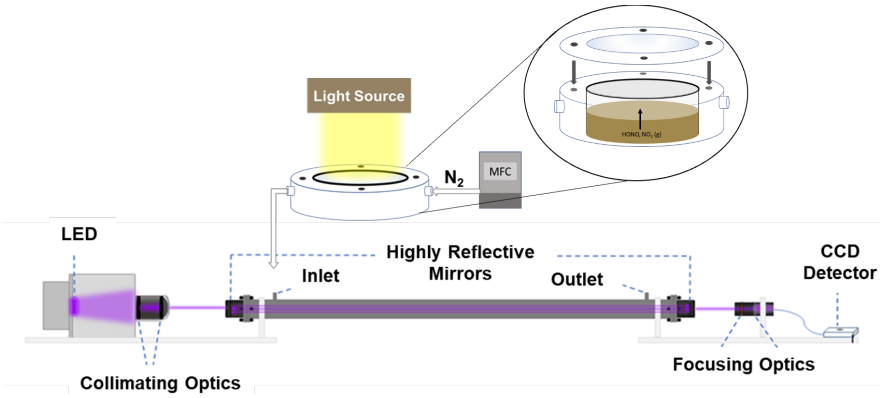

Figure 4.1 Schematic of the IBBCEAS used for NO_2 and HONO detection. The aqueous sample cell is irradiated with a broadband Xe-Arc lamp solar simulator. A continuous flow of nitrogen carries the gaseous products from the reaction cell into the cavity. LED = light emitting diode, MFC = mass flow controller, CCD = charged coupled device.

4.4 Results and Discussion

4.4.1 Characterization of nitrate and m-DOM solutions using UV-Vis Spectroscopy

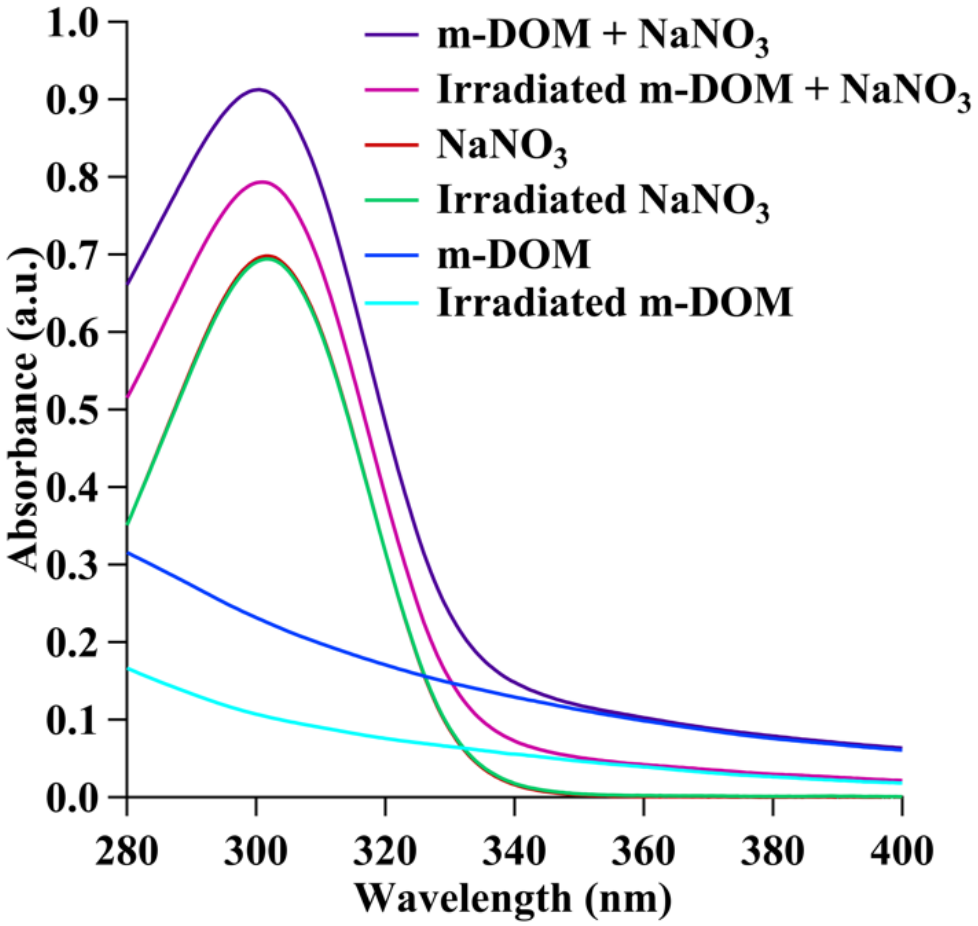

Figure 4.2 UV-Vis absorption of a 100 mM sodium nitrate solution, 0.10 mg/mL m-DOM solution, and a solution containing both sodium nitrate and m-DOM before and after a three-hour irradiation period. All solutions were acidified to pH 2.00 before irradiation.

The UV-Vis absorption spectra of the nitrate solutions with and without m-DOM show that irradiation with the solar simulator leads to a change in optical properties of only m-DOM in the solutions. The absorbance spectra of $NaNO_3$ solutions before (red) and after (green) irradiation are shown in Figure 4.2 where the characteristic absorption band with a λ_{max} at 305 nm, which

corresponds to the $n \rightarrow \pi^*$ transition of aqueous NO_3^-, is shown.[20,48] The UV-Vis absorption spectra of these solutions show no significant change in NO_3^- absorbance after three hours of broadband irradiation. This implies that the concentration of nitrate is relatively constant with respect to the amount of HONO and NO_2 being formed upon irradiation (*vide infra*). In contrast, for solutions of m-DOM alone, the spectra of m-DOM before (dark blue) and after (light blue) irradiation shows a significant decrease in absorption intensity after irradiation. Similarly, for solutions containing both NO_3^- and m-DOM there is a decrease in absorption intensity of about 15% after irradiation. Because there is no change in the nitrate solution absorbance after irradiation, in contrast to the decrease in absorbance in the solution with only m-DOM, the decrease in the solution with both nitrate and m-DOM is due to the changes in the absorption profile of m-DOM, suggesting changes in m-DOM during the course of irradiation. Although this study focuses on the gas-phase production of HONO, it can be seen that the m-DOM itself is also changing, likely oxidizing or forming organonitrates as has been previously observed by Ricker et al.[15]

In addition to UV-Vis spectroscopy, the surface activity of m-DOM was measured to better understand the role of the interface in the photosensitized formation of HONO. Measured values of the surface tension of different nitrate solutions with varying amounts of m-DOM are listed in Table 1. The initial surface tension of 73.8 ± 0.1 mN/m observed for the 100 mM $NaNO_3$ solution, in the absence of m-DOM, this value is higher than that of pure water, consistent with the behavior of solutions containing salts, which typically exhibit higher surface tensions.[49] As the concentration of m-DOM increases, the surface tension of the solution decreases from 72.3 ± 0.5 for a solution containing 0.01 mg/L m-DOM to 48.3 ± 0.1 for solutions containing 0.60 mg/mL m-DOM, suggesting that at least some of the organic compounds within m-DOM are surface active

and increasing the complexity at the interface during the photosensitized formation of gaseous HONO.

4.4.2 HONO formation from nitrate photochemistry in the presence of varying amounts of m-DOM

Solutions of 100 mM $NaNO_3$ with varying amounts of m-DOM (0, 0.01, 0.03, 0.05, 0.10, 0.20, 0.40, and 0.60 mg/mL) were irradiated with Xe-Arc broadband light. During the irradiation time, gaseous products HONO and NO_2 were measured using IBBCEAS. Figure 4.3 shows time profiles for the formation of HONO gas produced from these different solutions. The data presented in Figures 4.3A and 4.3B both show the HONO yields during the three hours period of irradiation with the solar simulator. The HONO measurements for the solutions containing only $NaNO_3$ and $NaNO_3$ plus 0.01 to 0.10 mg/mL of m-DOM are shown in Figure 4.3A, with a maximum enhancement of HONO formation taking place in solutions with 0.10 mg/mL of m-DOM. These experiments had the trend that the HONO yields increased with increasing m-DOM mass concentrations. The experiments where the solutions contained 0.20 - 0.60 mg/mL m-DOM are shown in Figure 4.3B with dashed traces as these lead to HONO enhancement in comparison to solutions containing only nitrate, but the enhancement decreased with increasing m-DOM mass concentration.

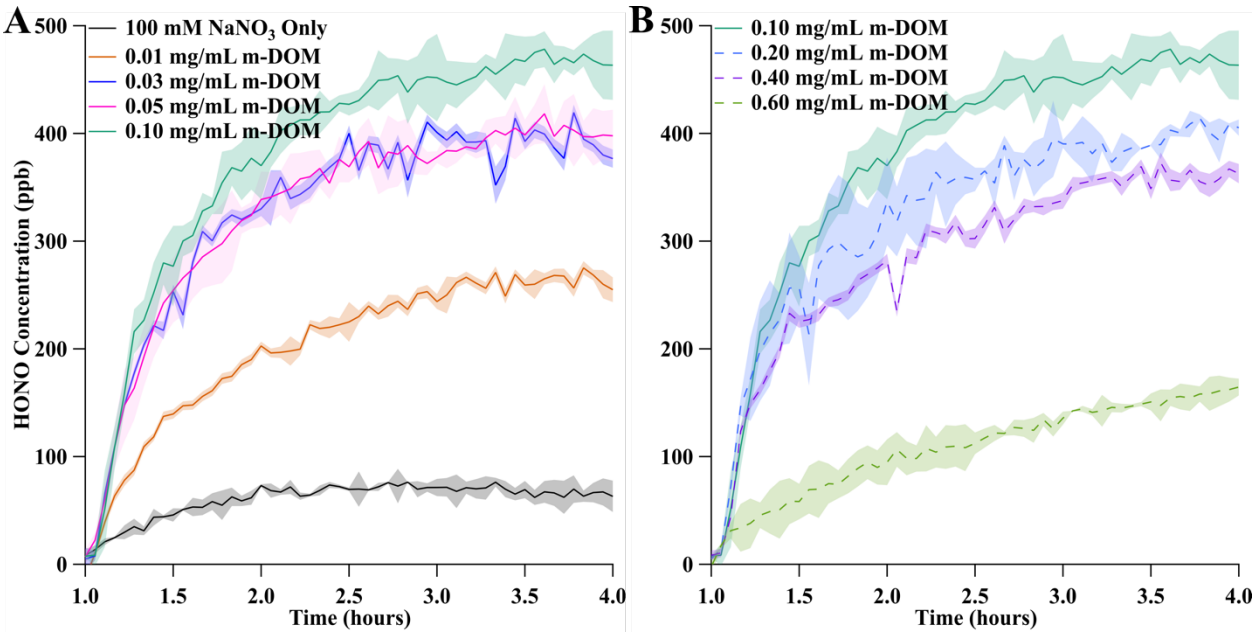

Figure 4.3 Temporal profiles of HONO formation from irradiating nitrate solutions alone and with varying m-DOM concentrations. The graph shows only the period when the samples were being irradiated which corresponds with time = 1 - 4 hours. The solid lines correspond to solutions containing 0.00 – 0.10 mg/mL m-DOM, showing an increase in enhancement with m-DOM and the dashed lines correspond to the solutions containing 0.20 – 0.60 mg/mL m-DOM as these led to an overall enhanced HONO amount but decreased with increasing m-DOM mass concentration. Shading for each curve represents either 1 standard deviation or the error associated with the fitting of data to a reference HONO cross-section spectrum.

Profiles of NO_2 yields measured for experiments containing only 100 mM $NaNO_3$ and 100 mM $NaNO_3$ plus varying m-DOM mass concentrations in mg/mL during the period of irradiation are shown in Figure 4.4. Unlike the HONO formation profiles, NO_2 reached steady state almost immediately and stayed that way for all experiments. Also different from HONO, NO_2 concentrations did not vary with a dependence on m-DOM concentration. The lack of enhancement in NO_2 formation from m-DOM supports the mechanisms suggested in previous work as they only enhance HONO and not NO_2 as well.[36] The only m-DOM mass concentration that led to a difference in NO_2 amounts was that of 0.60 mg/mL m-DOM. As will be discussed in a later section, this supports the discussion of increasing m-DOM surface coverage of the solutions

decreasing the partitioning abilities of HONO and NO_2 out of the solution.[48] The maximum measurements of HONO, $[HONO]_{Max}$, for all experiments occurred at the end of the three hour irradiation period, which was the point where the majority of the experiments reached steady state.

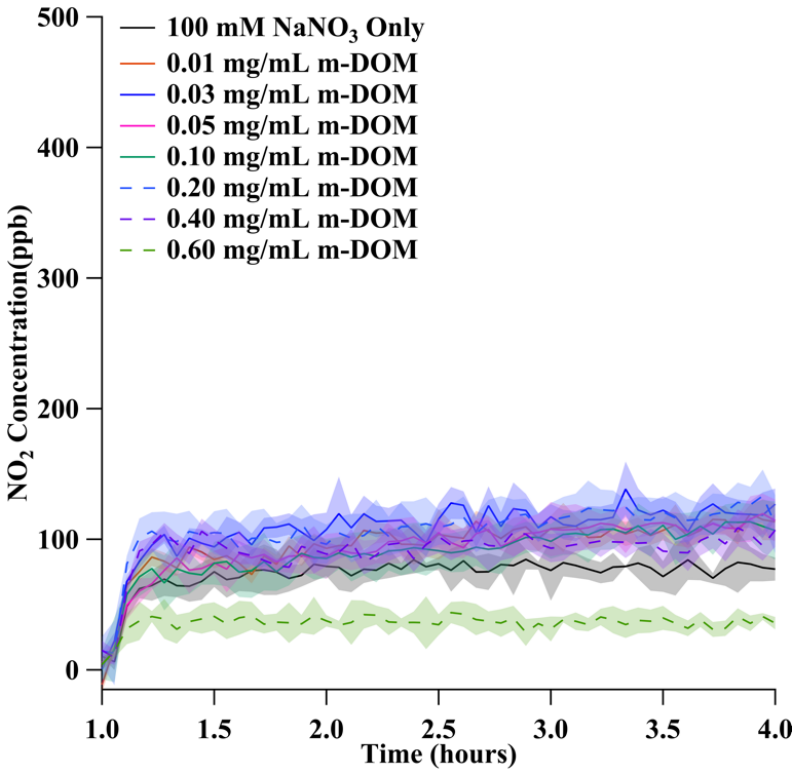

Figure 4.4 The NO_2 concentration measured in ppb during the irradiation period (t = 1 – 4 hours) of the experiments for all solutions containing acidified 100 mM $NaNO_3$ with varying amounts of m-DOM. The dashed traces correspond to the solutions that led to less HONO enhancement with increasing m-DOM concentration.

The maximum concentrations observed for HONO, $[HONO]_{Max}$, for the experiments demonstrate that the enhancement is m-DOM concentration dependent. The solutions that only contained nitrate led to a $[HONO]_{Max}$ value of 66 ppb and all amounts of m-DOM lead to more than that, increasing with increasing m-DOM concentrations up to 0.10 mg/mL where $[HONO]_{Max}$ peaked at 467 ppb. From 0.20-0.60 mg/mL, $[HONO]_{Max}$ decreased with 0.60 mg/mL m-DOM

having the lowest $[HONO]_{Max}$ at 161 ppb. These values are displayed in Figure 4.5 where it is apparent that the $[HONO]_{Max}$ has a nonlinear dependence on m-DOM mass concentrations.

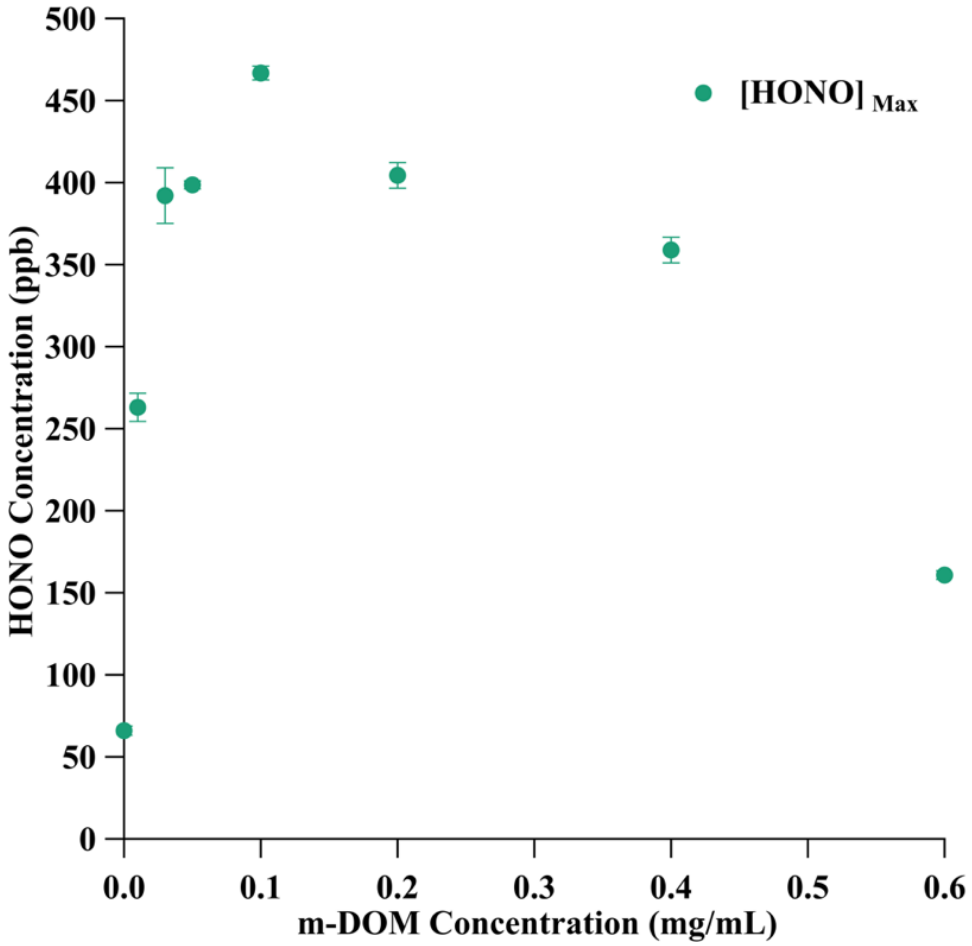

Figure 4.5 Maximum concentration of HONO in ppb measured from irradiating aqueous nitrate solutions as a function of m-DOM concentration. The error bars represent one standard deviation for the points that were taken to average the maximum HONO concentrations.

When comparing the experiments of 100 mM $NaNO_3$ plus 0.10 mg/mL m-DOM to that which only contained 100 mM $NaNO_3$ there is the greatest difference in the HONO profiles but not much for NO_2. Figure 4.6A shows HONO time profiles where there is a one-hour period before solutions are irradiated followed by a three-hour period of irradiation, denoted with the pink shading, and a five-hour period of measurement after the light is turned off. The HONO is

enhanced up 7 times at the end of the irradiation period. In contrast to this substantial difference in HONO yields, the NO_2 measurements did not change much with m-DOM in the nitrate solutions. Figure 4.6B shows the time profiles for NO_2 for the same experiments. There was no statistical difference in the measured NO_2 amounts for the first half of the irradiation period and in the second half there was a slight increase of 79 ppb for the solutions only containing nitrate and 111 ppb for the solutions containing nitrate and 0.10 mg/mL m-DOM. This lack of a significant difference in NO_2 profiles with and without m-DOM is also the case for all other m-DOM amounts except for 0.40 and 0.60 mg/mL which led to on average for the three hours 102 and 36 ppb, respectively.

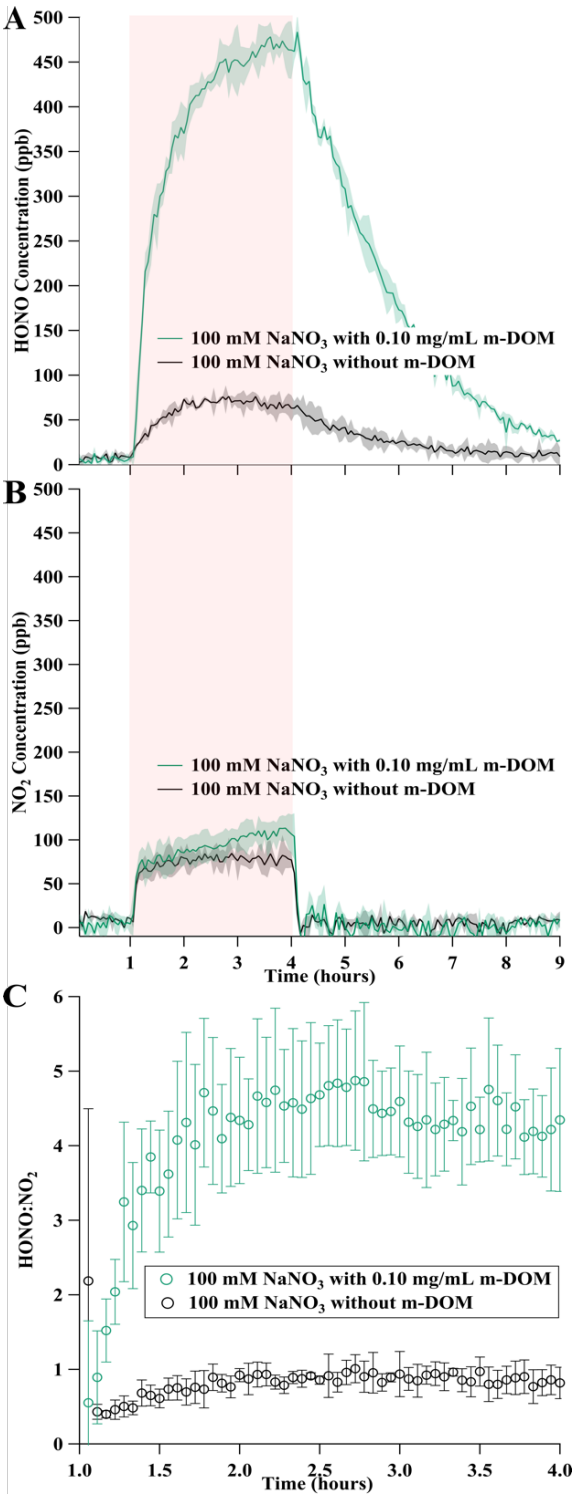

Figure 4.6 Time profile of gaseous HONO (A) and NO_2 (B) measured for solutions containing 100 mM $NaNO_3$, black trace, and 100 mM $NaNO_3$ + 0.1 mg/mL m-DOM, teal trace. The period of irradiation is denoted by the pink box in the graphs. The shading represents 1 standard deviation of triplicate experiments. (C) The HONO:NO_2 amounts for the same experiments only during the period of irradiation. The error bars represent error propagation for HONO and NO_2.

There are two major differences in the behavior of measured HONO and NO_2 gas from the irradiation of acidified nitrate solutions containing varying amounts of m-DOM. First, the profiles of HONO and NO_2 are significantly different. The rate at which NO_2 reaches steady state after the solar simulator is turned on and off is nearly immediate. In contrast, the formation of HONO takes longer to reach steady state during irradiation and its decay rate after irradiation stops is also significantly slower compared to that of NO_2. Second, once reaching steady state, the yield of NO_2 shows less significant variations compared to HONO with varying amounts of m-DOM. As mentioned above, for all experiments except those containing 0.40 and 0.60 mg/mL m-DOM, the concentration of NO_2 remains statistically similar across different m-DOM concentrations upon irradiation. These results can be attributed to the differences in the solubility of HONO and NO_2 in water. Specifically, the Henry's constant of NO_2 compared to HONO, is 2-3 orders of magnitude lower,[50,51] suggesting that measurements of NO_2 are carried out soon after its formation from nitrate photolysis compared to HONO which could be staying in solution much longer. Because HONO is significantly enhanced and NO_2 is not with m-DOM present in the irradiation of acidified nitrate solutions, the HONO:NO_2 ratios are affected by this.

The presence of m-DOM in nitrate solutions changes the measured HONO:NO_2 ratio of nitrate photolysis products. Aqueous nitrate photolysis has two product pathways, one that leads to NO_2^- and $O(^3P)$ (ϕ=0.001), and in the presence of excess protons, NO_2^- forms HONO. The other product pathway forms NO_2 and OH (ϕ=0.01).[52] From these reactions, it is expected that the HONO:NO_2 from solutions only containing $NaNO_3$ would be near 0.1 however that is not what was measured. Figure 4.6C shows that HONO:NO_2 ratio for the experiments of only nitrate and nitrate plus 0.10 mg/mL for only the period of irradiation. The experiments with only nitrate had a HONO:NO_2 ratio of ca. 0.50 for the first 30 minutes of irradiation and stabilized to 0.86 for the

rest of the experiment. The ratio being lower for the first 30 minutes is because of the slower formation rate HONO has compared to NO_2. A HONO:NO_2 ratio of 0.86 is high compared to the expected ratio of 0.10. This higher ratio, or higher than expected HONO values, comes from the fact that the solutions are acidified to pH 2.00 and as previously reported, more acidic nitrate solutions lead to more HONO being produced.[20,36] Additionally because HONO partitions out of the solution phase into the gas phase where the gas is then carried out of the reaction cell into the IBBCEAS with N_2, there is no aqueous and gas HONO equilibrium established and therefore because of Le'Chatliers Principle, more HONO is produced. For the solution containing 0.10 mg/mL m-DOM, the HONO:NO_2 is much higher. The ratio increases from ca. 0.50 to 4.33 in the first hour of irradiation. During the second hour, the ratio averages 4.63 and the last hour it averages 4.32. This decrease in the last hour of the experiment is because the NO_2 amount increases for these experiments during this point. To simplify the value, the last two hours are averaged and 100 mM $NaNO_3$ plus 0.10 mg/mL m-DOM has a HONO:NO_2 ratio of 4.47. This is ca. a five time increase in the HONO:NO_2 ratio compared to acidic aqueous nitrate photolysis without the presence of m-DOM. This HONO enhancement from marine relevant organics can increase the HONO:NO_2 up 4.47 compared to the expected 0.10 in the marine boundary layer (MBL); this is a factor that has yet to be considered in atmospheric models but should as the HONO:NO_2 is often a considered parameter.[21–23] In addition to the HONO yields, maximum measurements, and HONO:NO_2 ratios are enhanced by m-DOM, the formation and partitioning rates are affected.

This group has proposed that enhanced formation of HONO(g) by m-DOM in irradiated NO_3^-(aq) solutions via the formation of superoxide radicals, from the reaction of hydroxyl radicals with organic aliphatic compounds, followed by secondary reactions with superoxide radicals with NO and NO_2 leading to higher production of nitrite in the solution. This is furthered by the increase

in hydroxyl radicals in the solution from the hydrogen abstraction of H_2O with triplet excited state m-DOM.[36,42,53] This process increases nitrite levels in the solution, resulting in elevated HONO formation at the low pH values observed in sea spray aerosol.[54] This photo-enhanced mechanism can be simplified as the photolysis of nitrates in the absence and presence of m-DOM:

$$NO_3^-(aq) + h\nu \rightarrow NO_2^-(aq) + O(^3P). \qquad Eq.\,4.1$$

$$NO_3^-(aq) + h\nu \rightarrow NO_2(g) + O^- \qquad Eq.\,4.2$$

$$NO_3^-(aq) + h\nu \xrightarrow{m-DOM} NO_2^-(aq) + O(^3P) \qquad Eq.\,4.3$$

$$NO_3^-(aq) + h\nu \xrightarrow{m-DOM} NO_2(g) + O^- \qquad Eq.\,4.4$$

Reactions (4.1) and (4.2) represent the photolysis of aqueous NO_3^- in the absence of m-DOM.[52] Reaction (4.3) and (4.4) are a simplified reactions representing the more complex mechanism involving several different photo-enhanced pathways that lead to the increased formation of HONO and NO_2 in the presence of m-DOM.[35] The $NO_2^-(aq)$ from reactions 4.1 and 4.3 is protonated to form HONO(aq) at pH values below the pKa of HONO,[20] with the subsequent partitioning from the aqueous phase and into the gas phase, as shown below:

$$NO_2^-(aq) + H^+ \rightleftarrows HONO\,(aq) \xrightarrow{k} HONO(g) \qquad Eq.\,4.5$$

Under the experimental conditions, a continuous flow of nitrogen carries the gaseous HONO from the reaction cell into the IBBCEAS for detection, away from the solution, which prevents the establishment of the equilibrium in Reactions (4.5). The partitioning of HONO(g) of HONO into

the gas phase, as shown in Figure 4.3, follows pseudo-first order kinetics driven by Reaction (4.5), with a generalized rate law shown in Equation 4.6:

$$\frac{\mathrm{d[HONO(g)]}}{\mathrm{dt}} = k[\mathrm{HONO(aq)}] \qquad Eq\ 4.6$$

In the absence of m-DOM, the rate of formation of HONO(g) is k, while k^{m-DOM} corresponds to the rate constants in the presence of m-DOM. The integrated rate law for the formation of HONO(g) from yields:

$$[\mathrm{HONO(g)}] = [\mathrm{HONO(aq)}]_0 \left(1 - e^{-k_f^{m-DOM} t}\right) \qquad Eq.\ 4.7$$

Where k_f denotes the formation rate constant of HONO under daytime conditions, as shown in Figure 4.3. Concentrations of HONO shown in Figure 4.3, were fit to equation (4.7) to extract the formation rates of HONO(g), k_f or k_f^{m-DOM}. The fitted formation rates are summarized in Table 1.

Table 4.1 Surface tension measurements for the solutions with differing amounts of m-DOM where the first row corresponds to a solution of 100 mM $NaNO_3$ acidified to pH 2.00 with no m-DOM present. The uncertainty given is 1 standard deviation of triplicate measurements. Also in the table are the formation rates where k_{obs} observed corresponds to the solution for with no m-DOM and k_f^{m-DOM} for the solutions containing m-DOM. For simplicity, the table is labeled with the latter. The uncertainty of the formation rates represent the deviation of the slope of the fittings.

[m-DOM] (mg/mL)	**Surface Tension (mN/m)**	**Formation Rate k_f^{m-DOM} ($\times 10^{-4}$ s^{-1})**
0.00	73.8 ± 0.1	6.8 ± 0.4
0.01	72.3 ± 0.5	3.7 ± 0.1
0.03	70.0 ± 0.5	5.5 ± 0.2
0.05	66.6 ± 0.5	5.2 ± 0.1
0.10	62.3 ± 0.5	5.0 ± 0.1
0.20	50.9 ± 0.5	5.4 ± 0.2
0.40	48.5 ± 0.3	4.8 ± 0.2
0.60	48.3 ± 0.1	2.2 ± 0.1

All solutions containing any amount of m-DOM decreased the formation rate constant from (6.8 ± 0.4) x 10^{-4} s^{-1} to values at or below 5.5 x 10^{-4} s^{-1}. Notably, the difference between the solutions containing m-DOM was not significant for most cases with the average value for the experiments containing 0.03 – 0.20 mg/mL m-DOM being (5.3 ± 0.2) x 10^{-4} s^{-1}. The solution containing 0.01 mg/mL m-DOM led to a low formation constant of (3.7 ± 0.1) x 10^{-4} s^{-1} but this was one of the few experiments that was only done once and so not much can be concluded from this low formation value. The solutions that contained 0.40 and 0.60 mg/mL m-DOM led to lower k_f^{m-DOM} values of (4.8 ± 0.2) x 10^{-4} s^{-1} and (2.2 ± 0.1) x 10^{-4} s^{-1}, respectively. Both of these were lower than the average for the majority of the solutions and with the formation rate of the solutions containing the most amount of m-DOM being much lower, it is concluded that m-DOM lowers formation rates and does so with a dependence of increasing m-DOM concentration.

After 3 hours of irradiation, the broadband light was turned off with the concomitant decrease of HONO(g), as the partitioning in Reaction (4.5) is allowed to take place. The partitioning of HONO(aq) into HONO(g), was also fitted to the first-order kinetics Equation (4.8) for the solutions only containing nitrate and the solutions containing nitrate and 0.10 mg/mL m-DOM as these led to the most different amounts of m-DOM with k_d denoting the rate constant for the decay of gaseous HONO after broadband light was turned off

$$[\mathrm{HONO(g)}] = [\mathrm{HONO(g)}]_0 \left(e^{-k_d^{m-DOM} t}\right) \quad Eq\ 4.8$$

The decay rate constants do not differ from each other with the solutions containing only nitrate and those containing 0.10 mg/mL m-DOM both leading to a k_d/k_d^{m-DOM} of (1.4 ± 0.1) x 10^{-4} s^{-1}.

The surface activity of m-DOM in the aqueous nitrate solutions can explain the trends found in the HONO enhancement and observed formation rates. Evident in both the HONO formation profiles (Figure 4.3) and the $[HONO]_{Max}$ enhancement (Figure 4.5) with m-DOM present in the nitrate solutions, there is a trend where with increasing m-DOM up to 0.10 mg/mL, the HONO enhancement increases and decreases past that point. This makes 0.10 mg/mL of m-DOM present in 100 mM $NaNO_3$ acidified solutions an inflection point in the enhancement. Moreover, the observed formation rates of HONO are all lower than the rate of solutions only containing sodium nitrate, with a further decrease observed for the solutions containing the most amount of m-DOM. Interestingly, the surface tension of the solutions, found in Table 1, also decreased with increasing m-DOM mass concentration. Solutions containing 100 mM $NaNO_3$ had surface tension measurements of 73.8 ± 0.1 mN/m; the surface tension steadily decreased with

increasing m-DOM reaching as low as 48.3 ± 0.1 mN/m for solutions having 0.60 mg/mL. This decrease in surface tension is likely an indicator of surface coverage on the solutions by the surface-active compounds in m-DOM. This coverage of m-DOM can lower observed HONO enhancement in two ways. The first being that the coverage of the surface of the solutions by m-DOM can cause a physical impedance of HONO partitioning out of solution. The second being that with NO_3^-(aq) remaining water solvated in the bulk of the solution, there is a decrease the photosensitizing effect of the surface-bound m-DOM resulting in a slower rate of daytime HONO(g) formation.[23] This balance between enhancement due to the chemical mechanisms at play with the presence of m-DOM[36] and the surface activity of solutions due to m-DOM, can explain the inflection in HONO enhancement at 0.10 mg/mL of m-DOM in solution and the general lowering of formation rates of HONO.

This observation is in agreement with previous studies on the partitioning rates of NO_2 from irradiated potassium nitrate solutions, with non-polar organic compounds found to increase NO_2 solubility, while polar organics showed either no changes or small decreases in the partitioning of NO_2.[48] This solubility effect due to non-polar compounds is not likely a driving factor in the emission of HONO in this study because the organic compounds within m-DOM used in this study are assumed to be a mixture of polar and non-polar compounds, as the extraction cartridges used to extract m-DOM retain both polar and non-polar compounds.[38,55] The impact on HONO is likely attributed to the influence of surface-active m-DOM. Particularly, with the surface tension measurements of 48.3 ± 0.1 mN/m for the solution containing 0.60 mg/mL m-DOM and 48.5 ± 0.3 mN/m for the solution containing 0.40 mg/mL m-DOM, we propose that a critical surfactant concentration was reached where the m-DOM formed a monolayer on the surface. This would explain the drop in $[HONO]_{Max}$ values as well as the lower HONO formation rate for

solutions containing m-DOM. This m-DOM sample was generally characterized to be rich in polycyclic, aromatic, and unsaturated compounds;[38] meaning that, any of the present compound types could be aggregating on the surface of the solution depending on the molecules or they can be water solvated or enriched on the surface. Remarkably, the lack in change in HONO partitioning rates after exposure for solutions with only nitrate and nitrate plus 0.10 mg/mL m-DOM contradicts this explanation. Further investigation must be done in future studies to explain this difference as the HONO profiles after exposure to the solar simulator was not taken for the rest of the experiments performed here. It is important to point out that the difference in the formation rates are not artifacts of HONO sticking to the walls of the carrier lines or the instrument.

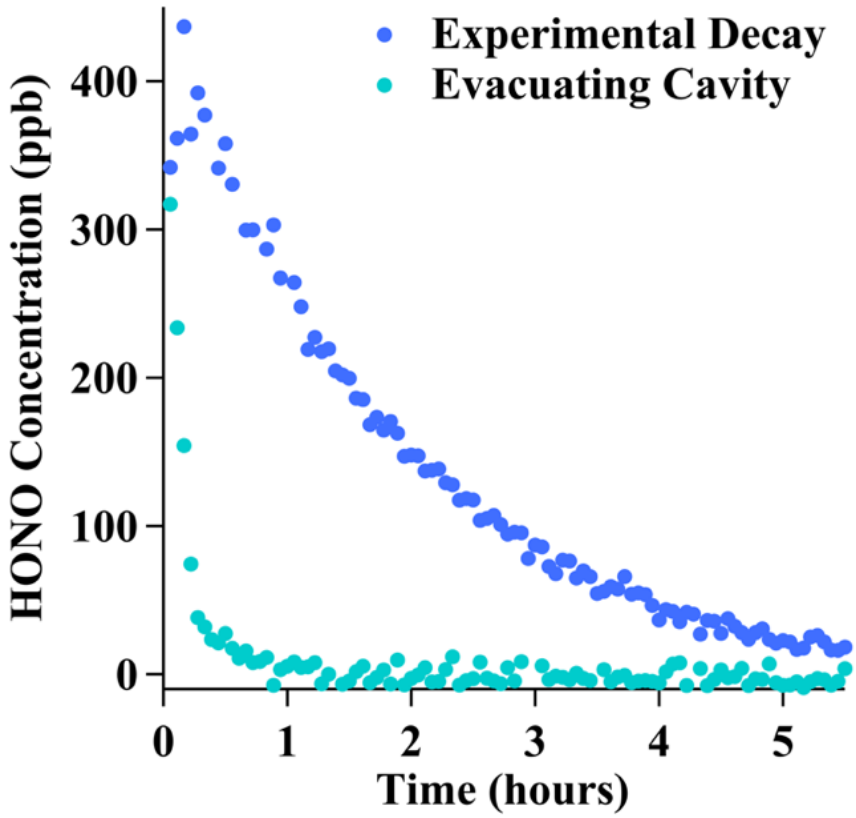

Figure 4.7 The decay (royal blue) or evacuation (cyan) of HONO was measured in the experimental set up. Time = 0 is the point where the acidified to pH 2.00 solutions of 100 mM $NaNO_3$ + 0.10 mg/mL m-DOM where no longer exposed to the solar simulator.

The HONO formation profiles for all solutions containing m-DOM shown in Figure 4.3 and the decay profiles for solutions containing only nitrate and nitrate plus 0.10 mg/mL m-DOM shown in Figure 4.6 are true kinetic observations. A control experiment was performed where solutions containing 100 mM $NaNO_3$ plus 0.10 mg/mL m-DOM was exposed to light from the Xe-Arc lamp solar simulator for three hours and the decay was measured by only turning off the lamp. This same experiment was done where the lamp was turned off as well as the path of the carrier gas from the reaction cell into the IBBCEAS was cutoff while keeping the rate of carrier gas the same. Figure 4.7 below shows that evacuation of HONO from the cavity happens within 30 minutes of cutting off the path from the reaction cell with the majority happening within the first

15 minutes. In contrast, keeping the carrier gas flowing over the reaction cell leads to a HONO decay profile that requires more than 5 hours to no longer detect HONO. Therefore, the profiles observed are indicative of kinetics of the gases partitioning into the gas and not HONO adsorbing to the walls of the experimental setup.

The enhancement in the photosensitization of nitrates to form HONO depends on m-DOM mass concentrations and can lead to an enhancement factor in the $[HONO]_{Max}$ of up to 7 times that of nitrate photolysis without the presence of m-DOM. This study builds on previous work in our group proposing that the enhancement of HONO in solutions containing m-DOM is due to both the secondary reactions of superoxide radicals with NO and NO_2 as well as the increase in hydroxyl radicals from the hydrogen abstraction of water by a triplet state chromophore.[36] In addition to these bulk solution enhancement mechanisms in HONO formation, the m-DOM surface coverage can also impact the observable partitioning of HONO where nitrate solutions led to a HONO formation rate of $6.8 \pm 0.4 \times 10^{-4}$ s^{-1} and all experiments with m-DOM present had a rate lower than that with the lowest being $2.2 \pm 0.1 \times 10^{-4}$ s^{-1}.

4.5 Conclusion and Atmospheric Impacts

The effect of varying amounts of m-DOM present in aqueous nitrate solutions on HONO formation was quantified. At the lower mass concentrations of m-DOM (0.01 – 0.10 mg/mL), the yields of HONO increase with increasing m-DOM leading to a maximum steady state concentration of 467 ppb compared to only 66 ppb for solutions only containing nitrate. Past this inflection point of 0.10 mg/mL m-DOM, increasing m-DOM concentration led to less HONO enhancement with 0.60 mg/mL m-DOM in the solution resulted in a maximum concentration of 161 ppb. This enhancement is not measured in NO_2 translating into $HONO:NO_2$ ratios of nitrate

photolysis products to increase from 0.86 for acidified nitrate solutions to 4.47 for acidified nitrate solutions in the presence of 0.10 mg/mL m-DOM. The rates of HONO partitioning into the gas phase upon irradiation lowered from $6.8 \pm 0.4 \times 10^{-4}$ s^{-1} to $2.2 \pm 0.1 \times 10^{-4}$ s^{-1} with m-DOM present. The differences in total yields, maximum concentrations, and rates of HONO from differing m-DOM amounts is attributed to higher concentrations of m-DOM decreasing the surface tension of the solutions. Higher concentrations of m-DOM lead to a physical barrier on the surface of the solutions that competes with the chemical enhancement mechanisms.

Though nitrate photolysis being the most significant source of daytime HONO formation in the MBL has been supported by many field and computational studies, all the components of the MBL conditions have not considered in the bigger picture. The enhancement of photolysis due to particulate nitrate compared to that of nitric acid has been suggested for the higher-than-expected nitrate to HONO amounts, the enhancement due to marine organics present in the environment has not. This study has provided concentration dependence of marine relevant organics on the enhancement of HONO that must be considered in MBL conditions. Though the total organic concentration in SSA is unclear, it is known that in ultrafine SSA, the composition is dominated by organic carbon (OC).[43–45] This study provides a range of what would likely be a high OC ratio SSA range for organic enhancement of HONO formation from nitrate photolysis in acidic SSA.[54]

Oceans cover over 70% of the Earth making the MBL an environment that cannot be overlooked in atmospheric chemistry. The MBL being a significant source of daytime HONO production provides a promising pathway of hydroxyl radical formation which is severely underappreciated in global atmospheric models. Nitrate photolysis in aged sea spray aerosols is likely a significant source as they have the ideal environment to lead to HONO being that nitrate is in an acidified environment and, most importantly, they are enriched in marine organics.

Enhancement reaction mechanisms have been previously proposed and with this new study, the surface coverage of marine organics has been introduced. The accumulation of marine organics on the SSA surface can affect the magnitude of HONO flux, making it an important factor to consider in the complex HONO formation factors in the MBL.

4.6 Acknowledgements

Chapter 4 contains unpublished material that has been submitted for publication in : Mora García, S. L.; Gutierrez, I.; Navea, J. G.; Grassian, V. H. Enhanced HONO Formation from Aqueous Nitrate Photochemistry in the Presence of Marine Relevant Organics: A Study of m-DOM Concentration on HONO Kinetics and Yields and the Synergistic Enhancement of Aliphatic and Photosensitizing Compounds in m-DOM. *Submitted*. The dissertation author was the primary investigator and author of this paper.

This work is supported by the National Science Foundation through the 995 NSF Center for Aerosol Impacts on the Chemistry of the Environment, a Center for Chemical Innovation (CHE-1801971). The authors would like to thank Viet Anh Nguyen for the acquisition of the UV-Vis data as well as Dr. Michael N. Sullivan, Dr. Jonathan Trueblood, and Dr. Kristin Wall for their work in the development of the experimental setup. Thank you to Prof. Mark Young and Heather Ricker for helpful discussions and Dr. Michael R. Alves for helpful discussions and his efforts in collecting m-DOM from the NSF-CAICE 2019 SeaSCAPE campaign.

4.7 Bibliography

(1) Atkinson, R.; Carter, W. P. L. Kinetics and Mechanisms of the Gas-Phase Reactions of Ozone with Organic Compounds under Atmospheric Conditions. *Chem. Rev.* **1984**, *84* (5), 437-470.

(2) Houle, F. A.; Hinsberg, W. D.; Wilson, K. R. Oxidation of a Model Alkane Aerosol by OH Radical: The Emergent Nature of Reactive Uptake. *Phys. Chem. Chem. Phys.* **2015**, *17* (6), 4412–4423.

(3) Trueblood, J. V.; Wang, X.; Or, V. W.; Alves, M. R.; Santander, M. V.; Prather, K. A.; Grassian, V. H. The Old and the New: Aging of Sea Spray Aerosol and Formation of Secondary Marine Aerosol through OH Oxidation Reactions. *ACS Earth. Space. Chem.* **2019**, *3* (10), 2307–2314.

(4) Kroll, J. H.; Lim, C. Y.; Kessler, S. H.; Wilson, K. R. Heterogeneous Oxidation of Atmospheric Organic Aerosol: Kinetics of Changes to the Amount and Oxidation State of Particle-Phase Organic Carbon. *J. Phys. Chem. A* **2015**, *119* (44), 10767–10783.

(5) Palm, B. B.; Campuzano-Jost, P.; Ortega, A. M.; Day, D. A.; Kaser, L.; Jud, W.; Karl, T.; Hansel, A.; Hunter, J. F.; Cross, E. S.; Kroll, J. H.; Peng, Z.; Brune, W. H.; Jimenez, J. L. In Situ Secondary Organic Aerosol Formation from Ambient Pine Forest Air Using an Oxidation Flow Reactor. *Atmos. Chem. Phys.* **2016**, *16* (5), 2943–2970.

(6) Leonardi, A.; Ricker, H. M.; Gale, A. G.; Ball, B. T.; Odbadrakh, T. T.; Shields, G. C.; Navea, J. G. Particle Formation and Surface Processes on Atmospheric Aerosols: A Review of Applied Quantum Chemical Calculations. *Int. J. Quantum. Chem.* **2020**, *120* (20), 1–18.

(7) Pimlott, M. A.; Pope, R. J.; Kerridge, B. J.; Latter, B. G.; Knappett, D. S.; Heard, D. E.; Ventress, L. J.; Siddans, R.; Feng, W.; Chipperfield, M. P. Investigating the Global OH

Radical Distribution Using Steady-State Approximations and Satellite Data. *Atmos. Chem. Phys.* **2022**, *22* (16), 10467–10488.

(8) Murray, L. T.; Fiore, A. M.; Shindell, D. T.; Naik, V.; Horowitz, L. W. Large Uncertainties in Global Hydroxyl Projections Tied to Fate of Reactive Nitrogen and Carbon. *Proc. Natl. Acad. Sci. USA* **2021**, *118* (43), 1–6.

(9) Perner, D.; Platt, U. Detection of Nitrous Acid in the Atmosphere by Differential Optical Absorption. *Geophys. Res. Lett.* **1979**, *6* (12), 917–920.

(10) Platt, U. The Origin of Nitrous and Nitric Acid in the Atmosphere. In *Chemistry of Multiphase Atmospheric Systems*; Wolfgang Jaeschke, Ed.; Springer Berlin Heidelberg: Berlin, 1986; pp 299–319.

(11) Oswald, R.; Behrendt, T.; Ermel, M.; Wu, D.; Su, H.; Cheng, Y.; Breuninger, C.; Moravek, A.; Mougin, E.; Delon, C.; Loubet, B.; Pommerening-Röser, A.; Sörgel, M.; Pöschl, U.; Hoffmann, T.; Andreae, M. O.; Meixner, F. X.; Trebs, I. HONO Emissions from Soil Bacteria as a Major Source of Atmospheric Reactive Nitrogen. *Science* **2013**, *341*, 1233–1235.

(12) Ramazan, K. A.; Syomin, D.; Finlayson-Pitts, B. J. The Photochemical Production of HONO during the Heterogeneous Hydrolysis of NO_2. *Phys. Chem. Chem. Phys.* **2004**, *6*, 3836–3843.

(13) Finlayson-Pitts, B. J.; Wingen, L. M.; Sumner, A. L.; Syomin, D.; Ramazan, K. A. The Heterogeneous Hydrolysis of NO_2 in Laboratory Systems and in Outdoor and Indoor Atmospheres: An Integrated Mechanism. *Phys. Chem. Chem. Phys.* **2003**, *5* (2), 223–242.

(14) Stemmler, K.; Ammann, M.; Donders, C.; Kleffmann, J.; George, C. Photosensitized Reduction of Nitrogen Dioxide on Humic Acid as a Source of Nitrous Acid. *Nature* **2006**, *440* (7081), 195–198.

(15) Ricker, H. M.; Leonardi, A.; Navea, J. G. Reduction and Photoreduction of NO_2 in Humic Acid Films as a Source of HONO, ClNO, N_2O, NO_X, and Organic Nitrogen. *ACS Earth. Space. Chem.* **2022**, *6* (12), 3066–3077.

(16) Pandit, S.; Mora García, S. L.; Grassian, V. H. HONO Production from Gypsum Surfaces Following Exposure to NO_2 and HNO_3: Roles of Relative Humidity and Light Source. *Environ. Sci. Technol.* **2021**, *55* (14), 9761–9772.

(17) Ostaszewski, C. J.; Stuart, N. M.; Lesko, D. M. B.; Kim, D.; Lueckheide, M. J.; Navea, J. G. Effects of Coadsorbed Water on the Heterogeneous Photochemistry of Nitrates Adsorbed on TiO_2. *J. Phys. Chem.* **2018**, *122*, 6360–6371.

(18) Lesko, D. M. B.; Coddens, E. M.; Swomley, H. D.; Welch, R. M.; Borgatta, J.; Navea, J. G. Photochemistry of Nitrate Chemisorbed on Various Metal Oxide Surfaces. *Phys. Chem. Chem. Phys* **2015**, *17*, 20775.

(19) Navea, J. G.; Grassian, V. H. Photochemistry of Atmospheric Particles. In *Encyclopedia of Interfacial Chemistry*; Klaus Wandelt, Ed.; Elsevier, 2018; pp 553–562.

(20) Scharko, N. K.; Berke, A. E.; Raff, J. D. Release of Nitrous Acid and Nitrogen Dioxide from Nitrate Photolysis in Acidic Aqueous Solutions. *Environ. Sci. Technol.* **2014**, *48* (20), 11991–12001.

(21) Ye, C.; Zhou, X.; Pu, D.; Stutz, J.; Festa, J.; Spolaor, M.; Tsai, C.; Cantrell, C.; Mauldin, R. L.; Campos, T.; Weinheimer, A.; Hornbrook, R. S.; Apel, E. C.; Guenther, A.; Kaser, L.; Yuan, B.; Karl, T.; Haggerty, J.; Hall, S.; Ullmann, K.; Smith, J. N.; Ortega, J.; Knote, C.

Rapid Cycling of Reactive Nitrogen in the Marine Boundary Layer. *Nature* **2016**, *532* (7600), 489–491.

(22) Reed, C.; Evans, M. J.; Crilley, L. R.; Bloss, W. J.; Sherwen, T.; Read, K. A.; Lee, J. D.; Carpenter, L. J. Evidence for Renoxification in the Tropical Marine Boundary Layer. *Atmos. Chem. Phys.* **2017**, *17* (6), 4081–4092.

(23) Andersen, S. T.; Carpenter, L. J.; Reed, C.; Lee, J. D.; Chance, R.; Sherwen, T.; Vaughan, A. R.; Stewart, J.; Edwards, P. M.; Bloss, W. J.; Sommariva, R.; Crilley, L. R.; Nott, G. J.; Neves, L.; Read, K.; Heard, D. E.; Seakins, P. W.; Whalley, L. K.; Boustead, G. A.; Fleming, L. T.; Stone, D.; Fomba, K. W. Extensive Field Evidence for the Release of HONO from the Photolysis of Nitrate Aerosols. *Sci. Adv.* **2023**, *9* (3), 1–10.

(24) Gen, M.; Liang, Z.; Zhang, R.; Go Mabato, B. R.; Chan, C. K. Particulate Nitrate Photolysis in the Atmosphere. *Environ. Sci.: Atmos*. **2022**, 2, 111–127.

(25) Kasibhatla, P.; Sherwen, T.; Evans, M. J.; Carpenter, L. J.; Reed, C.; Alexander, B.; Chen, Q.; Sulprizio, M. P.; Lee, J. D.; Read, K. A.; Bloss, W.; Crilley, L. R.; Keene, W. C.; Pszenny, A. A. P.; Hodzic, A. Global Impact of Nitrate Photolysis in Sea-Salt Aerosol on NOx, OH, and O_3 in the Marine Boundary Layer. *Atmos. Chem. Phys.* **2018**, *18* (15), 11185–11203.

(26) Baergen, A. M.; Donaldson, D. J. Photochemical Renoxification of Nitric Acid on Real Urban Grime. *Environ. Sci. Technol.* **2013**, *47* (2), 815–820.

(27) Liu, J.; Deng, H.; Li, S.; Jiang, H.; Mekic, M.; Zhou, W.; Wang, Y.; Loisel, G.; Wang, X.; Gligorovski, S. Light-Enhanced Heterogeneous Conversion of NO_2 to HONO on Solid Films Consisting of Fluorene and Fluorene/Na_2SO_4: An Impact on Urban and Indoor Atmosphere. *Environ. Sci. Technol.* **2020**, *54* (18), 11079–11086.

(28) Liu, J.; Li, S.; Mekic, M.; Jiang, H.; Zhou, W.; Loisel, G.; Song, W.; Wang, X.; Gligorovski, S. Photoenhanced Uptake of NO_2 and HONO Formation on Real Urban Grime. *Environ. Sci. Technol. Lett.* **2019**, *6* (7), 413–417.

(29) Liu, J.; Li, B.; Deng, H.; Yang, Y.; Song, W.; Wang, X.; Luo, Y.; Francisco, J. S.; Li, L.; Gligorovski, S. Resolving the Formation Mechanism of HONO via Ammonia-Promoted Photosensitized Conversion of Monomeric NO_2 on Urban Glass Surfaces. *J. Am. Chem. Soc.* **2023**, *145* (21), 11488–11493.

(30) Anastasio, C.; Liang, C. Photochemistry of Nitrous Acid (HONO) and Nitrous Acidium Ion (H_2ONO^+) in Aqueous Solution and Ice. *Environ. Sci. Technol.* **2009**, *43* (4), 1108–1114.

(31) Zhou, X.; Zhang, N.; Teravest, M.; Tang, D.; Hou, J.; Bertman, S.; Alaghmand, M.; Shepson, P. B.; Carroll, M. A.; Griffith, S.; Dusanter, S.; Stevens, P. S. Nitric Acid Photolysis on Forest Canopy Surface as a Source for Tropospheric Nitrous Acid. *Nat. Geosci.* **2011**, *4* (7), 440–443.

(32) Sörgel, M.; Trebs, I.; Serafimovich, A.; Moravek, A.; Held, A.; Zetzsch, C. Simultaneous HONO Measurements in and above a Forest Canopy: Influence of Turbulent Exchange on Mixing Ratio Differences. *Atmos. Chem. Phys.* **2011**, *11*, 841–855.

(33) Vogel, B.; Vogel, H.; Kleffmann, J.; Kurtenbach, R. Measured and Simulated Vertical Profiles of Nitrous Acid - Part II. Model Simulations and Indications for a Photolytic Source. *Atmos. Environ.* **2003**, *37* (21), 2957–2966.

(34) Ault, A. P.; Guasco, T. L.; Ryder, O. S.; Baltrusaitis, J.; Cuadra-Rodriguez, L. A.; Collins, D. B.; Ruppel, M. J.; Bertram, T. H.; Prather, K. A.; Grassian, V. H. Inside versus Outside: Ion Redistribution in Nitric Acid Reacted Sea Spray Aerosol Particles as Determined by Single Particle Analysis. *J. Am. Chem. Soc.* **2013**, *135* (39), 14528–14531.

(35) Hughes, L. S.; Allen, J. O.; Bhave, P.; Kleeman, M. J.; Cass, G. R.; Liu, D. Y.; Fergenson, D. P.; Morrical, B. D.; Prather, K. A. Evolution of Atmospheric Particles along Trajectories Crossing the Los Angeles Basin. *Environ. Sci. Technol.* **2000**, *34* (15), 3058–3068.

(36) Mora García, S. L.; Pandit, S.; Navea, J. G.; Grassian, V. H. Nitrous Acid (HONO) Formation from the Irradiation of Aqueous Nitrate Solutions in the Presence of Marine Chromophoric Dissolved Organic Matter: Comparison to Other Organic Photosensitizers. *ACS Earth. Space. Chem.* **2021**, *5* (11), 3056–3064.

(37) Han, C.; Yang, W.; Wu, Q.; Yang, H.; Xue, X. Heterogeneous Photochemical Conversion of NO_2 to HONO on the Humic Acid Surface under Simulated Sunlight. *Environ. Sci. Technol.* **2016**, *50* (10), 5017–5023.

(38) Alves, M. R.; Coward, E. K.; Gonzales, D.; Sauer, J. S.; Mayer, K. J.; Prather, K. A.; Grassian, V. H. Changes in Light Absorption and Composition of Chromophoric Marine-Dissolved Organic Matter across a Microbial Bloom. *Environ. Sci.: Process. Impacts.* **2022**, *24* (10), 1923–1933.

(39) Karimova, N. V.; Alves, M. R.; Luo, M.; Grassian, V. H.; Gerber, R. B. Toward a Microscopic Model of Light Absorbing Dissolved Organic Compounds in Aqueous Environments: Theoretical and Experimental Study. *Phys. Chem. Chem. Phys.* **2021**, *23* (17), 10487–10497.

(40) Karimova, N. V.; Luo, M.; Grassian, V. H.; Benny Gerber, R. Absorption Spectra of Benzoic Acid in Water at Different pH and in the Presence of Salts: Insights from the Integration of Experimental Data and Theoretical Cluster Models. *Phys. Chem. Chem. Phys.* **2020**, *22* (9), 5046–5056.

(41) Karimova, N.; Alija, O.; Mora García, S. L.; Grassian, V. H.; Gerber, R. B.; Navea, J. G. pH Dependence of the Speciation and Optical Properties of 4-Benzoylbenzoic Acid. *Phys. Chem. Chem. Phys.* **2023**, *25*, 17306–17319.

(42) Wang, X.; Dalton, E. Z.; Payne, Z. C.; Perrier, S.; Riva, M.; Raff, J. D.; George, C. Superoxide and Nitrous Acid Production from Nitrate Photolysis Is Enhanced by Dissolved Aliphatic Organic Matter. *Environ. Sci. Technol. Lett.* **2021**, *8* (1), 53–58.

(43) Bertram, T. H.; Cochran, R. E.; Grassian, V. H.; Stone, E. A. Sea Spray Aerosol Chemical Composition: Elemental and Molecular Mimics for Laboratory Studies of Heterogeneous and Multiphase Reactions. *Chem. Soc. Rev.* **2018**, *47* (7), 2374–2400.

(44) Cochran, R. E.; Laskina, O.; Jayarathne, T.; Laskin, A.; Laskin, J.; Lin, P.; Sultana, C.; Lee, C.; Moore, K. A.; Cappa, C. D.; Bertram, T. H.; Prather, K. A.; Grassian, V. H.; Stone, E. A. Analysis of Organic Anionic Surfactants in Fine and Coarse Fractions of Freshly Emitted Sea Spray Aerosol. *Environ. Sci. Technol.* **2016**, *50* (5), 2477–2486.

(45) Ault, A. P.; Moffet, R. C.; Baltrusaitis, J.; Collins, D. B.; Ruppel, M. J.; Cuadra-Rodriguez, L. A.; Zhao, D.; Guasco, T. L.; Ebben, C. J.; Geiger, F. M.; Bertram, T. H.; Prather, K. A.; Grassian, V. H. Size-Dependent Changes in Sea Spray Aerosol Composition and Properties with Different Seawater Conditions. *Environ. Sci. Technol.* **2013**, *47* (11), 5603–5612.

(46) Quinn, P. K.; Collins, D. B.; Grassian, V. H.; Prather, K. A.; Bates, T. S. Chemistry and Related Properties of Freshly Emitted Sea Spray Aerosol. *Chem. Rev*., **2015**, 115, 4383–4399.

(47) Sauer, J. S.; Mayer, K. J.; Lee, C.; Alves, M. R.; Amiri, S.; Bahaveolos, C.; Barnes, E. B.; Crocker, D. R.; Dinasquet, J.; Garofalo, L. A.; Kaluarachchi, C. P.; Dang, D.; Kilgour, D.; Mael, L.; Mitts, B. A.; Moon, D. R.; Morris, C. K.; Moore, A. N.; Ni, C.-M.; Pendergraft,

M. A.; Petras, D.; Simpson, R.; Smith, S.; Tumminello, P. R.; Walker, J. L.; DeMott, P. J.; Farmer, D. K.; Goldstein, A. H.; Grassian, V. H.; Jaffe, J. S.; Malfatti, F.; Martz, T. R.; Slade, J.; Tivanski, A. V.; Bertram, T. H.; Cappa, C. D.; Prather, K. A. The Sea Spray Chemistry and Particle Evolution Study (SeaSCAPE): Overview and Experimental Methods. *Environ. Sci.: Process. Impacts.* **2022**, *24*, 290–315.

(48) Reeser, D. I.; Kwamena, N. O. A.; Donaldson, D. J. Effect of Organic Coatings on Gas-Phase Nitrogen Dioxide Production from Aqueous Nitrate Photolysis. *J. Phys. Chem. C* **2013**, *117* (43), 22260–22267.

(49) Zhang, C.; Carloni, P. Salt Effects on Water/Hydrophobic Liquid Interfaces: A Molecular Dynamics Study. *J. Phys.: Condens. Matter.* **2012**, *24* (12).

(50) *NIST Chemistry WebBook Nitrogen Dioxide https://webbook.nist.gov/cgi/cbook.cgi?ID=C10102440&Mask=10#Solubility. (Accessed February 2023)*.

(51) *NIST Chemistry WebBook Nitrous Acid https://webbook.nist.gov/cgi/cbook.cgi?ID=C7782776&Mask=10#Solubility. (Accessed February 2023)*.

(52) Mack, J.; Bolton, J. R. Photochemistry of Nitrite and Nitrate in Aqueous Solution: A Review. *J. Photochem. Photobiol. A Chem.* **1999**, *128*, 1–13.

(53) McKay, G.; Rosario-Ortiz, F. L. Temperature Dependence of the Photochemical Formation of Hydroxyl Radical from Dissolved Organic Matter. *Environ. Sci. Technol.* **2015**, *49* (7), 4147–4154.

(54) Angle, K. J.; Crocker, D. R.; Simpson, R. M. C.; Mayer, K. J.; Garofalo, L. A.; Moore, A. N.; Mora García, S. L.; Or, V. W.; Srinivasan, S.; Farhan, M.; Sauer, J. S.; Lee, C.; Pothier,

M. A.; Farmer, D. K.; Martz, T. R.; Bertram, T. H.; Cappa, C. D.; Prather, K. A.; Grassian, V. H. Acidity across the Interface from the Ocean Surface to Sea Spray Aerosol. *Proc. Natl. Acad. Sci. USA* **2021**, *118* (2), 1–6.

(55) Dittmar, T.; Koch, B.; Hertkorn, N.; Kattner, G. A Simple and Efficient Method for the Solid-Phase Extraction of Dissolved Organic Matter (SPE-DOM) from Seawater. *Limnol. Oceanogr. Methods.* **2008**, *6* (6), 230–235.

Chapter 5 Synergistic Enhancement of HONO from Aliphatic and Photosensitizing Compounds in Marine Relevant Organic Compounds: A Study of Ethylene Glycol and 4-BBA on HONO Formation from Aqueous Nitrate Solutions

5.1 Abstract

Nitrous acid (HONO) concentrations have been found to peak in the marine boundary layer during the daytime, and therefore this suggests there is a photolytic source of HONO. This photolytic source has been suggested to be due to nitrate photochemistry. The higher-than-expected nitrate to HONO path in this environment has been thought to be due to the enhancement of HONO from particulate nitrate photochemistry compared to nitric acid photochemistry. However, the enhancement of HONO formation from nitrate photolysis in the presence of marine relevant organics has not been considered in modeling studies even though it is well-known that organic compounds, both light absorbing and non-light absorbing, play a role. Marine dissolved organic matter (m-DOM) can be used in studies focused on elucidating the role of marine relevant organics on HONO enhancement as it comes from the ocean and the organics present in sea spray aerosols come from the ocean via bubble bursting mechanisms. The details of how m-DOM impacts HONO formation due to the different reaction mechanisms from the light-absorption and non-light absorbing compounds within m-DOM remains unknown. To answer this question, mixtures of chromophoric (light absorbing) and aliphatic (non-light absorbing) molecular models 4-benzoylbenzoic acid (4-BBA) and ethylene glycol (EG) were introduced to acidic aqueous nitrate solutions and irradiated with a solar simulator to measure the gaseous HONO formed using Incoherent Cavity Enhanced Absorption Spectroscopy as described previously. Most interesting, is that all molecular proxy mixtures of both 4-BBA and EG resulted in more HONO than the

solutions containing only one of the molecular proxies at the same organic concentration. Thus, it is concluded that the mixtures of 4-BBA and EG enhance HONO formation in a synergistic manner such that the observations (HONO concentrations) are greater than the sum of the HONO concentrations from the single components. Furthermore, the solutions containing 1:1 or 3:1 4-BBA to EG concentrations led to the highest amounts of HONO and had the highest difference from the simulated amounts, i.e., the amounts calculated by adding the appropriate amounts of HONO from the individual proxy experiments. These results show that the hydroxyl radical from the photolysis of the chromophore is crucial to synergistic enhancement. Part of this study also focused on confirming that 4-BBA itself is an adequate molecular model for the chromophoric components of m-DOM. Taking nuclear magnetic resonance spectra of 4-BBA solutions of pH 1.0 to 7.0 allowed for the determination that the molecule is in the keto form and has a pKa of 3.41 ± 0.03 at atmospherically relevant conditions.

5.2 Introduction

Nitrous acid (HONO) is a widely studied trace gas in the atmosphere for its role as a significant source of hydroxyl (·OH) and nitric oxide (·NO) radicals from its photolysis that occurs at wavelengths within the solar spectrum.[1,2] The hydroxyl radical is one of the most important oxidizers in the atmosphere both because of its abundant sources and therefore availability and because of its high reactivity. In the marine boundary layer (MBL) specifically, oxidation by hydroxyl radicals leads to secondary marine aerosols which play a role in cloud formation.[3] The photodissociation of HONO also leads to nitric oxide, making it a part of the oxides of nitrogen cycle.[2] For this reason, the sources of HONO are important to understand. HONO sources in the

atmosphere have been widely studied but the MBL being a considerable source is a relatively new topic of interest in atmospheric chemistry.

For the last ten years, a photolytic source of HONO has been investigated in the MBL as it has been shown that HONO concentrations peak at solar noon.[4–8] Two mechanisms have been suggested as the source including the photosensitized reduction of NO_2 and nitrate photolysis with the latter having more evidence.[4,5,7,8] The evidence for nitrate photolysis, specifically particulate nitrate, derives from a decrease of particulate nitrate measurements when there is an increase in gaseous HONO measurements. Nitrate photolysis has two pathways, one leads to NO_2 and the other leads to NO_2^- and in the presence excess protons, above the pKa, leads to HONO.[9] Importantly, aliphatic compounds have been found to enhance HONO via reactions with ·OH, also a product of nitrate photolysis, leading to superoxide radicals which then reacts with NO and NO_2 leading to NO_2^-.[10] This is relevant in the MBL as nitrate exists in sea spray aerosols (SSA) and they are known to be rich in organics including aliphatic and condensed aromatic compounds.[11–13] Currently, computational studies do not consider the enhancement that marine organics would have in HONO formation where nitrate photolysis is taking place in the MBL.

This Ph.D. project has investigated the role of marine relevant organics on the enhancement of HONO from aqueous nitrate photolysis. The first study compared HONO enhancement from marine dissolved organic matter (m-DOM), humic acid (HA), 4-benzoylbenzoic acid (4-BBA), and ethylene glycol (EG) and found that m-DOM is the most efficient organic at enhancing HONO formation, proving that organics in the MBL in fact can significantly enhance HONO formation.[14] Additionally, mechanisms leading to the enhancements of HONO from m-DOM were proposed. The first was the increase in hydroxyl radicals from the H-abstraction from water by triplet state excited photosensitizing molecules in m-DOM.[15] The second was the formation of superoxide

radicals from the reaction of hydroxyl radicals with aliphatic organic compounds where the superoxide radicals react with NO and NO_2 to form HONO in acidic environments.[9,10,16] The second study investigated the dependence of HONO enhancement on m-DOM concentration. It was found that for m-DOM concentrations within 0.01-0.60 mg/mL m-DOM, HONO is enhanced up to a factor of about 7 with the most enhancement occurring at 0.10 mg/mL of m-DOM. In addition, the formation rates of HONO decreased for all solutions containing any amount of m-DOM. This is due to the surface-active molecules in m-DOM creating a barrier at the surface, as m-DOM was found to be highly surface active with surface tension decreasing with increasing m-DOM concentration. The main point in that study (Chapter 4) is that HONO formation due to m-DOM is a balance between the chemical enhancing mechanisms discussed in the first study and the physical barrier m-DOM creates on the surface of the solutions decreasing gaseous HONO measurements. Given m-DOM is composed of hundreds of different compounds, if not more, it is difficult to address specific mechanistic questions. Here we use two molecular models for m-DOM that represent light absorbing and non-light absorbing compounds and address the following question: Is the enhancement of HONO due to light absorbing and non-light absorbing compound types additive or synergistic?

This study aims to determine how the two types of HONO enhancing mechanisms affect overall measured enhancement by analyzing for additive or synergistic trends. We have proposed that HONO formation from nitrate photolysis is enhanced in the presence of m-DOM due to the chromophoric and aliphatic compounds in m-DOM.[14] The molecular proxies 4-BBA and EG can act as the chromophore and aliphatic compounds, respectively. The structures of these molecules can be found in Figure 5.1. Using these proxies in mixtures and comparing the HONO measurements to when only one of the proxies is present in the nitrate solutions can elucidate

possible synergism occurring. The proxies were introduced in ratios of 4-BBA:EG being 1:3, 1:1, and 3:1. Knowing the speciation of these molecular proxies in the solutions is imperative to confidently be able to use them as proxies for the compound type being studied.

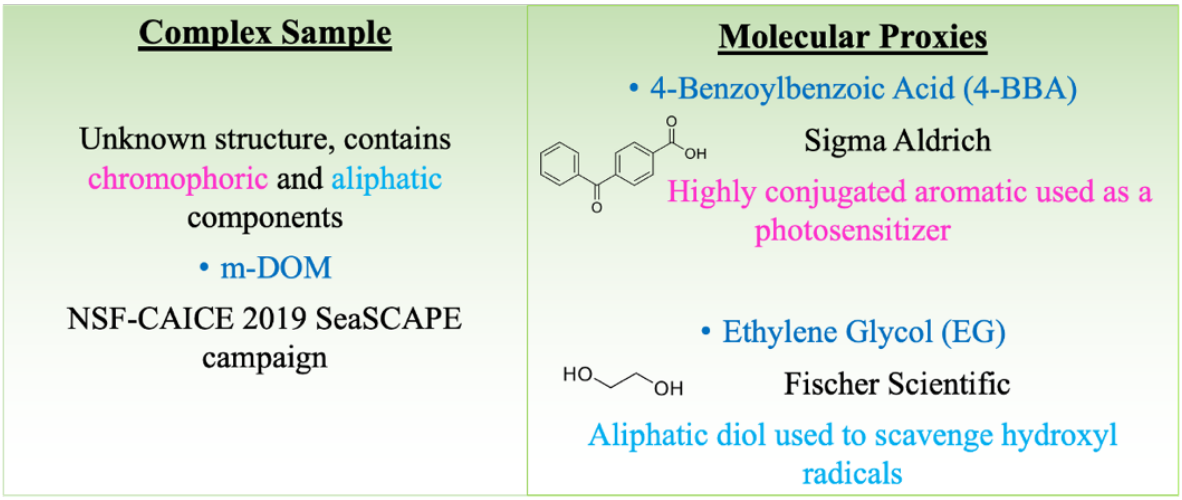

Figure 5.1 A comparison of the complex marine system organic being used, m-DOM, and the simple molecular proxies 4-BBA and EG being used in this study.

To be able to use 4-BBA and EG as proxies for chromophoric and aliphatic compounds, their speciation in the solutions of interest must be known. EG is miscible in water and does not absorb light at wavelengths greater than 280 nm, where the solar simulator used in this work begins to irradiate. Prior to the introduction of hydroxyl radicals from nitrate photolysis, its speciation stays in the diol form in solutions containing 100 mM $NaNO_3$.[10,17] The speciation of 4-BBA in the aqueous phase has been less certain. This molecule has been used as a model chromophore in atmospheric chemistry studies substantially but its form, whether it stays in the ketone form or forms a diol, and its pKa in atmospherically relevant conditions were not known. Protonation and deprotonation of keto organic acids such as 4-BBA, can hydrate under acidic conditions, leading to a keto-diol equilibrium.[18,19] This is important to know in atmospheric conditions as it can affect

the photoactivity of the molecule and its viability for use a model photosensitizer.[20–22] Therefore, as part of this study, we quantified the speciation of 4-BBA and the relevant pKa using proton nuclear magnetic resonance (^{1}H-NMR).

5.3 Experimental

5.3.1 ^{1}H-NMR Spectroscopy

Speciation of 4-BBA was carried out by analyzing the ^{1}H-NMR of 4-BBA at different pH's. A 110 μM 4-BBA stock solution was made by dissolving solid 4-BBA into pH unadjusted milli-Q water. Each solution at pH's 1.0, 2.0, 3.0, 3.5, 4.0, 5.0, 6.0, 7.0 was made from this stock solution by adjusting with HCl or NaOH and adding 5μM sodium trimethylsilylpropanesulfonate (DSS) purchased from Sigma Aldrich for the internal standard for peak locking. All solution contained 10% D_2O for instrument locking. The NMR used was a 500 Hz Jeol ECA NMR spectrometer with solvent suppression in the acquisition parameters. Because the signal of 4-BBA at this concentration is very low, 1024 scans were taken for each ^{1}H-NMR spectrum.[19]

5.3.2 UV-Vis Spectroscopy

An Agilent Cary 5000 UV-Vis-NIR Spectrophotometer was used to measure the absorbance of the molecular proxies to characterize light absorption in the region of the solar simulator. Spectra were recorded for solutions of 0.44 mM 4-BBA, 0.44 mM EG, and 0.03 mg/mL m-DOM all acidified to pH 2.00. The acquisition was done in the range of 280 – 500 nm wavelengths with a resolution of 0.5 nm.

5.3.3 Incoherent Broadband Cavity Enhanced Absorption Spectroscopy

The gaseous HONO and NO_2 measurements were acquired using an Incoherent Broadband Cavity Enhanced Absorption Spectrometer for which the experimental setup and analysis are described in detail in Chapters 2-4.[14,23] All solutions contained 100 mM $NaNO_3$ as the source of nitrate and were acidified with 0.5 M HCl, both from Sigma Aldrich. The solutions containing 0.03 mg/mL m-DOM was created by diluting from a 0.60 mg/mL m-DOM stock, originally made by adding a known weight of solid m-DOM from the NSF-CAICE 2019 SeaSCAPE campaign and adding the needed $NaNO_3$ amount. For the solutions containing molecular proxies, 4-benzoylbenzoic acid from Sigma-Aldrich and ethylene glycol from Fisher Scientific were used for sample preparation. The mixture concentrations were chosen to be 1:3, 1:1, and 3:1 4-BBA to EG where the total organic concentration was 0.44 mM.

5.4 Results and Discussion

5.4.1 Speciation of 4-Benzoyl Benzoic Acid and Its Optical Properties

Solutions of 100 μM 4-BBA adjusted to pH's 1.0 - 7.0 using HCl or NaOH were analyzed with ^{1}H-NMR. For all ^{1}H-NMR spectra, 5 distinct hydrogens were detected corresponding to the 5 hydrogens on the benzene rings. The peaks are most distinct in the spectra for pH 1.0 and are as follows. The triplet detected most upfield at 7.50 ppm was that of the hydrogens on the β-carbon to the ketone group on the least substituted benzene ring labeled D in Figure 5.2. The triplet next to that corresponds to the one hydrogen found on the para position to the ketone at 7.75 ppm, labeled E on Figure 5.2. The four hydrogens labeled B and C are doublets detected 7.84 and 7.88

ppm for pH 1.0 but they shift upfield and combine when at pH 3.5 and above. The hydrogens closest to the carbonyl group, labeled A, had a doublet signal detected at 8.17 and shifted the most with increasing pH up to 7.94 ppm at pH 7.0.

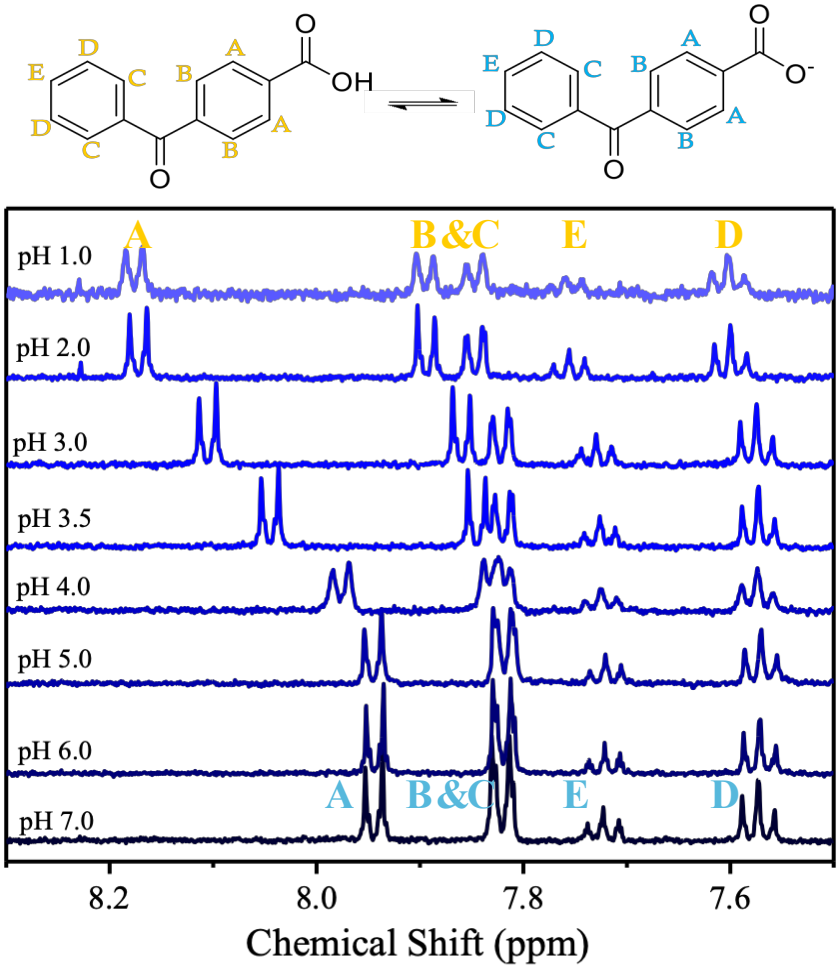

Figure 5.2 The ^{1}H-NMR spectra of 4-BBA at pH values of 1.0 to 7.0 with the chemical shifts for the unique hydrogens labeled for the protonated molecule in yellow deprotonated molecule in blue. The corresponding molecule diagrams are above.

It was hypothesized that 4-BBA would have two pKa's, one corresponding to the protonation of the molecule at the carbonyl group in the keto form of the molecule and the other corresponding to the protonation of the carbonyl group for the diol form of the molecule. This

hypothesis came from the findings of a previous study of a similar model photosensitizer molecule, pyruvic acid.[18] In the pH range tested, the only significant difference in the spectra was the upfield shifting of the hydrogen on the benzene ring adjacent to the carbonyl group. The shifting was caused by the deprotonation of the carbonyl groups beginning at pH 3.0 and was complete by pH 5.0. This results in the conclusion that there is only one pKa for 4-BBA at atmospherically relevant pH's and most importantly, informed that is the pKa corresponding to the protonation of the carbonyl group for the molecule in the keto form. These results were verified by the fact that the experimental spectra resembled those of the protonated and deprotonated keto forms of the molecule when comparing them to predicted spectra of the molecule at the possible four forms on MestreNova. Therefore, it is now known that 4-BBA exists in the protonated and deprotonated keto forms in the pH range of 1-7, as shown in Figure 5.2, with one pKa at 3.41 ± 0.03 which can be calculated from the spectra.

Calculations of pKa were done using the chemical shift of the doublet signal assigned to the hydrogens in the β-carbon with respect to the ketone group. At low pH values, this doublet shows downfield at around 8.17 ppm. As pH increases, the doublet shifts upfield to 7.94 ppm. This chemical shift can be expressed in terms of the mole fractions of the species in equilibrium:

$$\delta_{obs} = f_{HA}\delta_{HA} + f_{A^-}\delta_{A^-} \qquad Eq.5.1$$

where δ_{obs} is the observed chemical shift, and δ_{HA} and δ_{A^-}, are the chemical shift of protonated and deprotonated 4-BBA forms, respectively. f is the mole fraction:

$$f_{HA} = \frac{[H^+]}{[H^+] + K_a} \qquad Eq.5.2$$

$$f_{A^-} = \frac{K_a}{[H^+] + K_a} \quad Eq\ 5.3$$

The acid-base equilibrium constant, K_a, is extracted from the fitting of δ_{obs} vs pH to Eq. 5.1, as shown in Figure 5.3A, with the red line represents the fitting of the data. The fitting yields a $K_a = (3.9 \pm 0.3)\times10^{-4}$, for a pKa of 3.41 ± 0.03. This value is statistically similar to that found potentiometrically, as shown in Figure 5.3B: 3.41 ± 0.04.

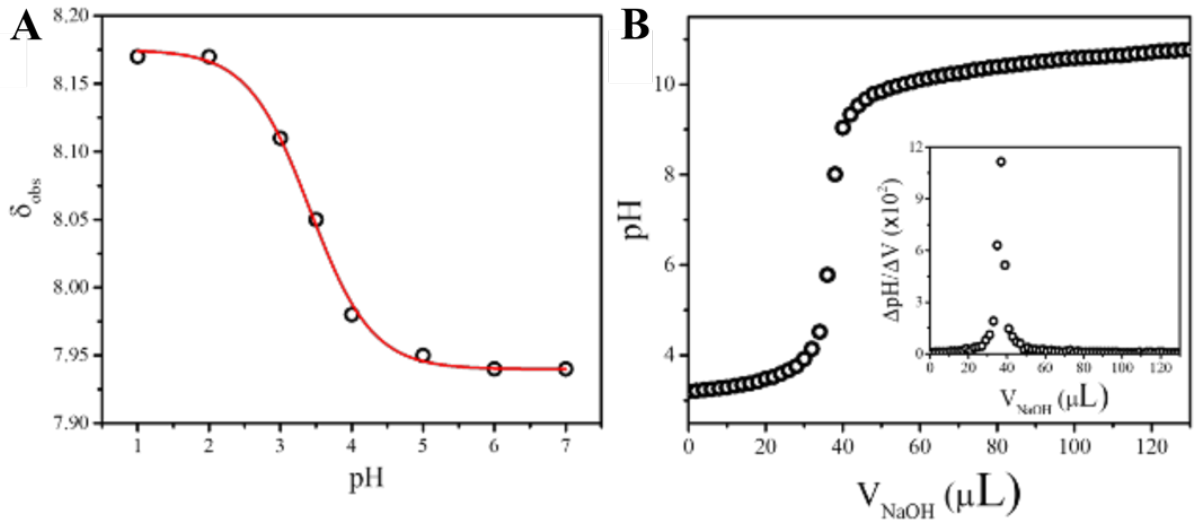

Figure 5.3 (A) Fitting of δ_{obs} vs pH to Equation 1. (B) potentiometric titration curve, with the insert showing the first order derivative of the titration.

Knowing that 4-BBA keeps its conjugated form in water at pH's relevant to the marine boundary layer, allows for its use as a molecular proxy of a marine relevant photosensitizer. Previous work has shown that the presence of m-DOM in irradiated aqueous nitrate solutions will lead to up to a 5-fold enhancement of HONO formation, with the enhancement being dependent on m-DOM concentration. The enhancement due to m-DOM in the solutions was proposed to be from the increase of ·OH in the solutions from the hydrogen abstraction of water from the triplet

state excited part of m-DOM, or m-CDOM. The increase in ·OH lead to an increase of superoxide radicals, from the reaction of ·OH with aliphatic organic compounds, which reacts with NO and NO_2 formed from nitrate photolysis to lead to nitrite. Nitrite in an acidic environment will lead to HONO.[14] To further elucidate information on the mechanisms of HONO enhancement, varying mixtures of 4-BBA and EG were added aqueous nitrate solutions to determine if the enhancement due to the reactions mentioned are synergistic.

5.4.2 Characterization of Molecular Proxies in water

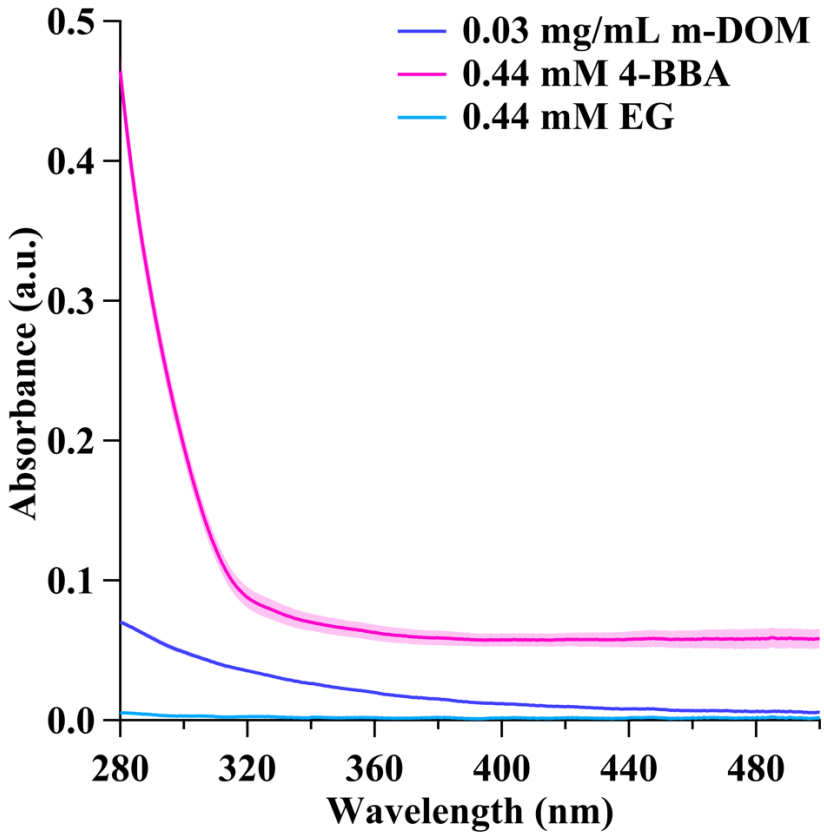

Figure 5.4 UV-Vis absorption of 0.03 mg/mL m-DOM (royal blue), 0.44 mM 4-BBA (pink) , and 0.44 mM EG (light blue) all acidified to pH 2.00 with HCl from 280 to 500 nm. These are triplicate measurements with shading as error bars (some are so small; they are difficult to see).

The absorbance spectra of the molecular proxies used in this study was taken and compared to m-DOM. The range of absorption was 280-500 nm as this is the range of absorption of m-DOM that overlaps with the solar spectrum.[21,24] Figure 5.4 displays m-DOM in dark blue having a broad absorption profile in the entire range. The absorption of 0.44 mM 4-BBA (pink) has a peak not shown in Figure 5.4 at 260 nm, but the tail of this absorption is shown and correspond to the both the $n \rightarrow \pi^*$ and $\pi \rightarrow \pi^*$transitions.[19] Lastly, 0.44mM EG (light blue) does not absorb light in this

region, having some absorption starting at energies higher than 280nm and peaking at 200 nm, which is higher energy than relevant in this study, making it a viable non-light absorbing aliphatic proxy.[17]

Additionally, the surface tension of the molecular proxy mixtures were taken of the solutions and compared to m-DOM as the surface tension of increasing m-DOM mass concentrations was found to influence the gaseous HONO measured. The chosen mixtures of 4-BBA and EG did not change the surface tension of the solutions to the same degree that m-DOM did. The solutions had surface tensions in the range of 72.9 - 74.6 mN/m (Table 5.1), meaning that the nitrate in the solution had a more significant effect on the surface tension than the organics at these concentrations did.[25] As the surface activity of the solutions containing the mixtures of 4-BBA and EG did not significantly differ, the difference in the amounts of HONO and NO_2 formation that will be discussed in the next section are not due to changes in the surface coverage of the solutions as was the case in the study with varying amounts of m-DOM in the solutions.

Table 5.1 Surface tension of solutions all containing 100 mM $NaNO_3$ and acidified to pH 2.00 with HCl. The uncertainty represents one standard deviation of triplicate experiments.

Organics Present in 100 mM $NaNO_3$ solutions acidified to pH 2.00	**Surface Tension (mN/m)**
None	73.8 ± 0.1
0.03 mg/mL m-DOM	70.0 ± 0.5
0.44 mM 4-BBA	72.3 ± 0.2
0.44 mM EG	73.1 ± 0.1
0.11 mM 4-BBA + 0.33 mM EG	73.5 ± 0.2
0.22 mM 4-BBA + 0.22 mM EG	74.6 ± 1.7
0.33 mM 4-BBA + 0.11 mM EG	72.9 ± 0.4

5.4.3 HONO and NO_2 measurements from nitrate solutions in the presence of 4-Benzoylbenzoic Acid and Ethylene Glycol

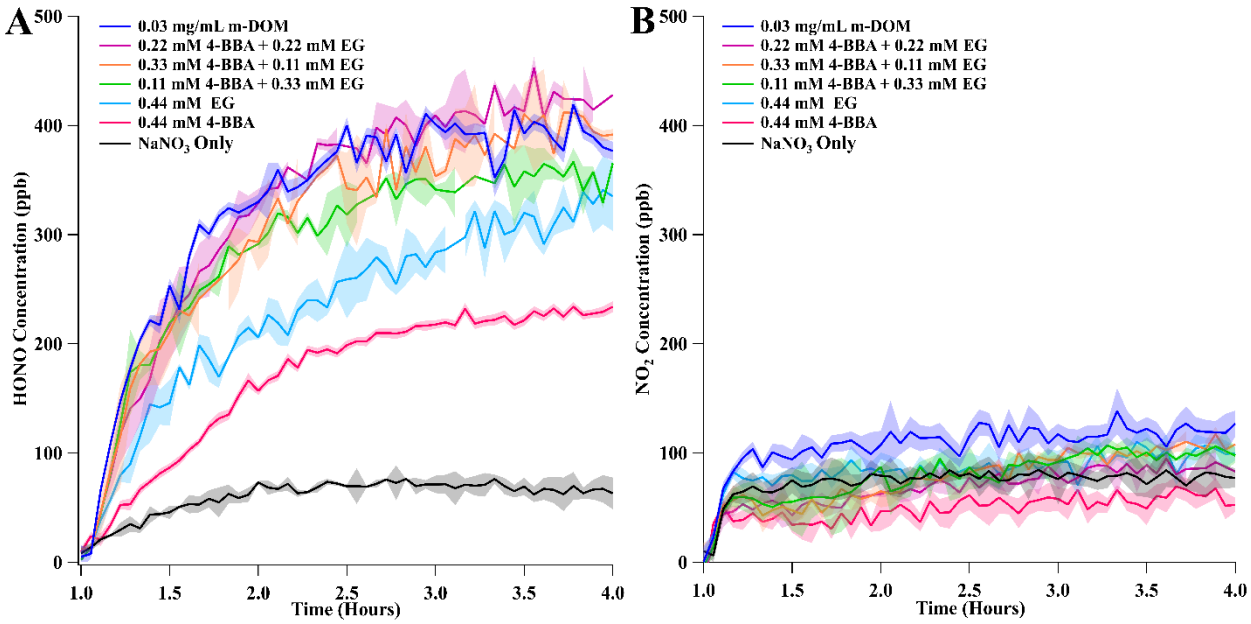

Figure 5.5 (A) HONO and (B) NO_2 time profiles of concentrations in ppb experimentally measured during the period of irradiation with a solar simulator of solutions containing 100 mM $NaNO_3$ + 0.03 mg/mL m-DOM or 0.44 mM 4-BBA or EG or varying mixtures of 4-BBA and EG. The shading shows 1 standard deviation of triplicate experiments, or the error associated with the fitting of data to a reference HONO cross-section spectrum.

Time profiles of HONO and NO_2 formation during the period of irradiation of solutions containing 100 mM $NaNO_3$ and mixtures of 4-BBA and EG are shown in Figure 5.5. The NO_2 measurements for these experiments did not differ much with the different solutions. All solutions led to NO_2 between 60 - 90 ppb for the entirety of the irradiation period, with the solutions containing 0.44mM 4-BBA led to slight less averaging at 50 ppb and the solution with 0.03 mg/mL m-DOM led to slightly more averaging at 100 ppb (Figure 5.5B). The left figure shows the amount of HONO measured from these solutions in comparison to solutions containing 0.03 mg/mL m-DOM in the royal blue trace, 0.44 mM 4BBA in the pink trace, 0.44 mM EG in the light blue trace,

and only nitrate solutions in the black trace. The solutions containing only 4-BBA and EG did not lead to as much HONO as the mixtures of 4-BBA and EG. When the total organic concentration was kept constant at 0.44 mM, the mixtures of 4-BBA and EG led significantly more HONO compared to 0.44 mM of either of the individual organic molecular model, suggesting synergism. Interestingly, the solutions containing 0.22 mM 4-BBA + 0.22 mM EG, magenta trace, lead to more HONO than the other two mixtures, apparent beginning 30 minutes into irradiation (t = 1.5 hours), until the end of the irradiation period. The solution containing 0.33 mM 4-BBA + 0.11 mM 4-BBA, orange trace, led to the same amount of HONO as the solution with 0.11 mM 4-BBA + 0.33 mM 4BBA, green trace, for the first hour and then led to ca. 25 ppb more at the end of the irradiation period. In comparison, to the solution containing 0.03 mg/mL m-DOM, the molecular proxy mixtures led to similar amounts of HONO. The HONO measured for this m-DOM mass concentration was chosen as the comparison because the surface tension was the most similar to the solutions containing 4-BBA and EG, 70.0 ± 0.5 mN/m compared to 72.9 – 74.6 mN/m (Table 5.1). In Chapter 4, it was discussed that the increased surface activity of increasing m-DOM amounts of the solution affected HONO partitioning out of the solution. By using 100 mM $NaNO_3$ with 0.03 mg/mL m-DOM, HONO enhancement due to chemical reactions is significant and the effect of the physical barrier impeding HONO from partition out of the solutions is avoided as that is not a factor that must be considered with the molecular proxy mixtures. Evidently, mixtures of 4-BBA and EG are a good model system for m-DOM in the quest to understand HONO enhancement mechanisms from marine relevant organics as they led to very similar amounts of HONO for the entirety of the irradiation period. This is not a direct comparison as the exact compounds in this m-DOM sample and their abundance are unknown but the categories of compounds in relative percentages are known and support the arguments in this work. Specifically,

aromatic ketones such as 4-BBA and aliphatics such as EG glycol are some of the major compound types found in this m-DOM sample.[21] Therefore, they can be used to investigate if the enhancement of HONO due to the photochemical and secondary reactions from aliphatics in solution is synergistic.

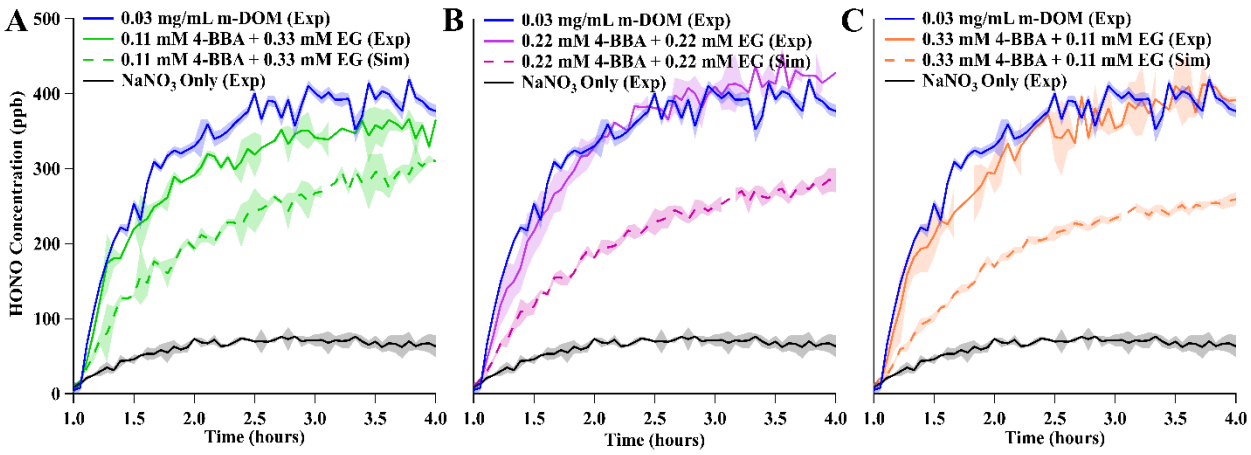

Figure 5.6 HONO concentrations in ppb measured (solid lines) from irradiation of solutions containing (A) 100 mM $NaNO_3$ plus 0.11 mM 4-BBA + 0.33 mM EG, (B) 0.22 mM 4-BBA + 0.22 mM EG, and (C) 0.33 mM 4-BBA + 0.11 mM EG. Also shown in dashed lines are the simulated amounts HONO expected from the amounts measured from the solutions containing 100 mM $NaNO_3$ plus 0.44 mM 4-BBA and 100 mM $NaNO_3$ plus 0.44 mM EG. The HONO irradiation profiles from solutions only containing 100 mM $NaNO_3$ and 100 mM $NaNO_3$ plus 0.03 mg/mL m-DOM are also shown for comparison. The experimental data is shown in solid lines and the simulated amounts in dashed lines. The shading represents the error from the fitting of the data to a HONO reference spectra using DOASIS for the experimental data and error propagation for the simulated amounts.

Simulated amounts of HONO were calculated for the mixtures of 4-BBA and EG from the solutions containing only 4-BBA or EG to compare to the measured HONO amounts of each mixture. The simulated HONO profiles were calculated by first dividing each time point of the profiles for the experiments with 100 mM $NaNO_3$ + 4-BBA and 100 mM $NaNO_3$ + EG by 4. Then the time points for the mixtures were done by adding the needed amounts of each individual

molecular proxy. For example, for the solution containing 0.11 mM 4-BBA and 0.33 mM EG, each time point was calculated by adding the HONO measurements of ¼ of 100 mM $NaNO_3$ + 4-BBA at the respective timepoint and ¾ of the 100 mM $NaNO_3$ + EG at the respective timepoint. These simulated time profiles for each mixture are shown in Figure 5.6 in the dashed lines. If the enhancement of HONO due to photosensitizing compounds (4-BBA) and aliphatic compounds (EG) were linearly additive, this is what the HONO time profiles would look like for the solutions containing the mixture of the two compounds.

Every simulated HONO formation profile for the mixtures was lower than the experimental amounts measured, suggesting a synergistic enhancement of HONO when both photosensitizing and aliphatic compounds are present in aqueous nitrate photolysis experiments. Figure 5.6 shows the measured amounts of the mixtures in the solid green, magenta, and orange traces where the average of the HONO for the last 30 minutes of irradiation were as follows: 352 ppb for 0.11 mM 4-BBA and 0.33 mM EG, 422 ppb for 0.22 mM 4-BBA and 0.22 mM EG, and 400 ppb for 0.33 mM 4-BBA and 0.11 mM EG. Also shown in Figure 5.6 are the simulated HONO amounts and the average for the last 30 minutes in the same order as the previous list are 306 ppb, 281 ppb, and 255 ppb. The difference in the experimental amounts and simulated amounts were between 46 and 145 ppb for all mixtures, with all experimental amounts being higher. Because the simulated profiles shown in this figure represent what the HONO enhancement would be if the enhancement due to both compound types was linearly additive and the experimental amounts exceed that, it is deduced that the enhancement of HONO is synergistic. Notably, the simulated HONO amounts increase with increasing EG concentration in the mixture, this is because the experiments only containing EG lead to more HONO than the experiments with only 4-BBA. However, that is not the trend that is seen in the experimental measurements where in actuality the experiments

containing equal parts 4-BBA and EG or more 4-BBA than EG led to the most amount of HONO an hour after the start of irradiation (time = 2 hours), with the experiment containing equal 4-BBA and EG amounts producing slightly more HONO. Also noteworthy is the fact that the difference in the experimental and simulated amounts was much higher for the solutions also containing equal parts 4-BBA and EG or more 4-BBA than EG, with the difference being 141 and 145 ppb, respectively and much less for the solution with less 4-BBA than EG, with the difference being 46 ppb. This difference can be partially attributed to the fact that the experiments with only EG leads to more HONO than the solutions with only 4-BBA, so the simulated amount is higher than that for the other two mixtures. However, another reasoning is that the solution containing 0.11 mM 4-BBA + 0.33 mM EG led to the least experimental amounts of HONO, making the difference between the experimental and simulated amounts lower.

The experiments with 0.22 mM 4-BBA + 0.22 mM EG and 0.33 mM 4-BBA + 0.11 mM EG led to the most amount of HONO and had a higher difference to the simulated amounts signifying that the synergism in the HONO enhancement is greater when there is equal to or greater concentration of 4-BBA than EG in the solutions. This synergistic enhancement from more photosensitizing molecules in the solution are not likely due to the photosensitized reduction of NO_2 to HONO because the measured amounts of NO_2 are not statistically different between the different mixtures experiments (Figure 5.5B). The more likely reasoning is that the photosensitizer 4-BBA abstracts a hydrogen from water when it is excited in the triplet state.[15] This leads to an increase in hydroxyl radicals which in the presence of aliphatic compounds like ethylene glycol, creates superoxide radicals. These superoxide radicals react with NO and NO_2 in the solution to lead to an enhancement of nitrite and in an acidic aqueous solution, lead to an increase in HONO.[14,16]

This study's significance is that in an environment where both photosensitizing and aliphatic compounds are present where nitrate photolysis is taking place, the two compound types synergistically enhance HONO. The first study that was presented in this project proposed that HONO enhancement due to m-DOM in the solutions was due to both aliphatic and photosensitizing compounds in the sample. This finding not only confirms that these mechanisms are responsible for the enhancement but also gives insight into the synergistic nature of the enhancement. This is especially crucial to know when considering this effect in real world conditions as m-DOM, and other organics in SSA, include a multitude of different compounds that act as photosensitizers or are aliphatic.[11,12,21]

5.5 Conclusion and Future Work

The previous chapters have shown that marine relevant organics can enhance HONO formation in the boundary layer; this study investigated if this enhancement is due to additive or synergistic enhancement from the different types of compounds in m-DOM. The chromophoric and aliphatic compounds in m-DOM lead to HONO enhancement via two different mechanisms, thus using molecular model compounds can give insight into specific mechanisms occurring. To be able to confidently use 4-BBA as a chromophoric model, its speciation in MBL conditions were determined using ^{1}H-NMR spectroscopy. It was determined that at pH values of 1.0 to 7.0, 4-BBA exists only in the keto form and has a pKa of 3.41 ± 0.03. This confirms that 4-BBA is photoactive in the solutions used in this study and therefore is a viable chromophore proxy for m-DOM. Therefore, mixes containing 1:3, 1:1; and 3:1 4-BBA to EG ratios for total of 0.44mM of organics were irradiated with 100 mM $NaNO_3$ solutions acidified to pH 2.

All irradiated nitrate solutions in the presence of mixtures of 4-BBA and EG containing 0.44 mM total organic led to more HONO enhancement (352, 422, and 400 ppb in that order) than 0.44 mM of either of the molecular proxies on their own signifying HONO enhancement from a mixture of chromophoric and aliphatic compounds in nitrate solutions is synergistic. Additionally, when comparing these experimental results to simulated amounts of what the solutions would be from a theoretical linear addition of HONO formation from the individual proxies, the experimental measurements were much higher; supporting the idea of a synergistic enhancement when there is a mixture of organics in the solutions. Importantly, the solutions with 1:1 and 3:1 4-BBA to EG led to the most amount of HONO experimentally and had the largest difference between the experimental and simulated values. This informs that the introduction of more hydroxyl radicals for the irradiation of the chromophore plays the larger role in a more efficient HONO enhancement. However, the solution with 1:3 4-BBA to EG was still experimentally higher than the simulated values, meaning the synergistic enhancement happens in all mixture conditions. Interestingly, compared to when there is 0.03 mg/mL m-DOM in the nitrate solutions, the molecular proxy mixtures led comparable amounts of HONO. There is one more m-DOM specific factor that would give more insight to the overall enhancement mechanism.

The molecules 4-benzoylbenzoic acid and ethylene glycol are advantageous models to study the HONO enhancement due to the chromophoric and aliphatic compounds in m-DOM because they are simple compounds, simplifying the possible reactions and they also have been used extensively in other studies; however, they do not mimic the increase surface activity in the solution with increasing concentration like m-DOM. Chapter 4 discussed that varying m-DOM mass concentrations can affect the maximum measurements of HONO produced as well as the rates of formation; this was because m-DOM is highly surface active and at higher concentrations

can act as a physical barrier. For future directions, introducing a molecule that is surface active such as nonanoic acid would be great to add to the molecular proxy mixture to better understand the m-DOM specific mechanisms that lead to such a high HONO enhancement.

Though nitrate photolysis being the most significant source of daytime HONO formation in the MBL has been supported by many field and computational studies, all the components of the MBL conditions have not considered in the bigger picture. The enhancement of photolysis due to particulate nitrate compared to that of nitric acid has been suggested for the higher-than-expected nitrate to HONO amounts, the enhancement due to marine organics present in the environment has not. This work, along with Chapters 3 and 4, can inform chemical models to better predict HONO, and therefore hydroxyl radical, sources and significance in the MBL. This project has provided information on mechanisms, concentration dependence, and now synergism effects on the enhancement of HONO due to marine organics that must be considered in MBL conditions. Though the total organic concentration in SSA is unclear, it is known that in ultrafine SSA, the composition is dominated by organic carbon (OC).[11,26,27] This study provides a range of what would likely be a high OC ratio SSA range for organic enhancement of HONO formation from nitrate photolysis in acidic SSA.[28]

5.6 Acknowledgements

Chapter 5 contains unpublished material that has been submitted for publication in : Mora García, S. L.; Gutierrez, I.; Navea, J. G.; Grassian, V. H. Enhanced HONO Formation from Aqueous Nitrate Photochemistry in the Presence of Marine Relevant Organics: A Study of m-DOM Concentration on HONO Kinetics and Yields and the Synergistic Enhancement of Aliphatic

and Photosensitizing Compounds in m-DOM. *Submitted*. The dissertation author was the primary investigator and author of this paper.

The authors would like to thank Prof. Mark Young and Prof. Imon Mandal for helpful comments, Anthony Mrse for assistance with NMR spectra analysis, and Alma Montserrat Palacios Puga and Gilberto Daniel Partida Coria for solution preparation in the ^{1}H-NMR experiments. Also, a big thank you to Viet Anh Nguyen for her help acquiring the UV-Vis data presented in this study. The authors would like to gratefully acknowledge support from the National Science Foundation through the Center for Aerosol Impacts on Chemistry of the Environment funded under the Centers for Chemical Innovation Program Grant CHE1801971.

5.7 Bibliography

(1) Alicke, B.; Geyer, A.; Hofzumahaus, A.; Holland, F.; Konrad, S.; Pätz, H. W.; Schäfer, J.; Stutz, J.; Volz-Thomas, A.; Platt, U. OH Formation by HONO Photolysis during the BERLIOZ Experiment. *J. Geophys. Res.: Atmos.* **2003**, *108* (D4), 8247.

(2) John H. Seinfeld; Spyros N. Pandis. *Atmospheric Chemistry and Physics: From Air Pollution to Climate Change*, Third.; John Wiley & Sons, Inc., 2016.

(3) Mayer, K. J.; Wang, X.; Santander, M. V.; Mitts, B. A.; Sauer, J. S.; Sultana, C. M.; Cappa, C. D.; Prather, K. A. Secondary Marine Aerosol Plays a Dominant Role over Primary Sea Spray Aerosol in Cloud Formation. *ACS Cent, Sci,* **2020**, *6* (12), 2259–2266.

(4) Kasibhatla, P.; Sherwen, T.; Evans, M. J.; Carpenter, L. J.; Reed, C.; Alexander, B.; Chen, Q.; Sulprizio, M. P.; Lee, J. D.; Read, K. A.; Bloss, W.; Crilley, L. R.; Keene, W. C.; Pszenny, A. A. P.; Hodzic, A. Global Impact of Nitrate Photolysis in Sea-Salt Aerosol on

NO_x, OH, and O_3 in the Marine Boundary Layer. *Atmos. Chem. Phys.* **2018**, *18* (15), 11185–11203.

(5) Ye, C.; Zhou, X.; Pu, D.; Stutz, J.; Festa, J.; Spolaor, M.; Tsai, C.; Cantrell, C.; Mauldin, R. L.; Campos, T.; Weinheimer, A.; Hornbrook, R. S.; Apel, E. C.; Guenther, A.; Kaser, L.; Yuan, B.; Karl, T.; Haggerty, J.; Hall, S.; Ullmann, K.; Smith, J. N.; Ortega, J.; Knote, C. Rapid Cycling of Reactive Nitrogen in the Marine Boundary Layer. *Nature* **2016**, *532* (7600), 489–491.

(6) Ye, C.; Zhang, N.; Gao, H.; Zhou, X. Photolysis of Particulate Nitrate as a Source of HONO and NO_x. *Environ. Sci. Technol.* **2017**, *51* (12), 6849–6856.

(7) Reed, C.; Evans, M. J.; Crilley, L. R.; Bloss, W. J.; Sherwen, T.; Read, K. A.; Lee, J. D.; Carpenter, L. J. Evidence for Renoxification in the Tropical Marine Boundary Layer. *Atmos. Chem. Phys.* **2017**, *17* (6), 4081–4092.

(8) Andersen, S. T.; Carpenter, L. J.; Reed, C.; Lee, J. D.; Chance, R.; Sherwen, T.; Vaughan, A. R.; Stewart, J.; Edwards, P. M.; Bloss, W. J.; Sommariva, R.; Crilley, L. R.; Nott, G. J.; Neves, L.; Read, K.; Heard, D. E.; Seakins, P. W.; Whalley, L. K.; Boustead, G. A.; Fleming, L. T.; Stone, D.; Fomba, K. W. Extensive Field Evidence for the Release of HONO from the Photolysis of Nitrate Aerosols. *Sci. Adv.* **2023**, *9* (3), 1–10.

(9) Mack, J.; Bolton, J. R. Photochemistry of Nitrite and Nitrate in Aqueous Solution: A Review. *J. Photochem. Photobiol. A Chem.* **1999**, *128*, 1–13.

(10) Scharko, N. K.; Berke, A. E.; Raff, J. D. Release of Nitrous Acid and Nitrogen Dioxide from Nitrate Photolysis in Acidic Aqueous Solutions. *Environ. Sci. Technol.* **2014**, *48* (20), 11991–12001.

(11) Bertram, T. H.; Cochran, R. E.; Grassian, V. H.; Stone, E. A. Sea Spray Aerosol Chemical Composition: Elemental and Molecular Mimics for Laboratory Studies of Heterogeneous and Multiphase Reactions. *Chem. Soc. Rev.* **2018**, *47* (7), 2374–2400.

(12) Wang, X.; Sultana, C. M.; Trueblood, J.; Hill, T. C. J.; Malfatti, F.; Lee, C.; Laskina, O.; Moore, K. A.; Beall, C. M.; McCluskey, C. S.; Cornwell, G. C.; Zhou, Y.; Cox, J. L.; Pendergraft, M. A.; Santander, M. V.; Bertram, T. H.; Cappa, C. D.; Azam, F.; DeMott, P. J.; Grassian, V. H.; Prather, K. A. Microbial Control of Sea Spray Aerosol Composition: A Tale of Two Blooms. *ACS Cent. Sci.* **2015**, *1* (3), 124–131.

(13) Miyazaki, Y.; Yamashita, Y.; Kawana, K.; Tachibana, E.; Kagami, S.; Mochida, M.; Suzuki, K.; Nishioka, J. Chemical Transfer of Dissolved Organic Matter from Surface Seawater to Sea Spray Water-Soluble Organic Aerosol in the Marine Atmosphere. *Sci. Rep.* **2018**, *8* (1), 1-10.

(14) Mora García, S. L.; Pandit, S.; Navea, J. G.; Grassian, V. H. Nitrous Acid (HONO) Formation from the Irradiation of Aqueous Nitrate Solutions in the Presence of Marine Chromophoric Dissolved Organic Matter: Comparison to Other Organic Photosensitizers. *ACS Earth. Space. Chem.* **2021**, *5* (11), 3056–3064.

(15) McKay, G.; Rosario-Ortiz, F. L. Temperature Dependence of the Photochemical Formation of Hydroxyl Radical from Dissolved Organic Matter. *Environ. Sci. Technol.* **2015**, *49* (7), 4147–4154.

(16) Wang, X.; Dalton, E. Z.; Payne, Z. C.; Perrier, S.; Riva, M.; Raff, J. D.; George, C. Superoxide and Nitrous Acid Production from Nitrate Photolysis Is Enhanced by Dissolved Aliphatic Organic Matter. *Environ. Sci. Technol. Lett.* **2021**, *8* (1), 53–58.

(17) Zhang, J.; Zhang, P.; Ma, K.; Han, F.; Chen, G.; Wei, X. Hydrogen Bonding Interactions between Ethylene Glycol and Water: Density, Excess Molar Volume, and Spectral Study. *Sci. China. B Chem.* **2008**, *51* (5), 420–426.

(18) Luo, M.; Shemesh, D.; Sullivan, M. N.; Alves, M. R.; Song, M.; Gerber, R. B.; Grassian, V. H. Impact of pH and NaCl and $CaCl_2$ Salts on the Speciation and Photochemistry of Pyruvic Acid in the Aqueous Phase. *J. Phys. Chem. A* **2020**, *124* (25), 5071–5080.

(19) Karimova, N.; Alija, O.; Mora García, S. L.; Grassian, V. H.; Gerber, R. B.; Navea, J. G. pH Dependence of the Speciation and Optical Properties of 4-Benzoylbenzoic Acid. *Phys. Chem. Chem. Phys.* **2023**, *25*, 17306–17319.

(20) McNeill, K.; Canonica, S. Triplet State Dissolved Organic Matter in Aquatic Photochemistry: Reaction Mechanisms, Substrate Scope, and Photophysical Properties. *Environ. Sci.: Process. Impacts.* **2016**, *18* (11), 1381–1399.

(21) Alves, M. R.; Coward, E. K.; Gonzales, D.; Sauer, J. S.; Mayer, K. J.; Prather, K. A.; Grassian, V. H. Changes in Light Absorption and Composition of Chromophoric Marine-Dissolved Organic Matter across a Microbial Bloom. *Environ. Sci.: Process. Impacts.***2022**, *24* (10), 1923–1933.

(22) Trueblood, J. V; Alves, M. R.; Power, D.; Santander, M. V; Cochran, R. E.; Prather, K. A.; Grassian, V. H. Shedding Light on Photosensitized Reactions within Marine-Relevant Organic Thin Films. *ACS Earth. Space .Chem.* **2019**, *3*, 1614–1623.

(23) Mora García, S. L.; Gutierrez, I.; Navea, J. G.; Grassian, V. H. Enhanced HONO Formation from Aqueous Nitrate Photochemistry in the Presence of Marine Relevant Organics: A Study of m-DOM Concentration on HONO Kinetics and Yields and the Synergistic Enhancement of Aliphatic and Photosensitizing Compounds in m-DOM. *Submitted*.

(24) Karimova, N. V.; Alves, M. R.; Luo, M.; Grassian, V. H.; Gerber, R. B. Toward a Microscopic Model of Light Absorbing Dissolved Organic Compounds in Aqueous Environments: Theoretical and Experimental Study. *Phys. Chem. Chem. Phys.* **2021**, *23* (17), 10487–10497.

(25) Zhang, C.; Carloni, P. Salt Effects on Water/Hydrophobic Liquid Interfaces: A Molecular Dynamics Study. *J. Phys.: Condens. Matter.* **2012**, *24* (12), 124109.

(26) Ault, A. P.; Moffet, R. C.; Baltrusaitis, J.; Collins, D. B.; Ruppel, M. J.; Cuadra-Rodriguez, L. A.; Zhao, D.; Guasco, T. L.; Ebben, C. J.; Geiger, F. M.; Bertram, T. H.; Prather, K. A.; Grassian, V. H. Size-Dependent Changes in Sea Spray Aerosol Composition and Properties with Different Seawater Conditions. *Environ. Sci. Technol.* **2013**, *47* (11), 5603–5612.

(27) Cochran, R. E.; Laskina, O.; Jayarathne, T.; Laskin, A.; Laskin, J.; Lin, P.; Sultana, C.; Lee, C.; Moore, K. A.; Cappa, C. D.; Bertram, T. H.; Prather, K. A.; Grassian, V. H.; Stone, E. A. Analysis of Organic Anionic Surfactants in Fine and Coarse Fractions of Freshly Emitted Sea Spray Aerosol. *Environ. Sci. Technol.* **2016**, *50* (5), 2477–2486.

(28) Angle, K. J.; Crocker, D. R.; Simpson, R. M. C.; Mayer, K. J.; Garofalo, L. A.; Moore, A. N.; Mora García, S. L.; Or, V. W.; Srinivasan, S.; Farhan, M.; Sauer, J. S.; Lee, C.; Pothier, M. A.; Farmer, D. K.; Martz, T. R.; Bertram, T. H.; Cappa, C. D.; Prather, K. A.; Grassian, V. H. Acidity across the Interface from the Ocean Surface to Sea Spray Aerosol. *Proc. Natl. Acad. Sci. USA* **2021**, *118* (2), 1–6.

Chapter 6 Conclusions and Future Directions

6.1 Conclusions

In this dissertation research, an in lab made Incoherent Broadband Cavity Enhanced Absorption Spectrometer (IBBCEAS) was used to simultaneously measure nitrous acid (HONO) and nitrogen dioxide (NO_2). This spectroscopic method is utilized in atmospheric chemistry for the direct measurement of multiple trace gases at atmospherically relevant pressures and concentrations simultaneously. This method operates without the need to convert gaseous samples, thus providing a direct and interference-free approach for trace gas detection. The technique incorporates Differential Optical Absorption Spectroscopy (DOAS), focusing on narrowband absorption features to differentiate between different absorbers and eliminate interference from atmospheric particles and molecules. A significant portion of the efforts of the dissertation presented involved optimizing the instrument for the use in the investigation of HONO enhancing mechanisms in the atmosphere. The instrument's optimization included changes to the cavity tube material, mirror cleaning, and alignment techniques leading to an increased maximum effective pathlength. To validate the instrument, successful calibration curves for known concentrations of NO_2 were obtained. Measuring known amounts of HONO with the instrument further confirmed the instrument's accuracy and reliability. The in lab made IBBCEAS served as a powerful tool in the presented projects, providing direct and simultaneous measurements of HONO and NO_2 leading to valuable insights to our understanding of HONO formation in the marine boundary layer.

The findings from three distinct studies shed light on the complex mechanisms underlying nitrous acid formation in the marine boundary layer (MBL); specifically, the focus on the role of marine-derived dissolved organic matter (m-DOM) has on HONO enhancement.

Chapter 3 presents an investigation into the enhancement of HONO formation in the MBL during daylight hours due to the presence of organics; importantly, showing for the first time that HONO can be enhanced by the presence of marine dissolved organic matter (m-DOM) from solar simulator irradiated nitrate solutions. The enhancement of HONO from the presence of m-DOM, humic acid (HA), ethylene glycol (EG), and 4-benzoylbenzoic acid (4-BBA) in irradiated aqueous nitrate solutions was compared. It was found that m-DOM was the most effective at enhancing HONO formation leading to a ca. 5-time enhancement. Therefore, the study identifies aged sea spray aerosols containing nitrate and m-DOM as significant contributors to elevated HONO levels in the MBL during the day. The proposed mechanism involves secondary reactions of superoxide radicals (formed from the reaction of hydroxyl radicals with aliphatic compounds in m-DOM) with nitrogen dioxide (NO_2) and nitric oxide ($\cdot NO$) leading to increased levels of nitrite. The chromophoric components in m-DOM enhanced HONO in two ways. The first was the formation of solvated electrons from the charge split of an excited chromophore, the solvated electron would react with nitrate to form nitrite or with molecular oxygen to form superoxide radicals ($\cdot O_2^-$). The second mechanism leads to the formation of hydroxyl radicals due to hydrogen abstraction of water by the triplet excited chromophore. Both mechanisms feed into the mechanisms of superoxide reactions with NO_2 and $\cdot NO$, leading to elevated amounts of nitrite which led to enhanced observed HONO because in an acidic environment, the protonated form of nitrite leads is the predominant species. These results support observations of a diurnal HONO cycle in the MBL and emphasize

the importance of considering complex marine relevant organics in atmospheric chemistry models for improved predictions of HONO and therefore hydroxyl radicals in the atmosphere.[1]

Chapter 4 further investigates the impact of m-DOM by varying m-DOM mass concentrations in aqueous nitrate solutions and measuring HONO formation upon broadband irradiation. The study reveals that at lower m-DOM concentrations (0.00 - 0.10 mg/mL), increasing amounts lead to enhanced HONO yields, but this effect diminishes beyond that and, though there is enhancement, it decreases with increasing m-DOM concentration (0.20 – 0.60 mg/mL). The rates of HONO partitioning into the gas phase decrease with m-DOM is present, especially at the higher mass concentrations where solutions not containing any m-DOM had a partitioning rate of $6.8 \pm 0.4 \times 10^{-4}$ s^{-1} and the solutions containing 0.60 mg/mL led to a partitioning rate of $2.2 \pm 0.1 \times 10^{-4}$ s^{-1}. The decrease in partitioning rates and decrease in HONO enhancement past 0.10 mg/mL m-DOM are attributed to the surface activity of m-DOM at these higher concentrations. In particular, the decrease in surface tension caused by higher m-DOM concentrations suggests surface coverage of the solutions from the surface-active molecules (aliphatic hydrocarbons and aromatic compounds) within m-DOM. This study emphasizes the balance between HONO enhancement from the chemical mechanisms elucidated in Chapter 3 and the physical barrier of the surface-active compounds within m-DOM, both factors can play a role within sea spray aerosols.[2]

Chapter 5 investigates whether the enhancement of HONO from nitrate photolysis containing the aliphatic, non-light absorbing, and chromophoric, light absorbing, compounds in m-DOM is additive or synergistic. Molecular model compounds, EG and 4-BBA, were added to nitrate solutions on their own or in a mixture of 1:3, 1:1, and 3:1 where the total amount of organic is kept the same at 0.44 mM. The study demonstrates synergistic effects, with mixed chromophoric

and aliphatic compounds leading to more substantial HONO enhancement compared to individual molecular proxies. Another factor that suggests synergism is that the theoretical amounts of HONO that would be measured if the HONO enhancement due to both types of compounds, EG and 4-BBA, was linearly additive was calculated and the experimental amounts were all greater than these calculated amounts. Importantly, the amounts of HONO measured from the solutions containing mixtures of EG and 4-BBA were comparable to the amount measured when 0.03 mg/mL of m-DOM, an m-DOM amount that led to surface tension values similar to the solutions containing the molecular models, was present in the solutions. This study further presents that the enhancement of HONO in the MBL from marine relevant organics is complex elucidating that the reaction mechanisms proposed lead to synergistic, not linear, enhancement. Additionally, proton nuclear magnetic resonance was used to determine the speciation of 4-BBA in MBL relevant conditions, where it was found that it exists only in the protonated and deprotonated keto form and has a pKa of 3.41 ± 0.03.[3]

To summarize the research discussed here, Figure 6.1 shows a flow chart pointing to efforts leading to publications and includes two other studies not mentioned in detail in the dissertation that also came out of two efforts. Chapter 1 introduces the need to study the effect of marine relevant organics on HONO formation in the MBL. The marine dissolved organic matter used in all studies was gathered from the NSF-CAICE 2019 SeaSCAPE campaign.[4] Being part of this campaign resulted in a co-authorship in a study that found that nascent sea spray aerosols are in fact acidic, with pH values of 2 - 4 depending on aerosol size, the pH value of 2 was used in these studies of HONO formation in part because of the SeaSCAPE measurements.[5] Chapter 2 covers the optimization, validation, and data analysis efforts for the in lab built IBBCEAS. The validation of this instrument also led to co-authorship on a study that probed HONO formation from NO_2

hydrolysis in the presence and absence of different light sources on gypsum surfaces, a possible route for HONO formation in indoor environments.[6] The use of m-DOM led to three different investigations regarding the enhancement of HONO from nitrate photochemistry in the presence of marine relevant organic compounds which are described in detail in Chapters 3 to 5.

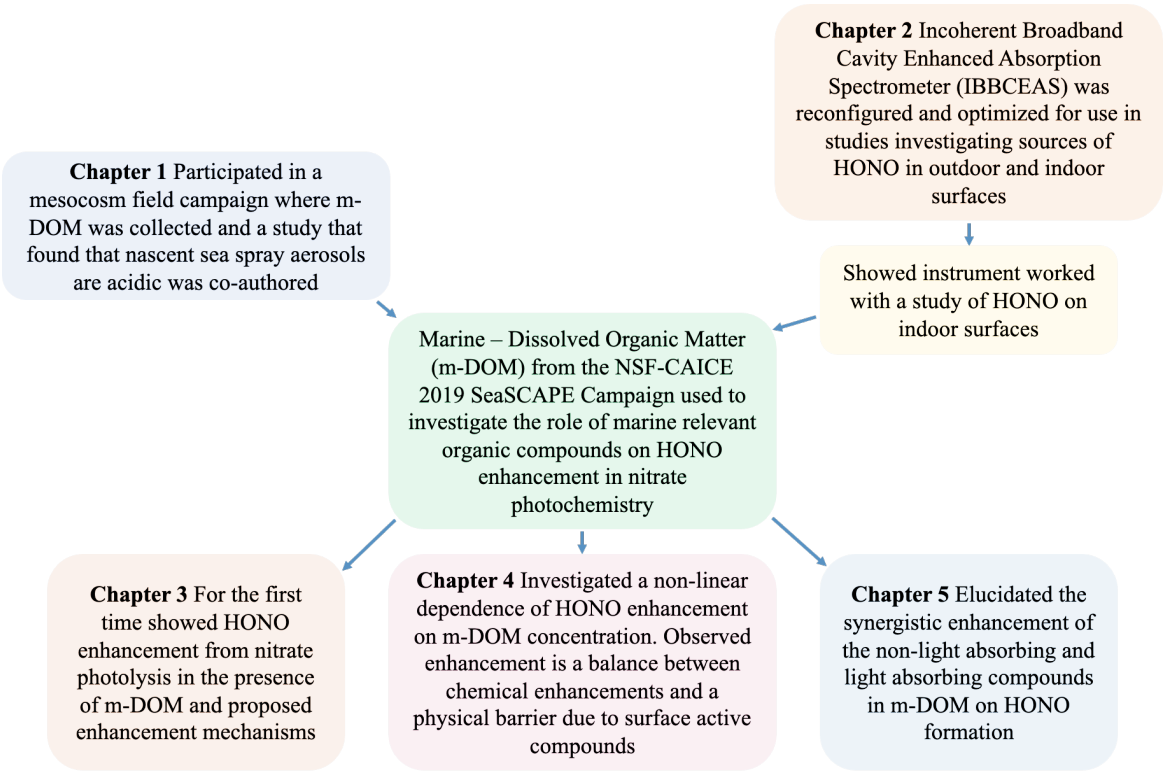

Figure 6.1 Summary of the chapters within this dissertation and the connection between them.

6.2 Future Directions

The future directions in the effort of shedding light on HONO sources in the MBL would include probing HONO from nitrate photolysis in the presence of other m-DOM samples and surface active and nitrogen containing molecular models. The m-DOM that was used in this study was m-DOM collected from the Pacific Ocean during the NSF-CAICE 2019 SeaSCAPE

Campaign. It has been ideal to use as a model of the complex organics that would be found in sea spray aerosols. What would be more beneficial is to also do these studies with other m-DOM samples from other geographical locations as m-DOM can differ in composition depending on the source. Studying other samples can give a better idea of what the global HONO flux from the enhancement of marine relevant organics is. With regards to the quest of trying to elucidate the mechanisms, there are two additional compound types that should be studied. The first is a surface-active compound as Chapter 4 showed that surface coverage by organics can impede HONO partitioning into the gas phase, therefore, adding a surface-active compound to the mixture of molecular models can provide more mechanistic insight on this hypothesis. A suggested compound would be nonanoic acid as it is a commonly used fatty acid molecular model in MBL studies as it has been found in sea spray aerosols; it is also highly surface-active as it is not soluble in water.[7] Further, introducing nitrogen containing chromophoric compounds would introduce a more marine relevant factor as recent studies published have found that the light absorbing parts of m-DOM have a high nitrogen composition percentage.[7,8] A suggested compound would be imidazole carboxaldehyde as it is a simple nitrogen containing chromophore and has been shown to be an effective photosensitizer in photochemical brown carbon studies.[9]

In conclusion, the studies presented in this dissertation advance our understanding of HONO formation in the MBL, highlighting the significance of marine organics in influencing HONO levels. The research provides insights into the complexity of the underlying mechanisms, concentration dependencies, and synergistic effects that must be considered in atmospheric chemistry models. These findings not only contribute to the broader understanding of HONO production but also offer valuable information for predicting hydroxyl radical sources in the MBL, the most important, but highly underappreciated in global models, oxidant in the atmosphere.

Future directions, include investigating HONO enhancement from nitrate photolysis due to other m-DOM samples and introducing both surface-active and nitrogen containing compounds in the molecular models study.

6.3 Bibliography

(1) Mora García, S. L.; Pandit, S.; Navea, J. G.; Grassian, V. H. Nitrous Acid (HONO) Formation from the Irradiation of Aqueous Nitrate Solutions in the Presence of Marine Chromophoric Dissolved Organic Matter: Comparison to Other Organic Photosensitizers. *ACS Earth. Space. Chem.* **2021**, *5* (11), 3056–3064.

(2) Mora García, S. L.; Gutierrez, I.; Navea, J. G.; Grassian, V. H. Enhanced HONO Formation from Aqueous Nitrate Photochemistry in the Presence of Marine Relevant Organics: A Study of m-DOM Concentration on HONO Kinetics and Yields and the Synergistic Enhancement of Aliphatic and Photosensitizing Compounds in m-DOM. *Submitted*.

(3) Karimova, N.; Alija, O.; Mora García, S. L.; Grassian, V. H.; Gerber, R. B.; Navea, J. G. pH Dependence of the Speciation and Optical Properties of 4-Benzoylbenzoic Acid. *Phys. Chem. Chem. Phys.* **2023**, *25*, 17306–17319.

(4) Sauer, J. S.; Mayer, K. J.; Lee, C.; Alves, M. R.; Amiri, S.; Bahaveolos, C.; Barnes, E. B.; Crocker, D. R.; Dinasquet, J.; Garofalo, L. A.; Kaluarachchi, C. P.; Dang, D.; Kilgour, D.; Mael, L.; Mitts, B. A.; Moon, D. R.; Morris, C. K.; Moore, A. N.; Ni, C.-M.; Pendergraft, M. A.; Petras, D.; Simpson, R.; Smith, S.; Tumminello, P. R.; Walker, J. L.; DeMott, P. J.; Farmer, D. K.; Goldstein, A. H.; Grassian, V. H.; Jaffe, J. S.; Malfatti, F.; Martz, T. R.; Slade, J.; Tivanski, A. V.; Bertram, T. H.; Cappa, C. D.; Prather, K. A. The Sea Spray

Chemistry and Particle Evolution Study (SeaSCAPE): Overview and Experimental Methods. *Environ. Sci.: Process. Impacts.* **2022**, *24*, 290–315.

(5) Angle, K. J.; Crocker, D. R.; Simpson, R. M. C.; Mayer, K. J.; Garofalo, L. A.; Moore, A. N.; Mora García, S. L.; Or, V. W.; Srinivasan, S.; Farhan, M.; Sauer, J. S.; Lee, C.; Pothier, M. A.; Farmer, D. K.; Martz, T. R.; Bertram, T. H.; Cappa, C. D.; Prather, K. A.; Grassian, V. H. Acidity across the Interface from the Ocean Surface to Sea Spray Aerosol. *Proc. Natl. Acad. Sci. USA* **2021**, *118* (2), 1–6.

(6) Pandit, S.; Mora García, S. L.; Grassian, V. H. HONO Production from Gypsum Surfaces Following Exposure to NO_2 and HNO_3: Roles of Relative Humidity and Light Source . *Environ. Sci. Technol.* **2021**, *55* (14), 9761–9772.

(7) Trueblood, J. V; Alves, M. R.; Power, D.; Santander, M. V; Cochran, R. E.; Prather, K. A.; Grassian, V. H. Shedding Light on Photosensitized Reactions within Marine-Relevant Organic Thin Films. *ACS Earth. Space. Chem.* **2019**, *3*, 1614–1623.

(8) Alves, M. R.; Coward, E. K.; Gonzales, D.; Sauer, J. S.; Mayer, K. J.; Prather, K. A.; Grassian, V. H. Changes in Light Absorption and Composition of Chromophoric Marine-Dissolved Organic Matter across a Microbial Bloom. *Environ. Sci.: Process. Impacts.* **2022**, *24* (10), 1923–1933.

(9) Palacios, L. G.; Arroyo, P. C.; Aregahegn, K. Z.; Steimer, S. S.; Bartels-rausch, T.; Nozière, B.; George, C.; Ammann, M.; Volkamer, R. Heterogeneous Photochemistry of Imidazole-2-Carboxaldehyde : HO_2 Radical Formation and Aerosol Growth. *Atmos. Chem. Phys.* **2016**, *16*, 11823–11836.